SUPPLEMENTARY INFORMATION

for

Cryptic phosphorylation in nucleoside natural product biosynthesis

Matthew M. Draelos[1], Anyarat Thanapipatsiri[2], Hilda Sucipto[2], and Kenichi Yokoyama[1,2*]

[1] Department of Chemistry, Duke University; [2] Department of Biochemistry, Duke University School of Medicine

* To whom correspondence should be addressed:

Tel: 919-684-8848

Email: ken.yoko@duke.edu

Table of Contents

Supplementary Table 1. Enzymes conserved between the nikkomycin and polyoxin pathways.

Streptomyces tendae	*Streptomyces cacaoi*	Amino acid identity	Predicted function [a]
NikI	PolD	50%	α-KG dependent dioxygenase
NikJ	PolH	70%	Radical SAM enzyme [b]
NikK	PolI	62%	PLP-dependent aminotransferase
NikL	PolJ	61%	Phosphatase
NikM	PolK	58%	α-KG dependent dioxygenase
NikN (N-terminal domain)	PolQ1	48%	Major facilitator superfamily
NikN (C-terminal domain)	PolQ2	63%	P-loop NTPase superfamily
NikO	PolA	63%	Enolpyruvyl transferase [b]
NikS	PolG	58%	ATP grasp family amide ligase

[a] Functional assignment is based upon amino acid sequence homology. [b] Catalytic function has been demonstrated.

Supplementary Table 2. Bacterial strains used in this study

Strain	Description/Chromosomal/Plasmid marker	Source/Reference
E. coli DH5α	*F- φ80lacZΔM15 Δ(lacZYA-argF)U169 deoR recA1 endA1 hsdR17(rk-, mk+) phoA supE44 thi-1 gyrA96 relA1 λ-*	Agilent technologies, US
E. coli DH10*β*	*F- mcrA* Δ(*mrr-hsd*RMS-*mcrBC*) *φ 80dlacZΔM15 ΔlacX74 endA1 recA1 deoR* Δ*(ara,leu)7697 araD139 galU galK nupG rpsL λ-*	Invitrogen, US
E. coli ET12567/ pUZ8002	*dam-13::Tn9 dcm-6 hsd*M *hsd*S CmR/ *tra, neo*, RP4	[1], [2]
S. cacaoi subsp. asoensis	Polyoxin producer	[3]
S. tendae Tü901	Nikkomycin producer	[4]
S. cacaoi Δ*polQ2*	*polQ2* markerless in-frame deletion mutant	This study
S. cacaoi Δ*polQ2* + pUWL201PWT/ *polQ2* (Δ*polQ2* + *polQ2*)	*S. cacaoi* Δ*polQ2* harboring pUWL201PWT/*polQ2* for a constitutive expression of *polQ2* under the control of the *ermE** promoter	This study
S. tendae Δ*nikK*::Kan^R	Insertion inactivation mutant of *nikK* by a replacement with Kan^R	This study
S. tendae Δ*nikK*::Kan^R pIJ10257/*nikK* (Δ*nikK* + *nikK*)	*S. tendae* Δ*nikK*::Kan^R with chromosamally integrated wt *nikK* gene under the control of the *ermE** promoter.	This study
S. tendae Δ*nikL*::Kan^R	Insertion inactivation mutant of *nikL* by a replacement with Kan^R	This study

Reference:

1 MacNeil, D. J. *et al.* Analysis of Streptomyces avermitilis genes required for avermectin biosynthesis utilizing a novel integration vector. *Gene* **111**, 61-68 (1992).

2 Paget, M. S., Chamberlin, L., Atrih, A., Foster, S. J. & Buttner, M. J. Evidence that the extracytoplasmic function sigma factor sigmaE is required for normal cell wall structure in Streptomyces coelicolor A3(2). *Journal of bacteriology* **181**, 204-211 (1999).

3 Suzuki, S. *et al.* A New Antibiotic, Polyoxin A. *The Journal of antibiotics* **18**, 131 (1965).

4 Dahn, U. *et al.* Stoffwechselprodukte von mikroorganismen. 154. Mitteilung. Nikkomycin, ein neuer hemmstoff der chitinsynthese bei pilzen. *Archives of microbiology* **107**, 143-160 (1976).

Supplementary Table 3. Plasmids for gene disruption and complementation

Plasmid/Cosmid	Relevant genotype/Descriotion	Source/Reference
pJET 1.2 Blunt	AmpR, cloning vector	Thermo Fisher Scientific, US
pKC1139	*aac(3)IV, E. coli-Streptomyces* shuttle plasmid containing a *Streptomyces* temperature-sensitive origin of replication	[5]
pIJ10257	HygR, *φ*BT1 *attP-int* derived integration vector for the conjugal transfer of DNA from *E. coli* to *Streptomyces* spp. containing 330-bp *ermE*p* (*Kpn*I-*Pst*I) with ribosome binding site and multicloning site from pIJ8723 cloned into pMS81 cut with *Kpn*I-*Nsi*I	[6]
pUWL201PWT	A derivative of pUWL201PW[7] containing an *oriT* sequence inserted into the *Pst*I site	This study
pKC1139/Δ*nikJ*::Kan^R	A derivative of pKC1139 containing kanamycin resistance marker (Kan^R), left and right flanking regions of *nikJ* for *nikJ* insertion inactivation	This study
pKC1139/Δ*polQ2*	A derivative of pKC1139 containing left and right flanking regions of *polQ2* for *polQ2* markerless in-frame deletion	This study
pKC1139/Δ*nikK*::Kan^R	A derivative of pKC1139 containing kanamycin resistance marker (Kan^R), left and right flanking regions of *nikK* for *nikK* insertion inactivation	This study
pKC1139/Δ*nikL*::Kan^R	A derivative of pKC1139 containing kanamycin resistance marker (Kan^R), left and right flanking regions of *nikL* for *nikL* insertion inactivation	This study
pKC1139/Δ*nikM*::Kan^R	A derivative of pKC1139 containing kanamycin resistance marker (Kan^R), left and right flanking regions of *nikM* for *nikM* insertion inactivation	This study
pIJ10257/*nikK*	pIJ10257 containing cloned *nikK* coding sequence	This study
pUWL201PWT/*polQ2*	pUWL201PWT containing cloned *polQ2* coding sequence	This study

Reference:

5 Bierman, M. *et al.* Plasmid cloning vectors for the conjugal transfer of DNA from Escherichia coli to Streptomyces spp. *Gene* **116**, 43-49 (1992).

6 Hong, H. J., Hutchings, M. I., Hill, L. M. & Buttner, M. J. The role of the novel Fem protein VanK in vancomycin resistance in *Streptomyces coelicolor*. *The Journal of biological chemistry* **280**, 13055–13061 (2005).

7 Doumith, M. *et al.* Analysis of genes involved in 6-deoxyhexose biosynthesis and transfer in Saccharopolyspora erythraea. *Molecular & general genetics : MGG* **264**, 477-485 (2000).

Supplementary Table 4. Primers used in this study

Oligomer	Sequence 5'-3'	Description
KA09F	CATATGGTGCCGGCGCGGGAAGGGGC	Cloning of *nikK*
KA09R	GGATCCTCATGCCACCCCTTCGCGGTACCG	
KA16F	GAATTCCCCGACCCCTTGGACGCCACCGTG	Forward primer for upstream region of *polQ2* knockout
KA16R	CATATGGTCTGCGGGCTCGGTCATGCGGG	Reverse primer for upstream region of *polQ2* knockout
KA17F1	CATATGCGCACCCACGACGGTTCCCGC	Forward primer for downstream region of *polQ2* knockout
KA17R1	AAGCTTCTGGAGGACTTTGTGCTCGAAGTCAA CGGTGGC	Reverse primer for downstream region of *polQ2* knockout
KA18F	CGCACCCGTGATGACCGTC	Sequencing of *polQ2* knockout construct
KA18R	GCGACATCGTGGGCGACC	
KA23F	CCACGGTGAGCCCATGACC	Verification of *polQ2* knockout construct and mutant
KA23R	GTCACCCACGAGGCGTTCAC	
KanR	TCAGAAGAACTCGTCAAGAAG	Kanamycin gene amplification for insertion inactivation
HSU-Nik11	GATACAAAGCTTGAACGGCGGCTCACG	*nikK* gene insertion inactivation, sequencing and genotype verification
HSU-Nik12	GCTCTCCCGCAGGAAG	
HSU-Nik13	CCCTTCCTGCGGGAGAGCCCGGAATTGCCAGC TG	
HSU-Nik14	GCCTTCTTGACGAGTTCTTCTGACGTCAGGTC GTCGCC	
HSU-Nik15	TCTATGGAATTCCGTGTTCGGCTTCGATC	
HSU-Nik16	GATACAAAGCTTGGAGGAACTGGCCGAGC	*nikL* gene insertion inactivation, sequencing and genotype verification
HSU-Nik17	ATCGCGCACGTTGGG	
HSU-Nik18	CTGCCCAACGTGCGCGATCCGGAATTGCCAGC TG	
HSU-Nik19	GCCTTCTTGACGAGTTCTTCTGAACGCTCCAC GGCCTC	
HSU-Nik20	TCTATGGAATTCCAGGTCACCGCTCCAC	
LIC-MBP-polJ-F	TACTTCCAATCCAATGCCGTGACCACCGGAGC CCGCC	Cloning of PolJ into pMCSG9

LIC-MBP-polJ-R	TTATCCACTTCCAATGTTATCAATCAGCGTCATGTCGTTCTCTCC	
polJ-F	CATATGACCACCGGAGCCCGCCG	Cloning of PolJ into pET28b
polJ-R	AAGCTTCAATCAGCGTCATGTCGTTCTCTCC	
LIC-MBP-polQ2-F	TACTTCCAATCCAATGCCATGACCGAGCCCGCAGACCCGC	Cloning of PolQ2 into pMCSG9
LIC-MBP-polQ2-R	TTATCCACTTCCAATGTTATCACGCGCGGGAACCGTCGTGGG	
LIC-MBP-nikK-F	TACTTCCAATCCAATGCCGTGCCGGCGCGGGAAGG	Cloning of NikK into pMCSG9
LIC-MBP-nikK-R	TTATCCACTTCCAATGTTATCATGCCACCCCTTCGCGGTACCG	
LIC-MBP-nikM-F	TACTTCCAATCCAATGCCATGTCCCTAGTCGACATCGAGACC	Cloning NikM into pMCSG9
LIC-MBP-nikM-R	TTATCCACTTCCAATGTTATCACGGGCGGACGAAGTGCAC	
nikL-F	CATATGGTTCCGGGCCTGCCCAACG	Cloning NikL into pET28
nikL-R	AAGCTTCACAGACGAACGGGATGGGTGAAC	

[a] Underlined regions denote restriction sites (*Hind*III: AAGCTT; *Nde*I: CATATG, *Eco*RI: GAATTC, *Bam*HI: GGATCC) or T4 DNA Polymerase LIC handles (TACTTCCAATCCAATGCC and TTATCCACTTCCAATGTTA).

1: MBP-PolQ2 (64.1 kDa)
2: MBP-PolJ (73.7 kDa)
3: 6xHis-PolJ (31.2 kDa) [red asterisk (*)]
4: 6xHis-PolK (26.2 kDa)
5: MBP-NikM (66.6 kDa)
6: MBP-NikK (83.03 kDa)
7: 6xHis-PolD (26.3 kDa)
8: 6xHis-NikS (50.1 kDa)
M: MW marker

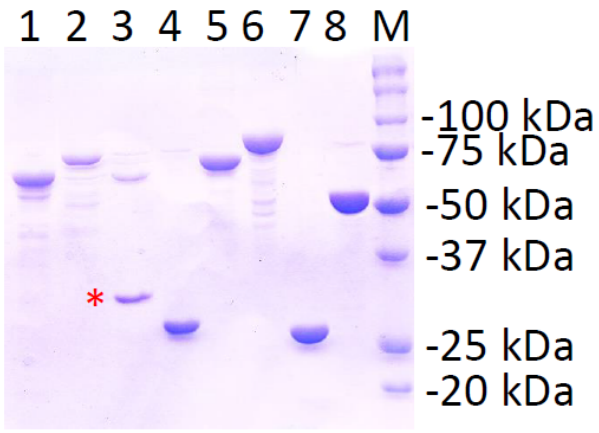

Supplementary Figure 1. SDS-PAGE (12.5%) gel of purified enzymes in this study.
Purifications were repeated for at least twice as either His-tagged or MBP-fusion proteins for each enzyme with reproducible purity and yield.

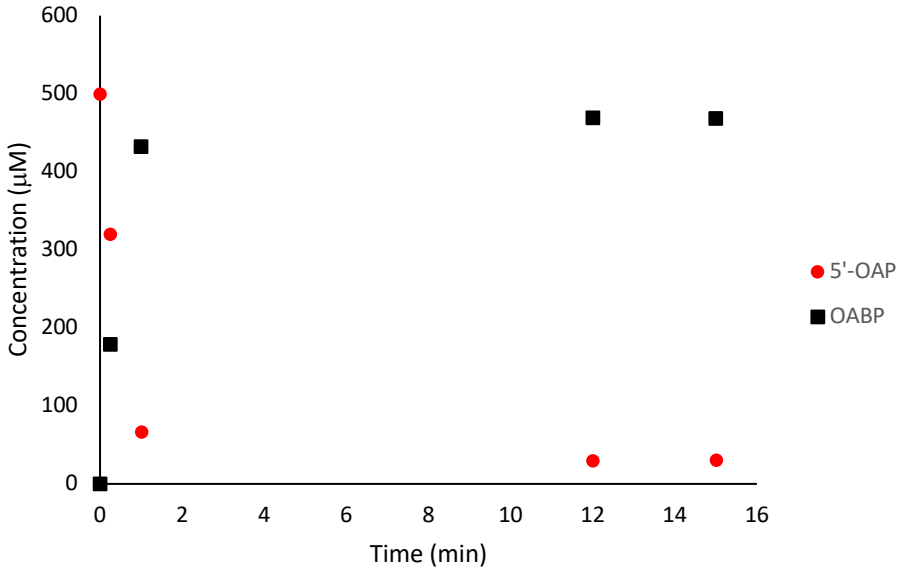

Supplementary Figure 2. Time course of a PolQ2 assay with 5'-OAP as substrate.
Typical reaction time course for phosphorylation of 5'-OAP into OABP by PolQ2. PolQ2 (35 μM) was incubated with 500 μM of 5'-OAP in Buffer A supplemented with 4 mM $MgCl_2$ and 2 mM ATP at 25 °C. Turnover rate with these conditions is ~0.1-0.21 min^{-1} depending on enzyme preparation. The data shown is from a single, representative experiment.

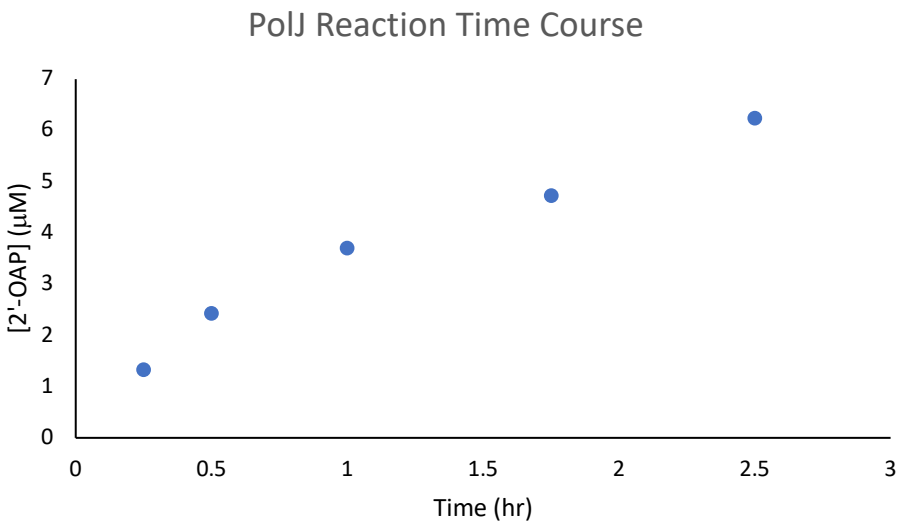

Supplementary Figure 3. Time course of a PolJ assay with OABP as substrate.
Reaction conditions: MBP-PolJ (2.2μM) was incubated with 100 uM OABP and 10 mM $MgCl_2$ in 50 mM Tris pH 8 at 25 °C. Turnover rates of ~0.016 min^{-1} were typically observed. These data were consistent in three separate experiments from three different enzyme preps; the data shown is from a single, representative experiment.

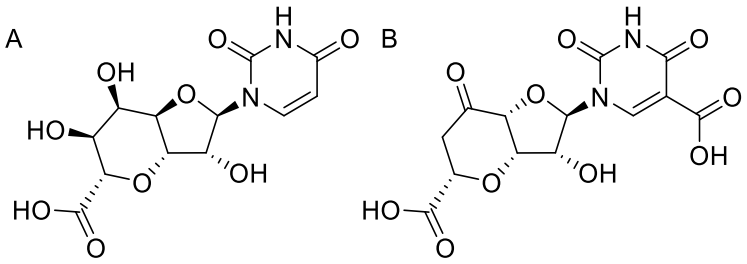

Supplementary Figure 4. Structures of Nikkomycin S_{OZ} and octosyl acid C.
Nikkomycin S_{OZ}[8] (**a**) and octosyl acid C[9] (**b**) were previously isolated from nikkomycin and polyoxin producers, respectively. Given our in vitro characterization of oxygenases PolK and NikM, these species are likely shunt metabolites derived from the promiscuous oxidative activities of these enzymes.

Reference:

8 Schuz, T. C., Fiedler, H. P., Zahner, H., Rieck, M. & Konig, W. A. Metabolic Products of Microorganisms .263. Nikkomycins Sz, Sx, Soz and Sox, New Intermediates Associated to the Nikkomycin Biosynthesis of Streptomyces-Tendae. *J Antibiot* **45**, 199-206 (1992).

9 Isono, K., Crain, P. F. & Mccloskey, J. A. Isolation and Structure of Octosyl Acids - Anhydrooctose Uronic Acid Nucleosides. *J Am Chem Soc* **97**, 943-945 (1975).

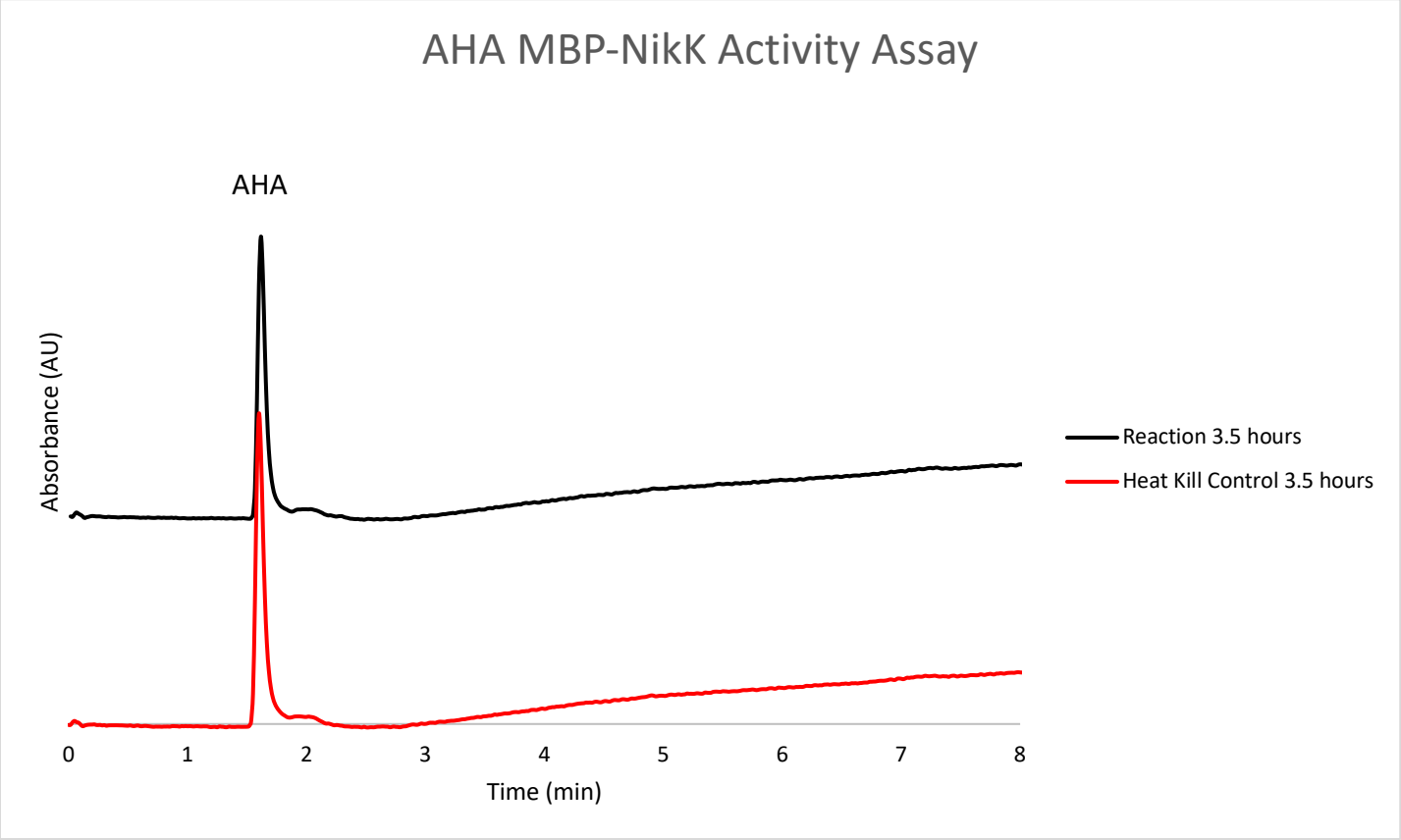

Supplementary Figure 5. HPAEC analysis of the NikK activity assay with AHA as substrate. NikK (30 μM) was incubated with AHA (0.75 mM) and α-KG (1 mM) in 40 mM Tris pH 9.0 at 25 °C. After 3.5 hours no product formation and no decrease in the AHA peak was observed in the reaction (black line) compared to the control with heat-inactivated NikK (red line). This observation suggests that AHA is unlikely to be the substrate for NikK.

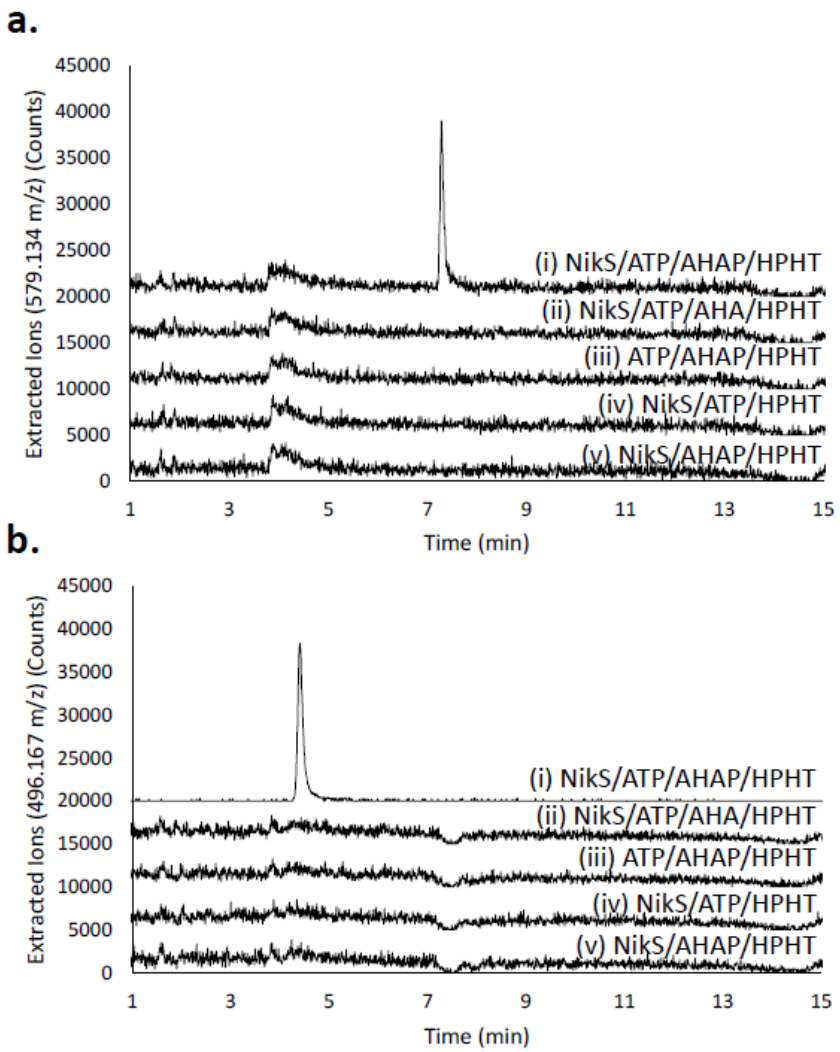

Supplementary Figure 6. Extracted Ion Chromatograms for nikkomycin Z phosphate and nikkomycin Z from NikS assays with AHAP or AHA.

a. Non-CIP treated reactions and controls. **b.** CIP-treated reactions and controls.

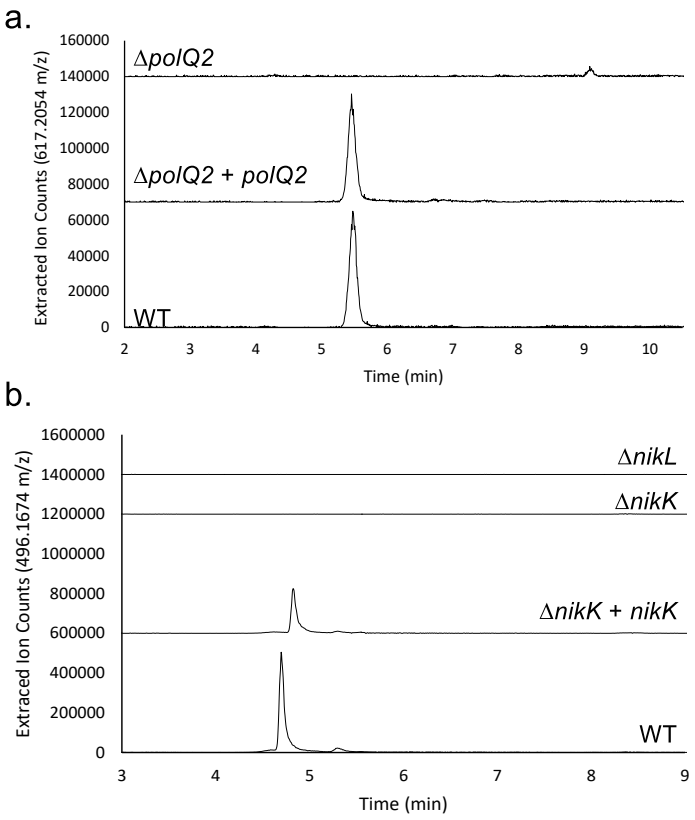

Supplementary Figure 7. LCMS characterization of metabolites produced by wt and mutant *S. cacaoi* and *S tendae*.

a. LC-HRMS analysis of culture media of *S. cacaoi* wt, Δ*polQ2*, and Δ*polQ2* complemented with *polQ2* (Δ*polQ2* + *polQ2*). Shown are EIC for polyoxin A (*m/z* 617.2054 ± 0.0031). **b.** LC-HRMS analysis of culture media of *S. tendae* wt, Δ*nikL*::*kan*^{R}, Δ*nikK*::*kan*^{R}, and Δ*nikK*::*kan*^{R} complemented with *nikK* (Δ*nikK* + *nikK*). Shown are EIC for nikkomycin Z (*m/z* 496.1674 ± 0.0024).

BGCs with kinase [a]	BGCs without kinase [b]
Nikkomycin[10]	Showdomycin[27]
Polyoxin[11]	Puromycin[28]
Malayamycin[12]	Tunicamycin[29,30]
Pseudouridimycin[13]	Oxetanocin[31]
Muraymycin[14]	Toyocamycin[32]
Caprazamycin[15]/A-90289[16]/muraminomycin[17]/liposidomycin[18]	Minimycin[33]
Capuramycin[19]	Mildiomycin[34]/Blasticidin S[35]/Gougerotin[36]
Amipurimycin[20]	Herbicidin[37]
A-94964[21]	Pacidamycin/napsamycin[38]
Aristeromycin[22]/coformycin[23]	Jawsamycin[39]
Formycin[24]	
Tubercidin[25]	
Albomycin[26]	

Supplementary Figure 8. Reported nucleoside BGCs categorized by conservation of kinases. Red highlights represent BGCs with P-loop NTPase superfamily members; blue, aminoglycoside 3'-phosphotransferase family; green, PfkB (ribokinase) family carbohydrate kinase; orange, nucleoside/nucleotide kinase family; purple, BGCs with phosphatases. [a] 17 of the 29 reported BGCs contain kinases. Nine of those kinases belonged to the P-loop NTPase superfamily (highlighted in red), and thus related to PolQ2. Eight other pathways (highlighted in blue, green and orange) contained kinases in distinct families that are all related to phosphorylation of nucleoside or carbohydrates. Therefore, these enzymes could also be responsible for phosphorylation of nucleoside biosynthetic intermediates. CapP from the capuramycin pathway was shown to phosphorylate the final metabolites and proposed to be responsible for self-resistance[40]. The reported K_m and k_{cat}/K_m values for CapP towards one of the final metabolites (A-503083A) was reported as 175 μM and 4380 M^{-1} s^{-1}, respectively, which may be compared to those for Mur28 towards muraymycin D2 (170 μM and 510 M^{-1} s^{-1}) and ADR-GlyU (38 μM and 33000 M^{-1} s^{-1}). CapP's activity towards biosynthetic intermediates have not been reported. Intriguingly, some of these pathways (amipurimycin and tubercidin) also have MFS transporter, reminiscent of polyoxin and nikkomycin BGCs. [b] 12 of 29 reported BGCs do not contain kinase. However, even among these BGCs without kinase, six BGCs contained phosphatases, which may suggest that they are biosynthesized from nucleotide precursors that need to be dephosphorylated later in the biosynthesis. The timing of dephosphorylation could be important for the efficient metabolic flux as well as self-resistance. For example, in oxetanocin biosynthesis, nucleoside 5'-diphosphate was the substrate of oxetan ring formation, and dephosphorylation is the final step of the biosynthesis[31].

Reference:

10 Bruntner, C., Lauer, B., Schwarz, W., Mohrle, V. & Bormann, C. Molecular characterization of co-transcribed genes from Streptomyces tendae Tu901 involved in the biosynthesis of the peptidyl moiety of the peptidyl nucleoside antibiotic nikkomycin. *Mol Gen Genet* **262**, 102-114 (1999).

11 Chen, W. *et al.* Characterization of the polyoxin biosynthetic gene cluster from Streptomyces cacaoi and engineered production of polyoxin H. *J Biol Chem* **284**, 10627-10638 (2009).

12 Hong, H., Samborskyy, M., Zhou, Y. & Leadlay, P. F. C-Nucleoside Formation in the Biosynthesis of the Antifungal Malayamycin A. *Cell Chem Biol* **26**, 493-501 e495 (2019).
13 Sosio, M. *et al.* Analysis of the Pseudouridimycin Biosynthetic Pathway Provides Insights into the Formation of C-nucleoside Antibiotics. *Cell Chem Biol* **25**, 540-549 e544 (2018).
14 Cheng, L. *et al.* Identification of the gene cluster involved in muraymycin biosynthesis from Streptomyces sp NRRL 30471. *Mol Biosyst* **7**, 920-927 (2011).
15 Kaysser, L. *et al.* Identification and manipulation of the caprazamycin gene cluster lead to new simplified liponucleoside antibiotics and give insights into the biosynthetic pathway. *J Biol Chem* **284**, 14987-14996 (2009).
16 Funabashi, M. *et al.* The biosynthesis of liposidomycin-like A-90289 antibiotics featuring a new type of sulfotransferase. *Chembiochem* **11**, 184-190 (2010).
17 Chi, X. *et al.* The muraminomicin biosynthetic gene cluster and enzymatic formation of the 2-deoxyaminoribosyl appendage. *Medchemcomm* **4**, 239-243 (2013).
18 Kaysser, L., Siebenberg, S., Kammerer, B. & Gust, B. Analysis of the liposidomycin gene cluster leads to the identification of new caprazamycin derivatives. *Chembiochem* **11**, 191-196 (2010).
19 Funabashi, M. *et al.* Identification of the biosynthetic gene cluster of A-500359s in Streptomyces griseus SANK60196. *J Antibiot* **62**, 325-332 (2009).
20 Kang, W. J. *et al.* Identification of the Amipurimycin Gene Cluster Yields Insight into the Biosynthesis of C9 Sugar Nucleoside Antibiotics. *Org Lett* **21**, 3148-3152 (2019).
21 Shiraishi, T., Nishiyama, M. & Kuzuyama, T. Biosynthesis of the uridine-derived nucleoside antibiotic A-94964: identification and characterization of the biosynthetic gene cluster provide insight into the biosynthetic pathway. *Org Biomol Chem* **17**, 461-466 (2019).
22 Kudo, F., Tsunoda, T., Takashima, M. & Eguchi, T. Five-Membered Cyclitol Phosphate Formation by a myo-Inositol Phosphate Synthase Orthologue in the Biosynthesis of the Carbocyclic Nucleoside Antibiotic Aristeromycin. *Chembiochem* **17**, 2143-2148 (2016).
23 Xu, G. *et al.* Coordinated Biosynthesis of the Purine Nucleoside Antibiotics Aristeromycin and Coformycin in Actinomycetes. *Appl Environ Microbiol* **84**, e01860-01818 (2018).
24 Wang, S. A. *et al.* Identification of the Formycin A Biosynthetic Gene Cluster from Streptomyces kaniharaensis Illustrates the Interplay between Biological Pyrazolopyrimidine Formation and de Novo Purine Biosynthesis. *J Am Chem Soc* **141**, 6127-6131 (2019).
25 Liu, Y. *et al.* Discovery and characterization of the tubercidin biosynthetic pathway from Streptomyces tubercidicus NBRC 13090. *Microb Cell Fact* **17**, 131 (2018).
26 Zeng, Y. *et al.* Biosynthesis of Albomycin delta(2) Provides a Template for Assembling Siderophore and Aminoacyl-tRNA Synthetase Inhibitor Conjugates. *Acs Chemical Biology* **7**, 1565-1575 (2012).
27 Palmu, K. *et al.* Discovery of the Showdomycin Gene Cluster from Streptomyces showdoensis ATCC 15227 Yields Insight into the Biosynthetic Logic of C-Nucleoside Antibiotics. *Acs Chemical Biology* **12**, 1472-1477 (2017).
28 Lacalle, R. A., Tercero, J. A. & Jimenez, A. Cloning of the Complete Biosynthetic Gene-Cluster for an Aminonucleoside Antibiotic, Puromycin, and Its Regulated Expression in Heterologous Hosts. *Embo J* **11**, 785-792 (1992).
29 Chen, W. Q. *et al.* Characterization of the tunicamycin gene cluster unveiling unique steps involved in its biosynthesis. *Protein Cell* **1**, 1093-1105 (2010).
30 Wyszynski, F. J., Hesketh, A. R., Bibb, M. J. & Davis, B. G. Dissecting tunicamycin biosynthesis by genome mining: cloning and heterologous expression of a minimal gene cluster. *Chemical Science* **1**, 581-589 (2010).
31 Bridwell-Rabb, J., Kang, G., Zhong, A., Liu, H. W. & Drennan, C. L. An HD domain phosphohydrolase active site tailored for oxetanocin-A biosynthesis. *P Natl Acad Sci USA* **113**, 13750-13755 (2016).
32 McCarty, R. M. & Bandarian, V. Deciphering deazapurine biosynthesis: Pathway for pyrrolopyrimidine nucleosides toyocamycin and sangivamycin. *Chem Biol* **15**, 790-798 (2008).
33 Kong, L. *et al.* Divergent Biosynthesis of C-Nucleoside Minimycin and Indigoidine in Bacteria. *iScience* **22**, 430-440 (2019).

34 Wu, J., Li, L., Deng, Z. X., Zabriskie, T. M. & He, X. Y. Analysis of the Mildiomycin Biosynthesis Gene Cluster in Streptoverticillum remofaciens ZJU5119 and Characterization of MilC, a Hydroxymethyl cytosyl-glucuronic Acid Synthase. *Chembiochem* **13**, 1613-1621 (2012).
35 Cone, M. C., Yin, X. H., Grochowski, L. L., Parker, M. R. & Zabriskie, T. M. The blasticidin S biosynthesis gene cluster from Streptomyces griseochromogenes: Sequence analysis, organization, and initial characterization. *Chembiochem* **4**, 821-828 (2003).
36 Niu, G. Q., Li, L., Wei, J. H. & Tan, H. R. Cloning, Heterologous Expression, and Characterization of the Gene Cluster Required for Gougerotin Biosynthesis. *Chem Biol* **20**, 34-44 (2013).
37 Lin, G. M., Romo, A. J., Liem, P. H., Chen, Z. & Liu, H. W. Identification and Interrogation of the Herbicidin Biosynthetic Gene Cluster: First Insight into the Biosynthesis of a Rare Undecose Nucleoside Antibiotic. *J Am Chem Soc* **139**, 16450-16453 (2017).
38 Kaysser, L. *et al.* Identification of a Napsamycin Biosynthesis Gene Cluster by Genome Mining. *Chembiochem* **12**, 477-487 (2011).
39 Hiratsuka, T. *et al.* Biosynthesis of the Structurally Unique Polycyclopropanated Polyketide-Nucleoside Hybrid Jawsamycin (FR-900848)**. *Angew Chem Int Edit* **53**, 5423-5426 (2014).
40 Yang, Z. *et al.* Functional and kinetic analysis of the phosphotransferase CapP conferring selective self-resistance to capuramycin antibiotics. *J Biol Chem* **285**, 12899-12905 (2010).

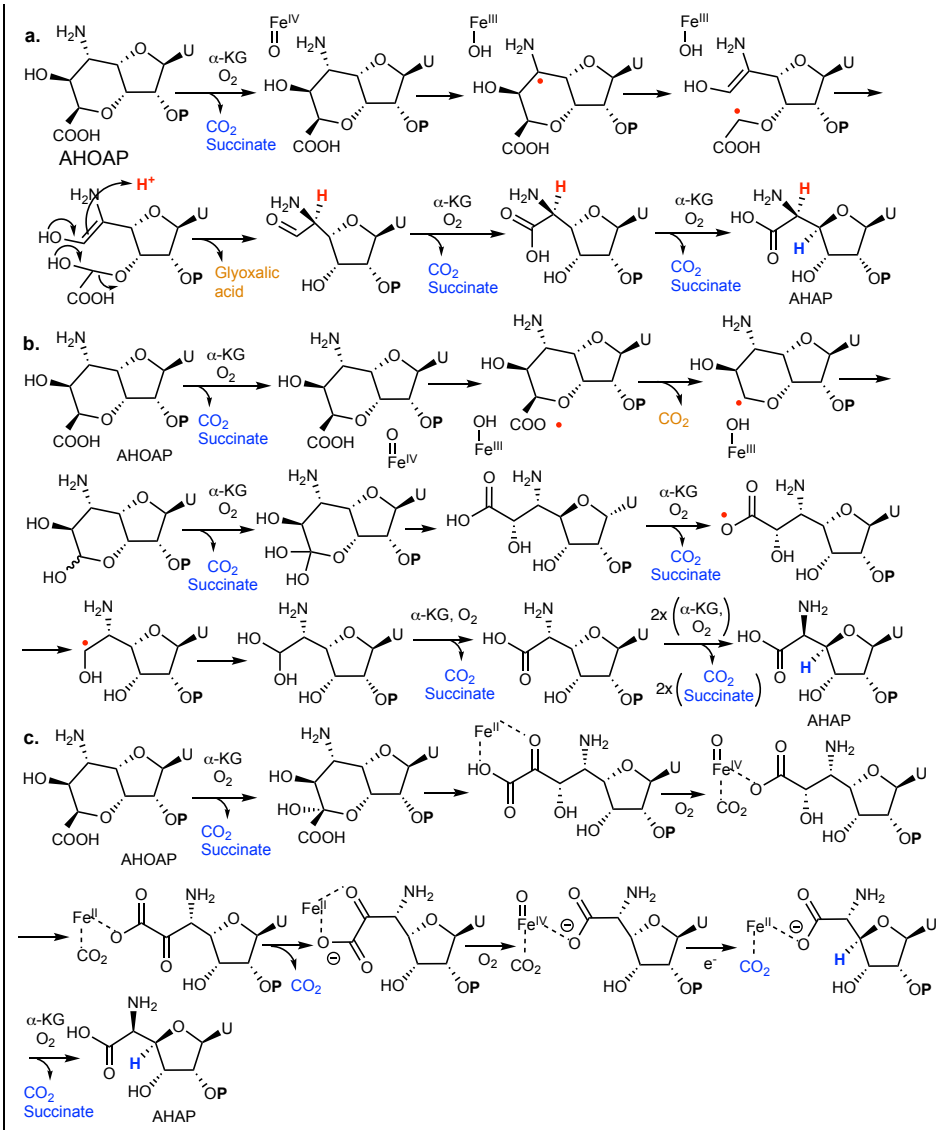

Supplementary Figure 9. Possible mechanisms for PolD with AHOAP.
Shown are possible mechanisms for C-C bond cleavage of AHOAP into AHAP by PolD. **a.** Radical formation at the 5' position initiates the homolytic cleavage of the 5'-6' C-C bond. Subsequent hydroxylation of the 7' radical and hydrolysis of the resulting hemi-acetal yields glyoxylate. **b.** A processive decarboxylation with succinate and CO_2 being the primary by-products. **c.** α-ketoacid intermediates are used to activate O_2 to catalyze either hydroxylation or epimerization.

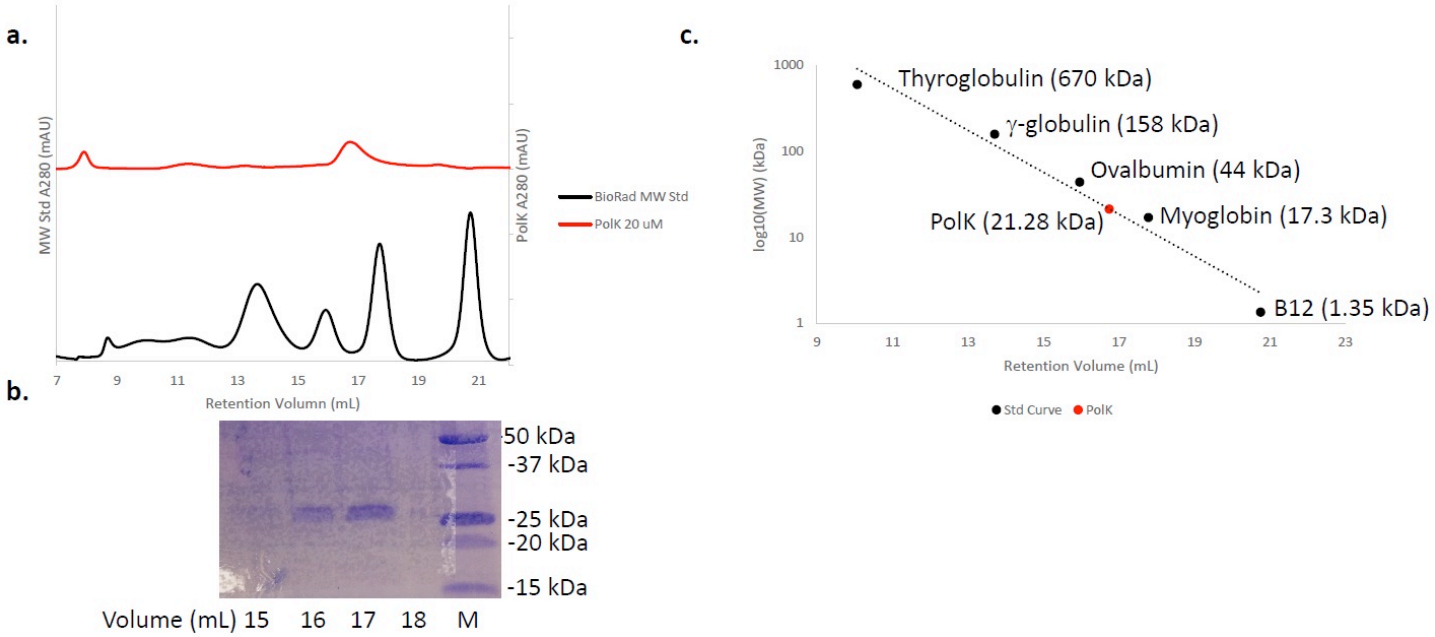

Supplementary Figure 10. Determination of the oligomeric state of PolK by size exclusion chromatography (SEC).

a. SEC chromatogram of PolK (top trace) and Bio-Rad SEC molecular weight standard (bottom). **b.** SDS-PAGE of SEC fractions. **c.** Standard curve based on the molecular weight standard chromatogram in **a**. The native molecular weight of PolK was determined as 21.3 kDa, which is consistent with the theoretical molecular weight of PolK monomer (26.2 kDa). These results were reproducible in two enzyme preparations.

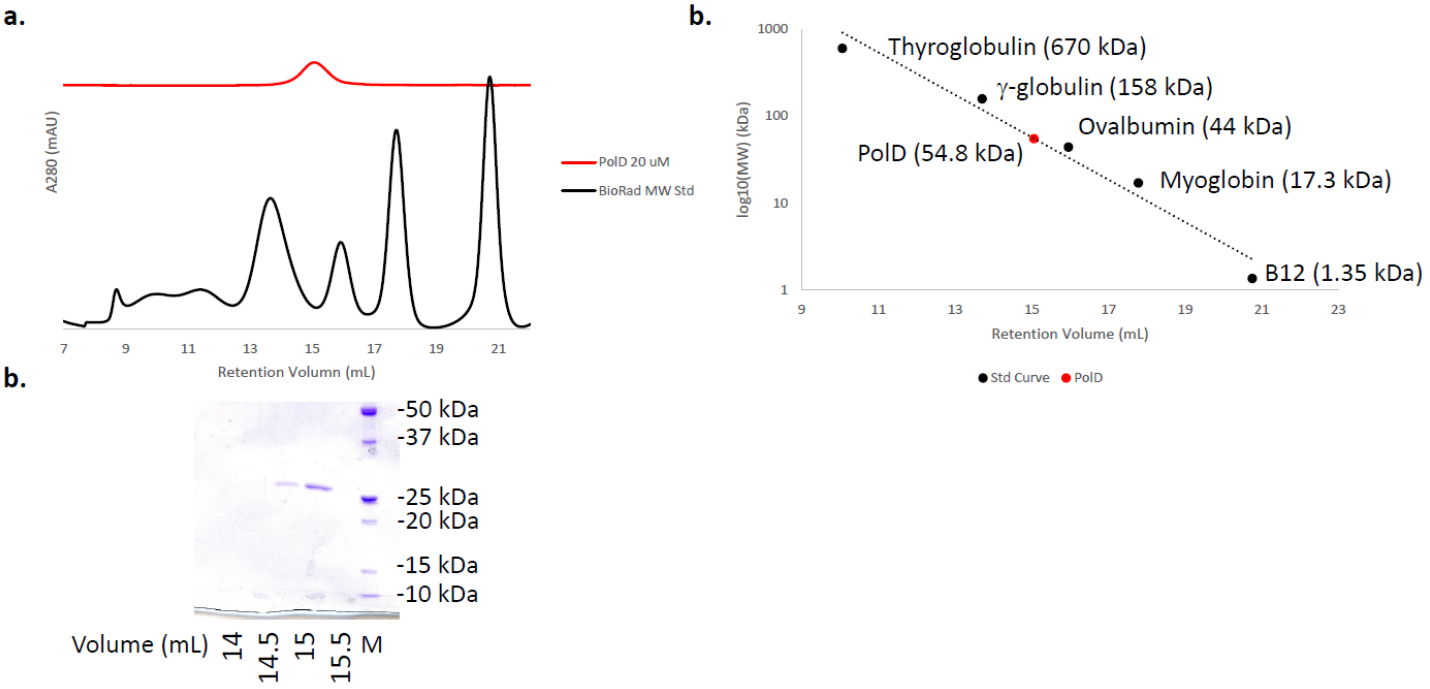

Supplementary Figure 11. Determination of the oligomeric state of PolD by SEC
a. SEC chromatogram of PolD (top trace) and Bio-Rad SEC molecular weight standard (bottom). **b.** SDS-PAGE of SEC fractions. **c.** Standard curve based on the molecular weight standard chromatogram in **a**. The native molecular weight of PolD was determined as 54.8 kDa, which is consistent with the theoretical molecular weight of PolD dimer (52.6 kDa). These results were reproducible in two enzyme preparations.

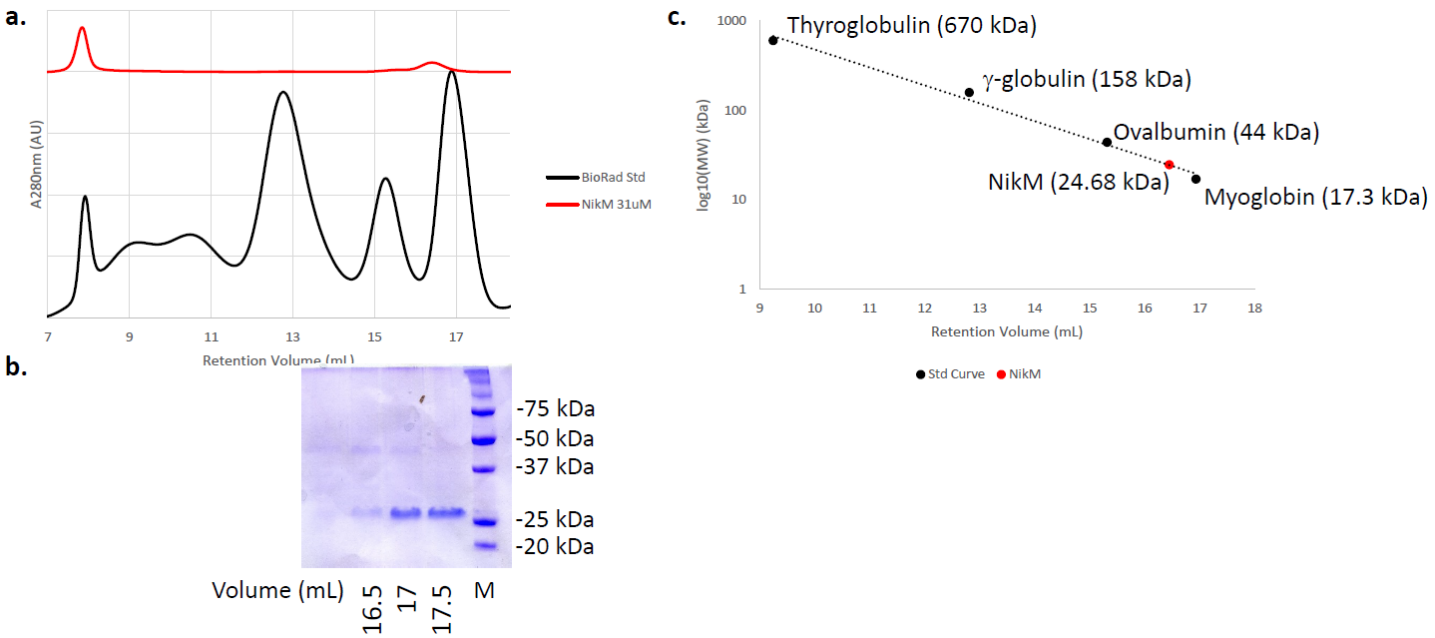

Supplementary Figure 12. Determination of the oligomeric state of NikM by SEC.
a. SEC chromatogram of NikM (top trace) and Bio-Rad SEC molecular weight standard (bottom). **b.** SDS-PAGE of SEC fractions. **c.** Standard curve based on the molecular weight standard chromatogram in **a**. The native molecular weight of NikM was determined as 24.7 kDa, which is consistent with the theoretical molecular weight of NikM monomer (26.3 kDa). These results were conducted once.

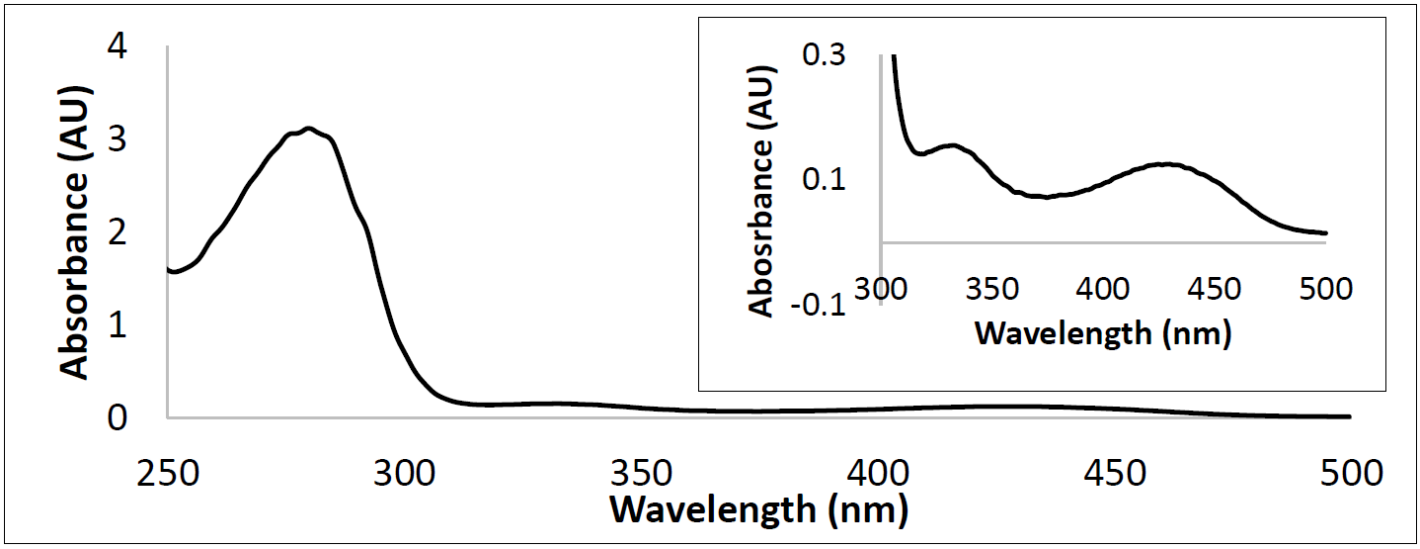

Supplementary Figure 13. UV-vis spectrum of NikK.

The spectrum was determined for 16 μM MBP-NikK. Based on the reported extinction coefficient of PLP at 388 nm (5305 cm^{-1} mM^{-1}; pH 7.5)[41], 0.92 eq. of PLP was co-purified with MBP-NikK, assuming one PLP-binding site per monomer. The concentration of MBP-NikK was determined by Bradford Assay with BSA as a standard. These data were collected in duplicate.

Reference:

41 Ghatge, M. S. *et al.* Pyridoxal 5 '-Phosphate Is a Slow Tight Binding Inhibitor of E. coli Pyridoxal Kinase. *Plos One* **7**, e41680 (2012).

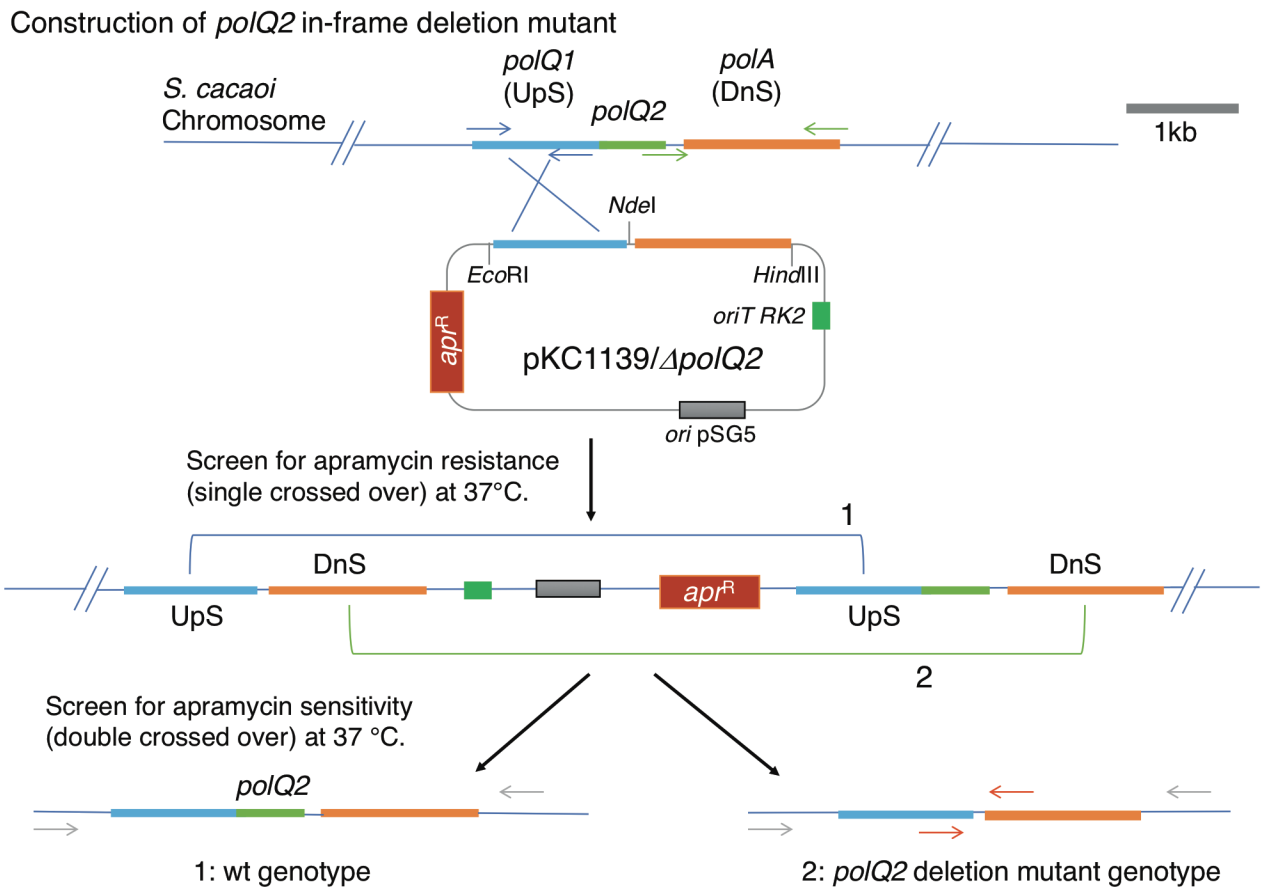

Supplementary Figure 14. Schematic representation of markerless in-frame deletion of *polQ2*. UpS (upstream) and DnS (downstream) represent 5' and 3' flanking region of *polQ2*, respectively. Blue and green arrows indicate primers used to amplify the upstream 5' flanking fragment and downstream 3' flanking fragments, respectively, from the *S. cacaoi* genomic DNA in order to generate the pKC1139/Δ*polQ2* construct. Grey arrows indicate the first pair of verification primers used to amplify and distinguish the wt and Δ*polQ2* mutant genotypes. Red arrows indicate the second pair of primer used to amplify and confirm the deleted region in the Δ*polQ2* mutant.

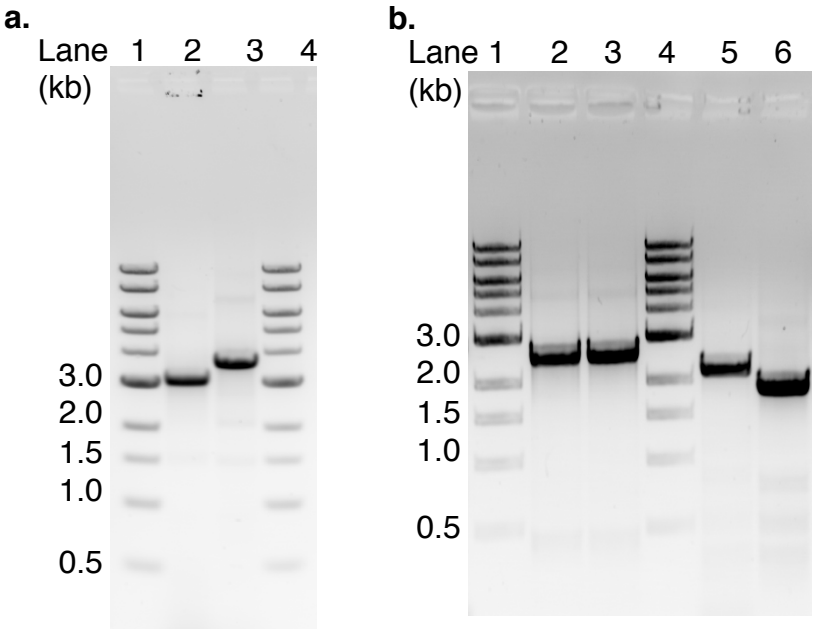

Supplementary Figure 15. PCR verification of gene disruption mutants of *S. cacaoi* and *S. tendae*. **a.** PCR verification of *polQ2* in-frame deletion, Lanes 1 and 4: NEB 1 kb DNA marker, Lanes 2 and 3: PCR products from *S. cacaoi* Δ*polQ2* (3,018 bp) and wt (3,585 bp), respectively. **b.** PCR verification of *nikK* and *nikL* disruption, Lanes 1 and 4: NEB 1 kb DNA marker, Lanes 2 and 3: PCR products from *S. tendae* Δ*nikK*::Kan^R (2,378 bp) and wt (2,452 bp), respectively, Lanes 5 and 6: PCR products from *S. tendae* Δ*nikL*::Kan^R (2,158 bp) and wt (1,833 bp). The identity of the PCR products was confirmed by DNA sequencing. Identical results were obtained for all the clones (2-3) isolated for each mutant strains.

a. Nikkomycin gene inactivation-PCR design using overlapping PCR

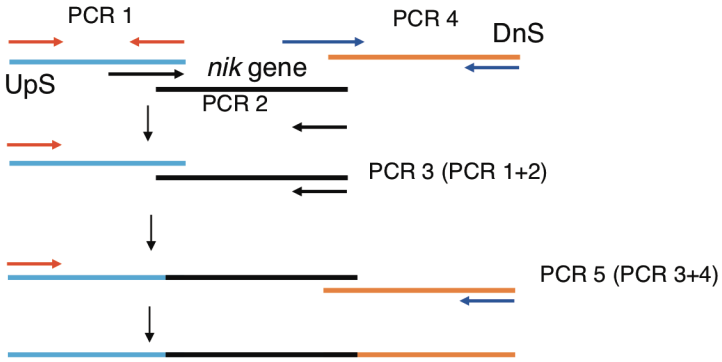

Genes	Primers				
	PCR 1	PCR 2	PCR 3 (PCR 1+2)	PCR 4	PCR 5 (PCR 3+4)
NikK	HSU-Nik11 HSU-Nik12	HSU-Nik13 KanR	HSU-Nik11 KanR	HSU-Nik14 HSU-Nik15	HSU-Nik11 HSU-Nik15
NikL	HSU-Nik16 HSU-Nik17	HSU-Nik18 KanR	HSU-Nik16 KanR	HSU-Nik19 HSU-Nik20	HSU-Nik16 HSU-Nik20

b. Insertion inactivation of *nik* genes

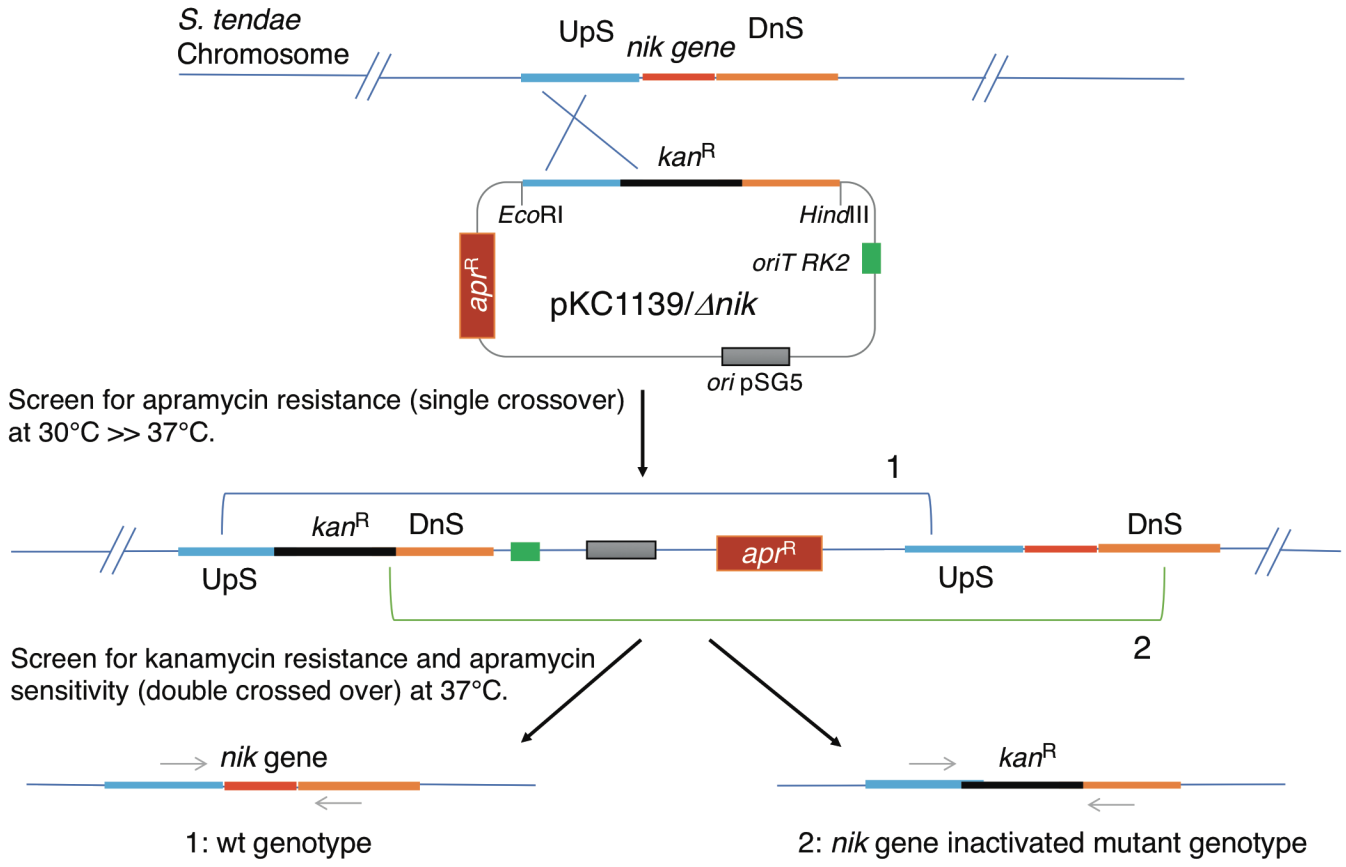

Supplementary Figure 16. Schematic representation of *nik* gene disruption.
a. Overlapping PCR design for kanamycin resistance gene insertion inactivation of *nik* genes. The primers used to amplify each PCR product from *S. tendae* genomic DNA are described in the table. **b**. Schematic representation of disruption of *nik* genes. UpS (upstream) and DnS (downstream) represent target's 5' flanking region and target's 3' flanking region, respectively. The scale bar is not shown as the lengths of the DNA

fragments are different depending on the target *nik* gene. Grey arrows indicate verification primers used to distinguish and confirm the wt and *nik* gene inactivated mutant genotypes.

SUPPLEMENTARY NOTE
for

Cryptic phosphorylation in nucleoside natural product biosynthesis

Preparation of 2',5'-octosyl acid bisphosphate (OABP, 8)

For isolation of OABP (**8**), an MBP-PolQ2 reaction (100 mL) was performed with 5'-OAP as a substrate under the conditions described in the Methods section. The reaction was incubated at 25 °C overnight, boil quenched for 10 min at 95 °C, and clarified by centrifugation at 11,000 x g for 10 min. The supernatant was loaded onto a QAE Sephadex A25 column (70 mL; bicarbonate form; GE Healthcare Life Sciences) pre-equilibrated in 100 mM NH_4HCO_3 pH 7.6. The column was washed with 10 CV of 100 mM NH_4HCO_3 pH 7.6, and the elution was conducted in a gradient from 200-500 mM NH_4HCO_3 pH 7.6 over 10 CV. Fractions containing OABP (**8**) were identified by HPAEC and were collected for lyophilization. OABP (**8**) was lyophilized three times prior to structural characterization. ^{1}H NMR (700 MHz, D_2O): δ 1.91 (t; 14.0 Hz; 1H); 2.46 (dt; 14.0 Hz, 2.1 Hz; 1H); 4.08 (dt; 10.5 Hz, 2.1 Hz; 1H); 4.14 (dd; 10.4 Hz, 4.9 Hz; 1H); 4.63 (dd; 12.4 Hz, 2.8 Hz; 1H); 4.82 (dd; 7.1 Hz, 4.9 Hz; 1H), 4.99 (br; 1H), 5.85 (d; 8.4 Hz; 1H); 5.93 (s; 1H), 7.91 (d; 8.4 Hz; 1H). ^{13}C NMR (125 MHz, D_2O): δ 36.59, 70.34, 71.86, 76.84, 78.64, 79.75, 95.38, 105.47, 146.04, 154.60, 162.36, 175.62. 31P NMR (200 MHz, D_2O): δ 1.35 (s); 1.75 (br). LC-HRMS (ESI-TOF) *m/z* $[M-H]^-$ calculated for $C_{12}H_{16}N_2O_{14}P_2$ 473.000; found 472.999.

Summary of NMR data for OABP (8).

No.	^{1}H δ (ppm) (multiplicity; J_{H-H} (Hz))	^{13}C δ (ppm)	COSY
2	-	154.60	-
4	-	162.36	-
5	5.85 (d; 8.4)	105.47	H-6
6	7.91 (d; 8.4)	146.07	H-5
1'	5.93 (s)	95.38	-
2'	4.82 (dd; 7.1, 4.9)	78.64	H-3'
3'	4.14 (dd; 10.4, 4.9)	71.86	H-2', H-4'
4'	4.08 (dt; 10.5, 2.1)	79.75	H-3', H-5'
5'	4.99 (br)	70.34	H-6'$_a$, H-6'$_b$
6' a	2.46 (dt; 14.0, 2.1)	36.59	H-6'$_b$, H-7'
6' b	1.91 (t; 14.0)		H-6'$_a$, H-7'
7'	4.63 (dd; 12.4, 2.8)	76.84	H-6'$_a$, H-6'$_b$
8'	-	175.62	-

Chemical shifts were referenced to sodium 3-(trimethylsilyl)-2,2,3,3-d4-proponate.

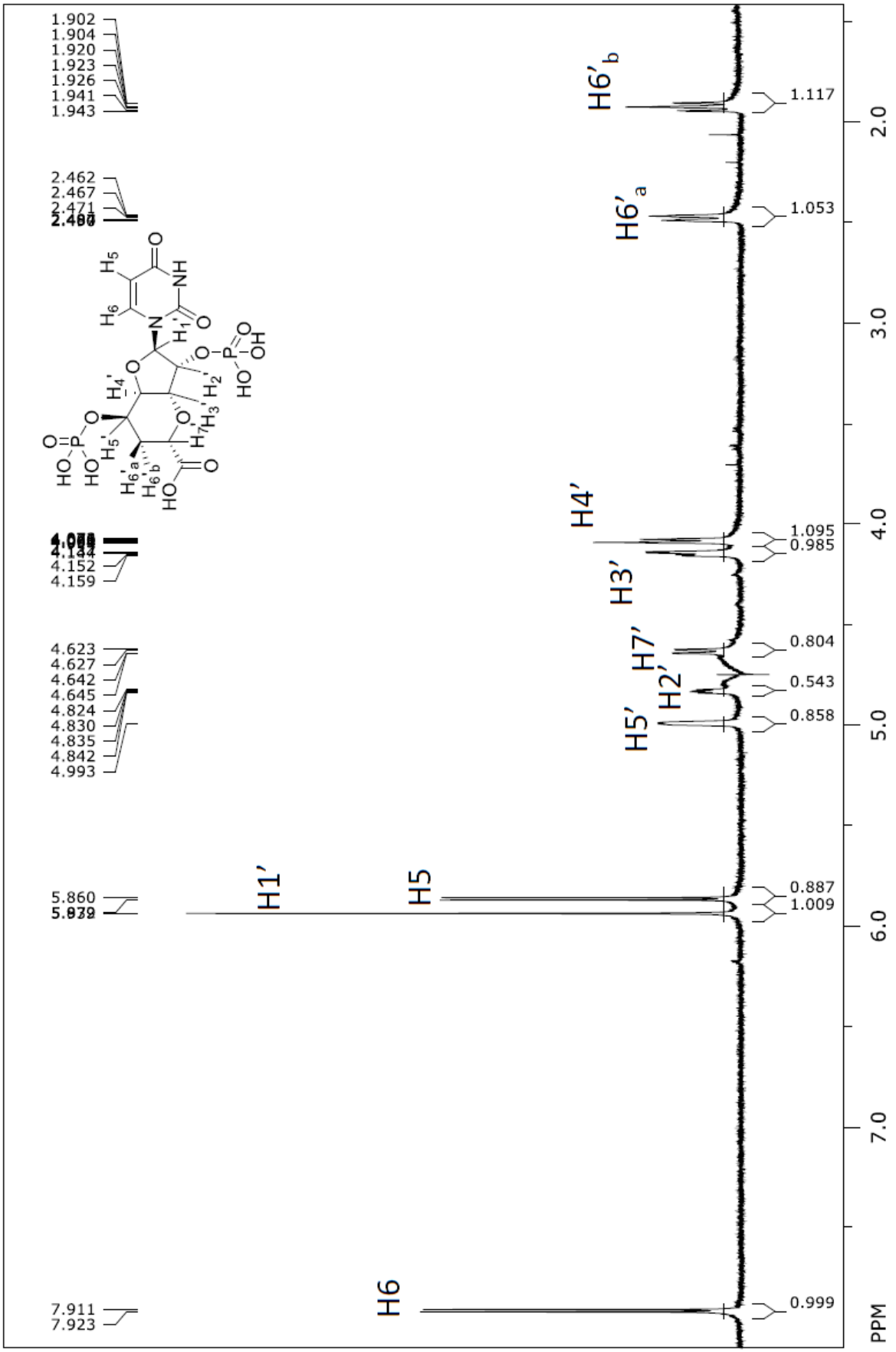

^{1}H NMR spectrum of OABP (8) at 700 MHz in D_2O.

The chemical shifts were referenced to sodium 3-(trimethylsilyl)-2,2,3,3-d4-proponate.

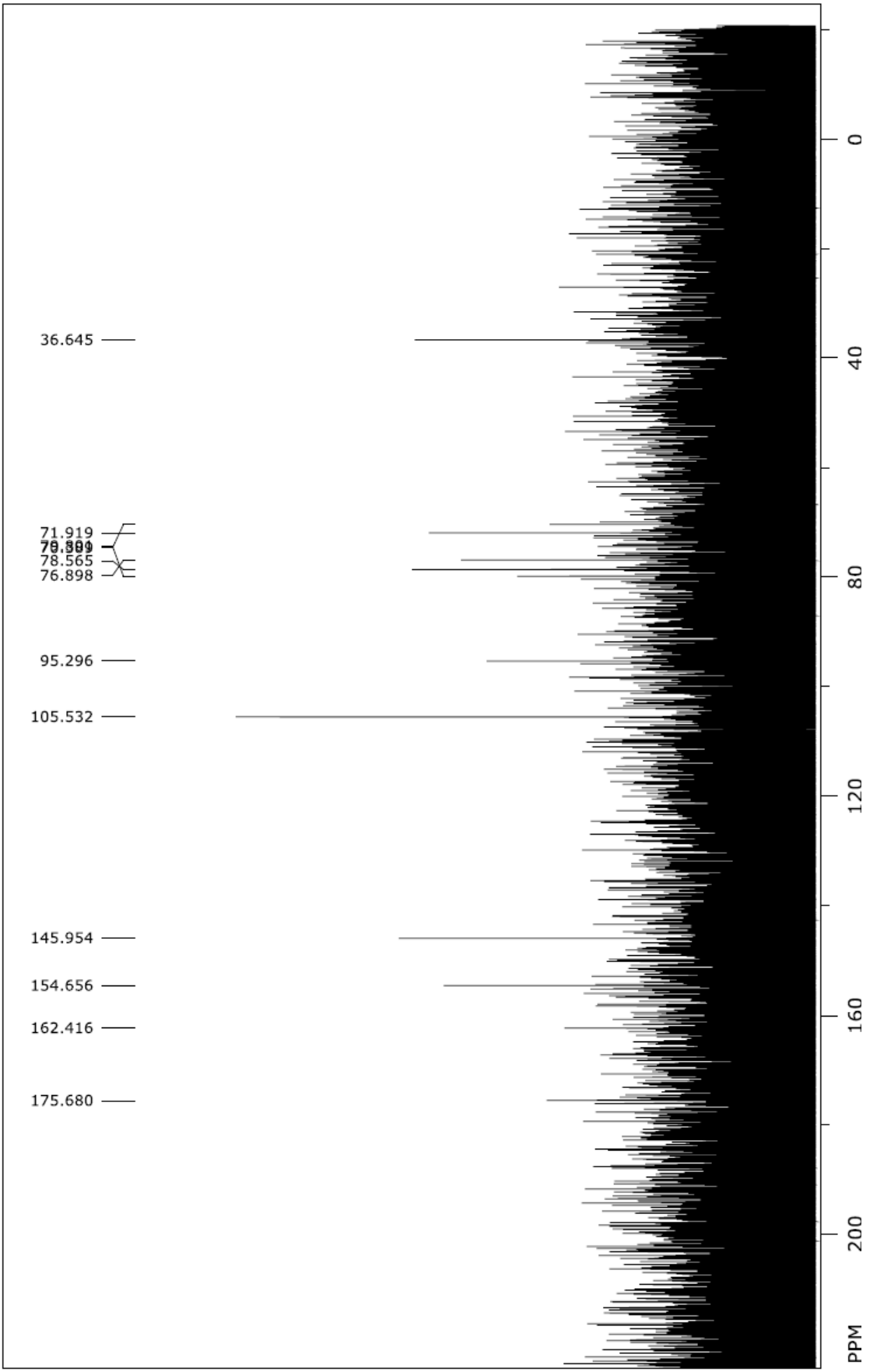

^{13}C NMR spectrum of OABP (8) at 201.5 MHz in D_2O.

The chemical shifts were referenced to sodium 3-(trimethylsilyl)-2,2,3,3-d4-proponate.

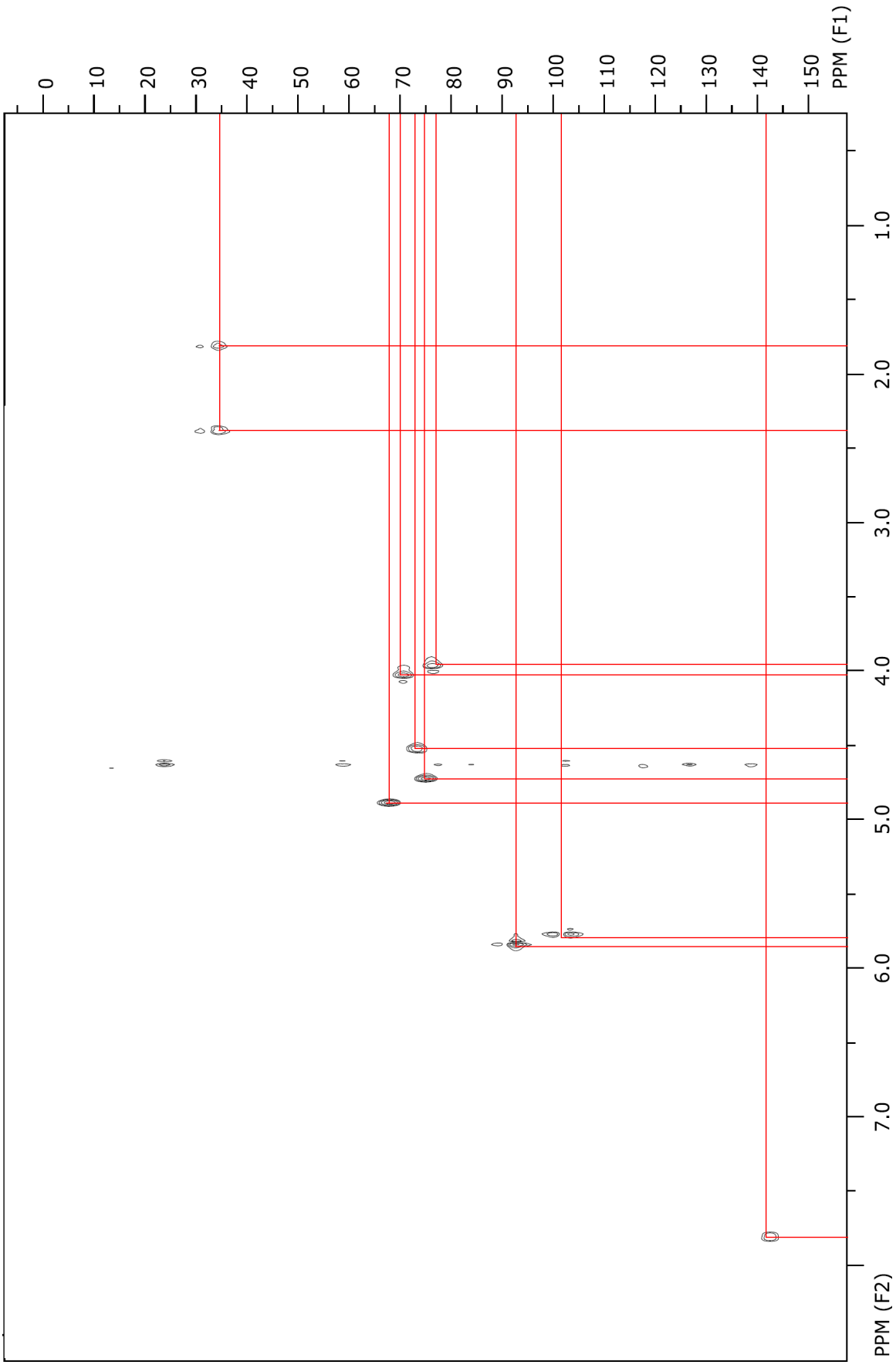

^{1}H-^{13}C HMQC spectrum of OABP (8) at 700 MHz in D_2O.

The chemical shifts were referenced to sodium 3-(trimethylsilyl)-2,2,3,3-d4-proponate.

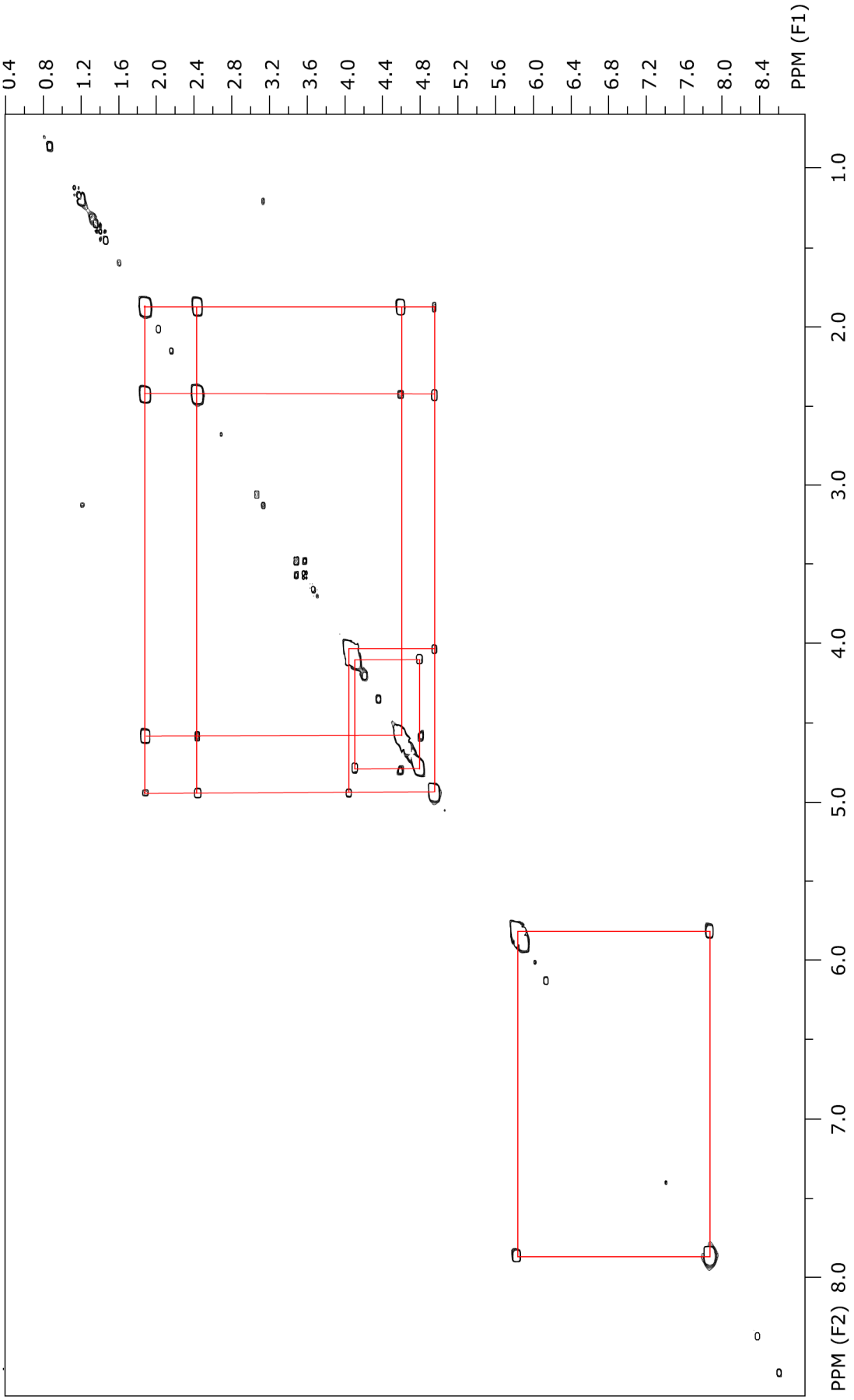

^{1}H-^{1}H COSY spectrum of OABP (8) at 700 MHz in D_2O.

The chemical shifts were referenced to sodium 3-(trimethylsilyl)-2,2,3,3-d4-proponate.

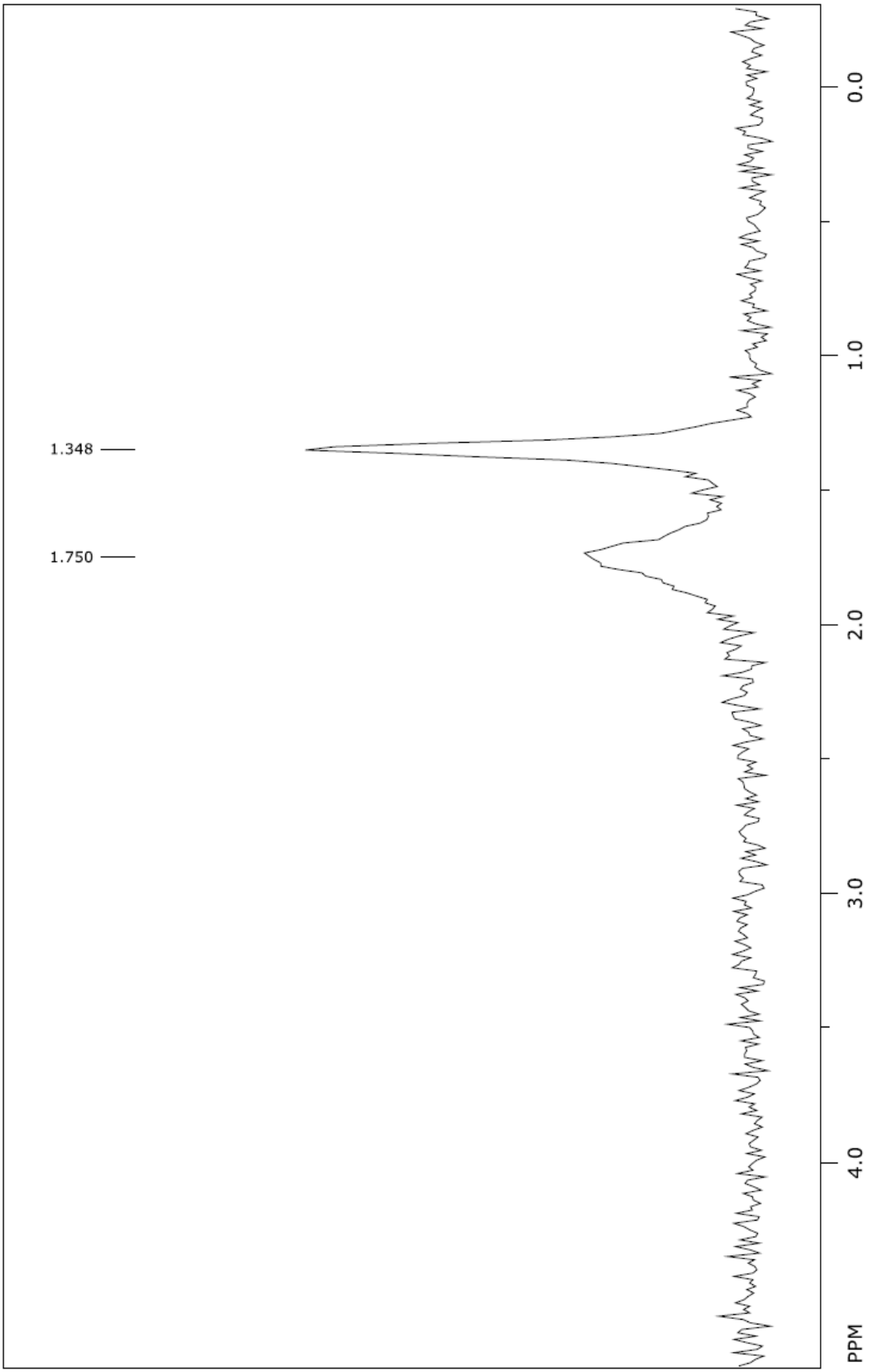

^{31}P NMR spectrum of OABP (8) at 201.6 MHz in D_2O.

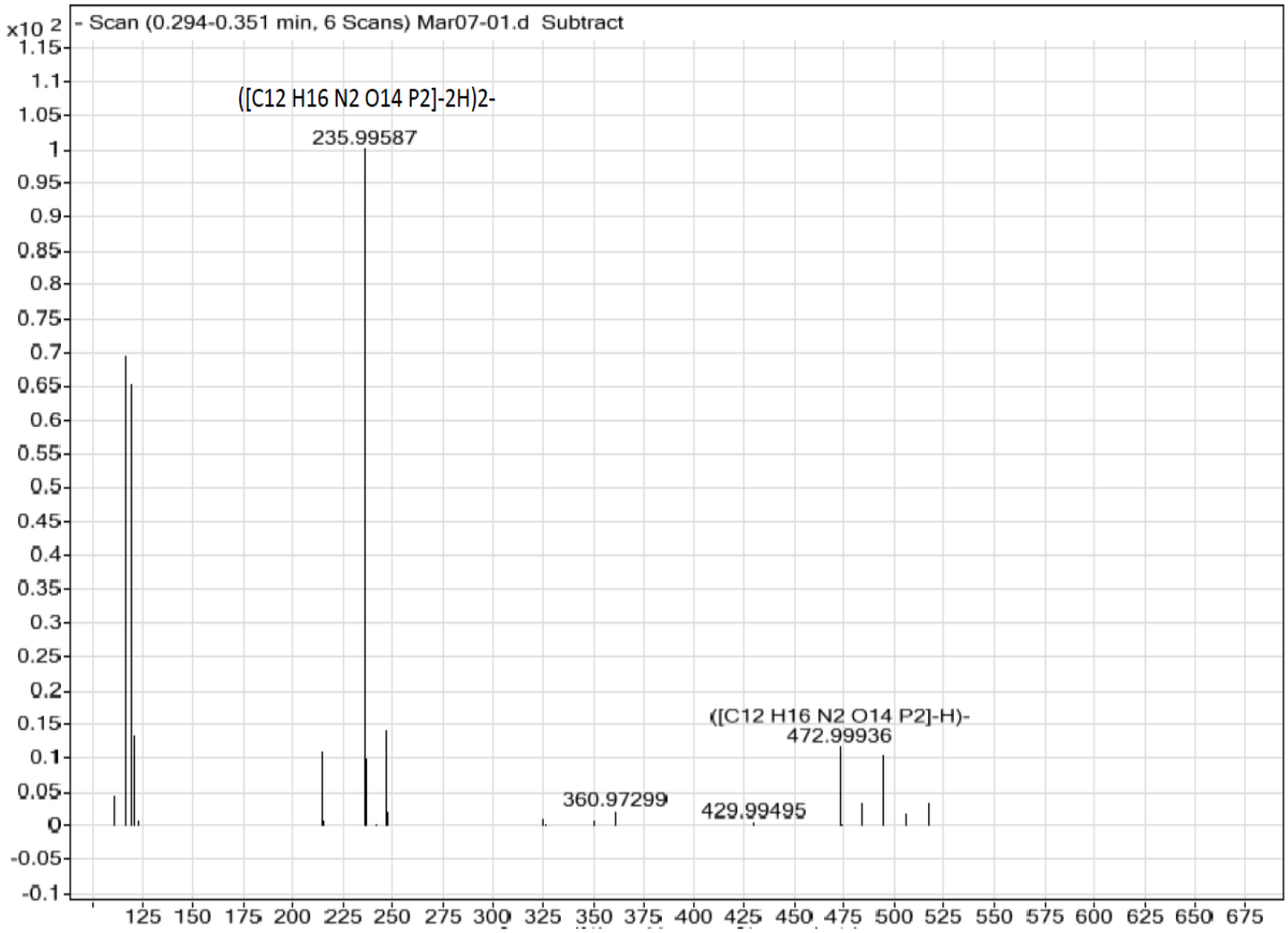

HRMS of OABP (8).

m/z $[M-H]^-$ calculated for $C_{12}H_{16}N_2O_{14}P_2$ 473.000; found 472.999.

Preparation of octosyl acid 2' phosphate (2'-OAP, 12)

To isolate 2'-OAP (**12**), PolJ reaction (8 x 15 mL) was performed with OABP as a substrate under the condition described in the Methods section. After overnight incubation at 25 °C, the reaction was boil-quenched for 10 min at 95 °C and clarified by centrifugation at 11,000 x g for 10 min. The supernatant was loaded onto a QAE Sephadex A25 column (8 mL; bicarbonate form) pre-equilibrated in dH_2O. Then, the column was washed with 10 CV of 150 mM NH_4HCO_3 pH 7.6, and elution was performed by a linear gradient 150 - 500 mM NH_4HCO_3 pH 7.6 over 10 CV. 2'-OAP was eluted after approximately four CV. Fractions containing 2'-OAP were identified by HPAEC, combined and lyophilized three times prior to structural characterization. ^{1}H NMR (800 MHz, D_2O): δ 1.88 (t; 13 Hz; 1H); 2.22 (d, 15.0 Hz; 1H); 3.99 (d; 10.5 Hz); 4.24 (br; 1H); 4.41 (d; 12.0; 1H); 4.59 (s; 1H); 4.89 (br t; 6.0; 1H); 5.89 (d; 8.0; 1H); 5.94 (s; 1H); 7.75 (d; 8.0; 1H). ^{13}C NMR (201.5 MHz, D_2O): δ 37.10, 66.53, 73.01, 75.83, 77.32, 79.32, 96.69, 104.57, 146.82, 153.62, 162.82, 169.06. ^{31}P NMR (200 MHz, D_2O): δ 3.01 (s). LC-HRMS (ESI-TOF) *m/z* $[M-H]^-$ calculated for $C_{12}H_{14}N_2O_{11}P$ 393.034; found 393.034.

Summary of NMR data for 2'-OAP (12).

No.	^{1}H δ (ppm) (multiplicity; J_{H-H} (Hz))	^{13}C δ (ppm)	^{31}P δ (ppm)	COSY
2	-	147.85	-	-
4	-	154.65	-	-
5	5.89 (d, 8.0)	105.32	-	H-6
6	7.75 (d, 8.0)	147.29	-	H-5
1'	5.94 (s)	96.59	-	-
2'	4.89 (br t, 6.0)	77.16	3.01	H-3'
3'	4.24 (br)	73.73	-	H-2', H-4'
4'	3.99 (d, 10.5)	80.35	-	H-3', H-5'
5'	4.59 (s)	67.08	-	H-4', H-6'$_a$
6' a	2.22 (d, 15.0)	37.73	-	H-5', H-6'$_b$
6' b	1.88 (t, 13.5)		-	H-5', H-6'$_a$
7'	4.41 (d, 12.0)	78.35	-	H-6'$_b$
8'	-	170.09	-	-

^{1}H and ^{13}C chemical shifts were referenced to sodium 3-(trimethylsilyl)-2,2,3,3-d4-proponate. ^{31}P chemical shifts were referenced to orthophosphoric acid

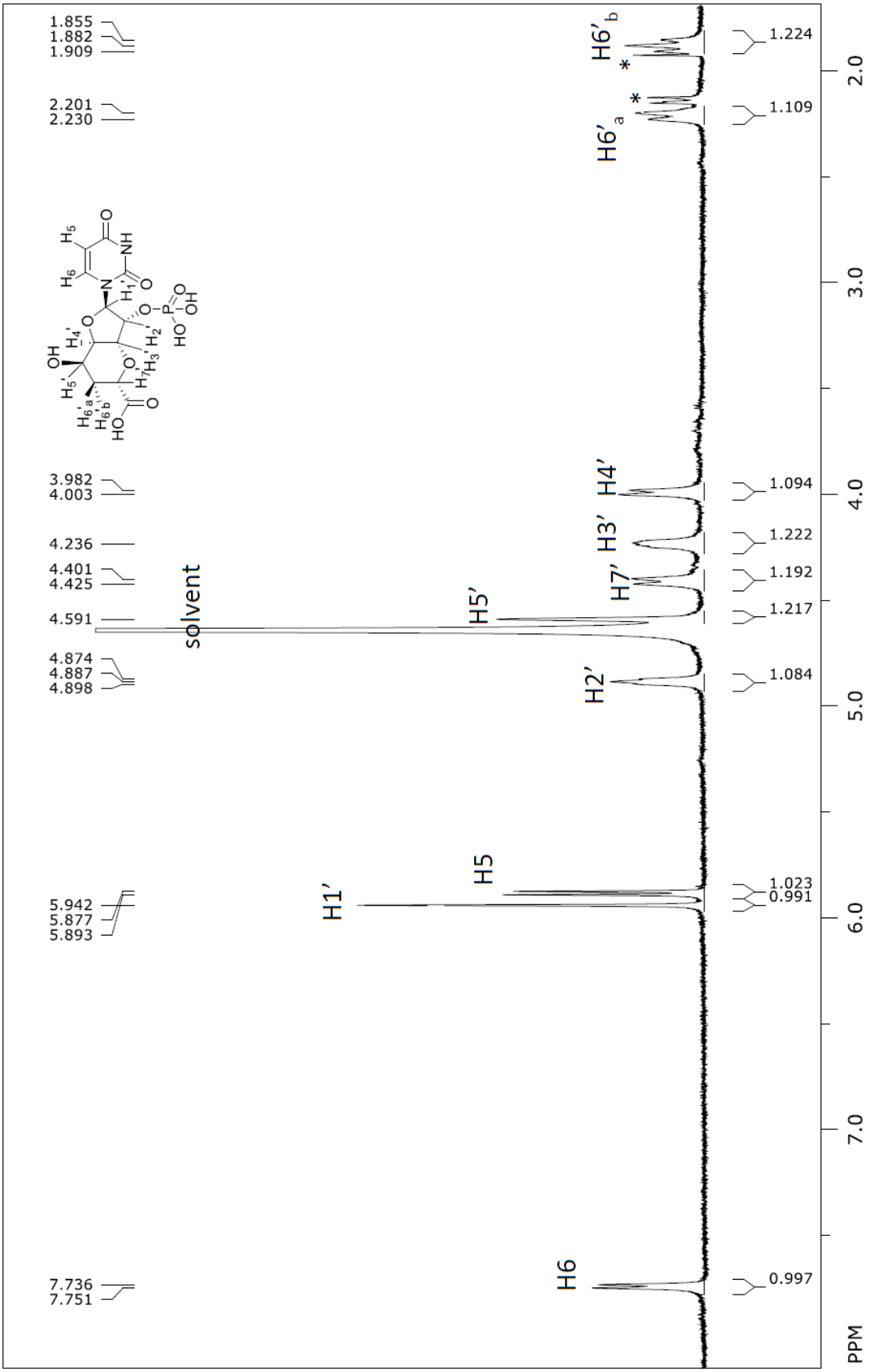

^{1}H NMR spectrum of 2'-OAP (12) at 700 MHz in D_2O.

The spectrum was determined at 40 °C. Asterisks are unknown impurities. Chemical shifts were referenced to sodium 3-(trimethylsilyl)-2,2,3,3-d4-proponate. 2'-OAP was isolated from PolJ enzyme assay.

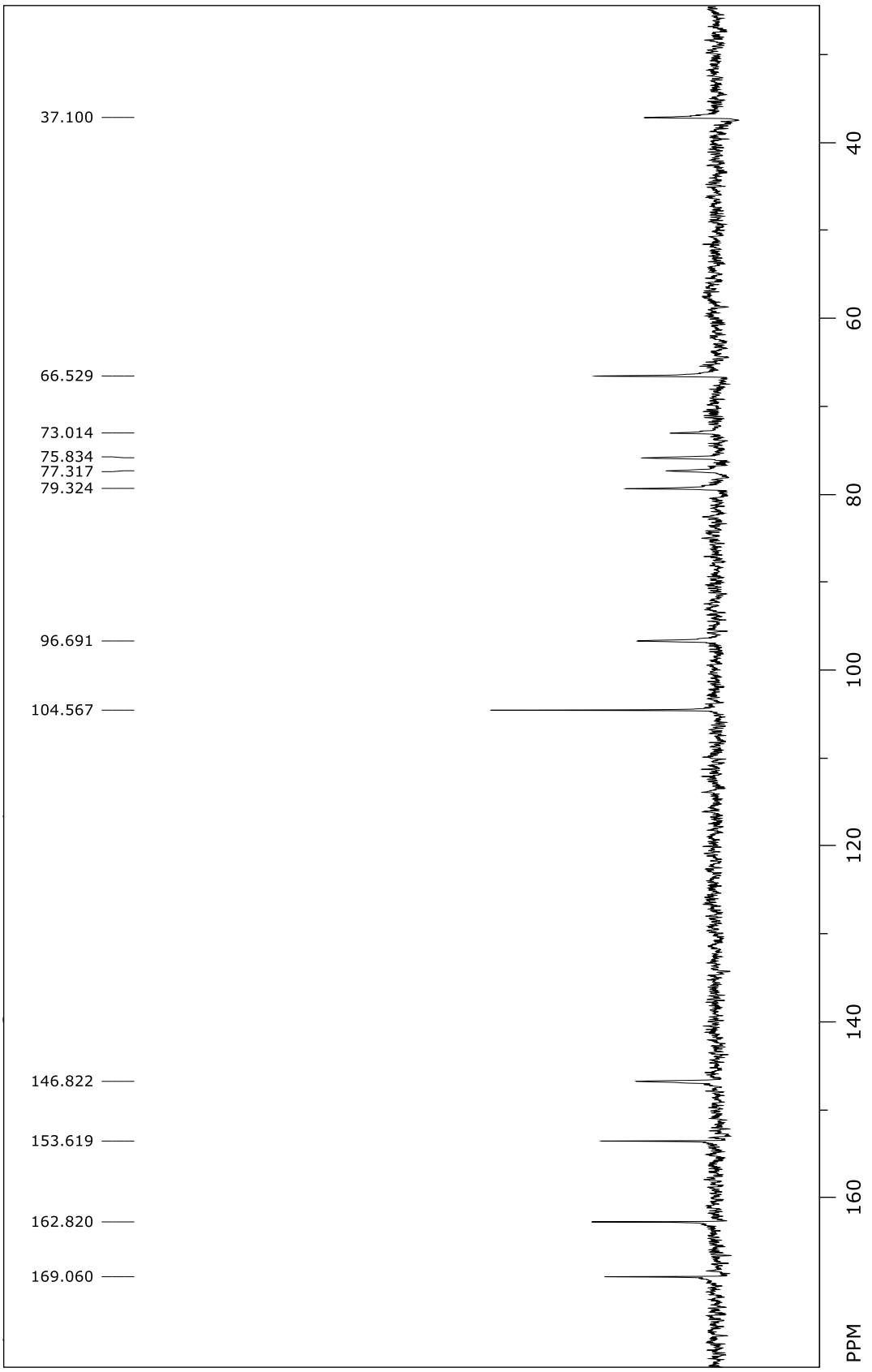

^{13}C NMR spectrum of 2'-OAP (12) at 201.5 MHz in D_2O.
The spectrum was determined at 25 °C.

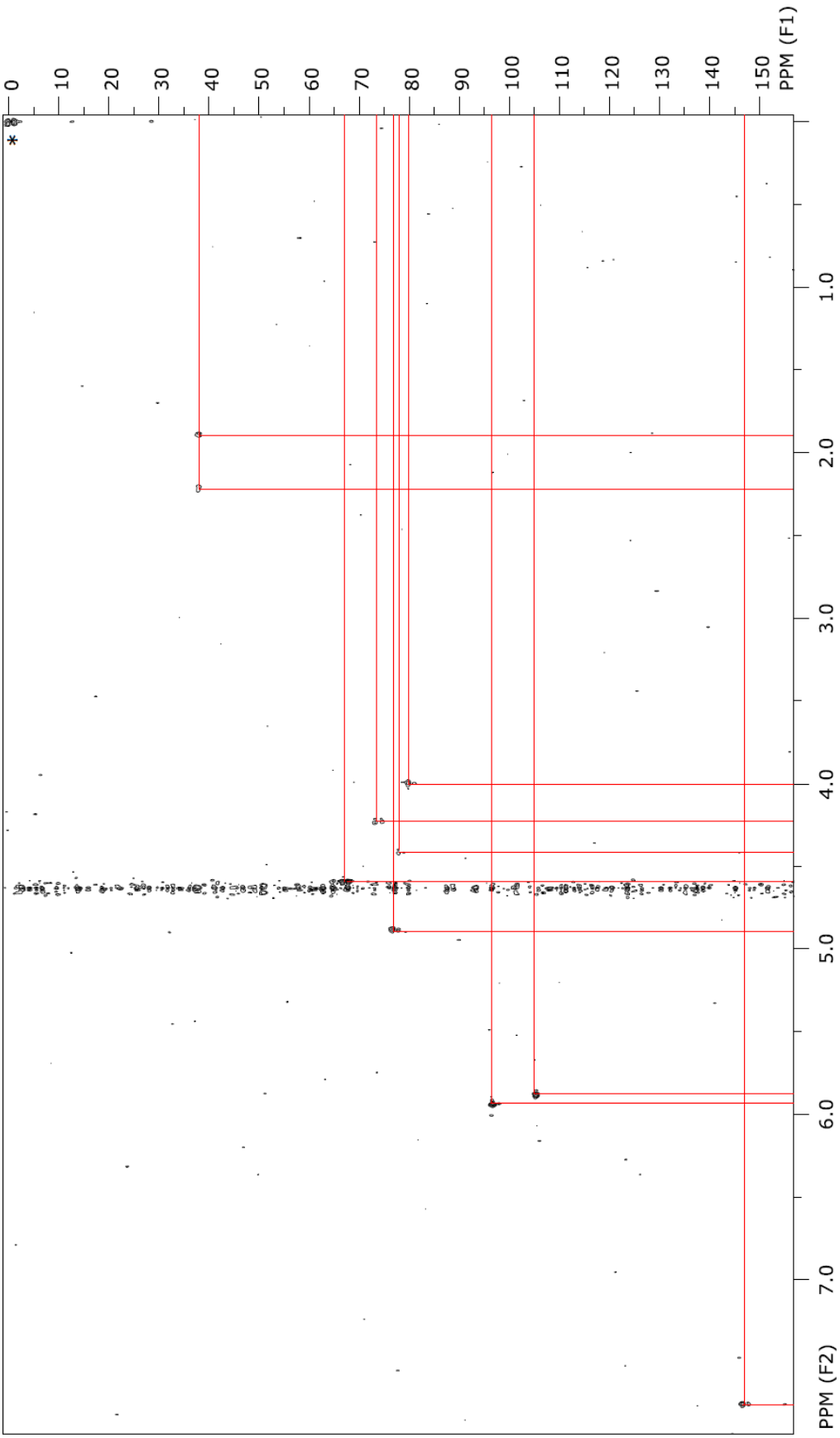

^{1}H-^{13}C HMQC spectrum of 2'-OAP (12) at 800 MHz in D_2O.

The spectrum was collected at 40 °C. The chemical shifts were referenced to sodium 3-(trimethylsilyl)-2,2,3,3-d4-proponate.

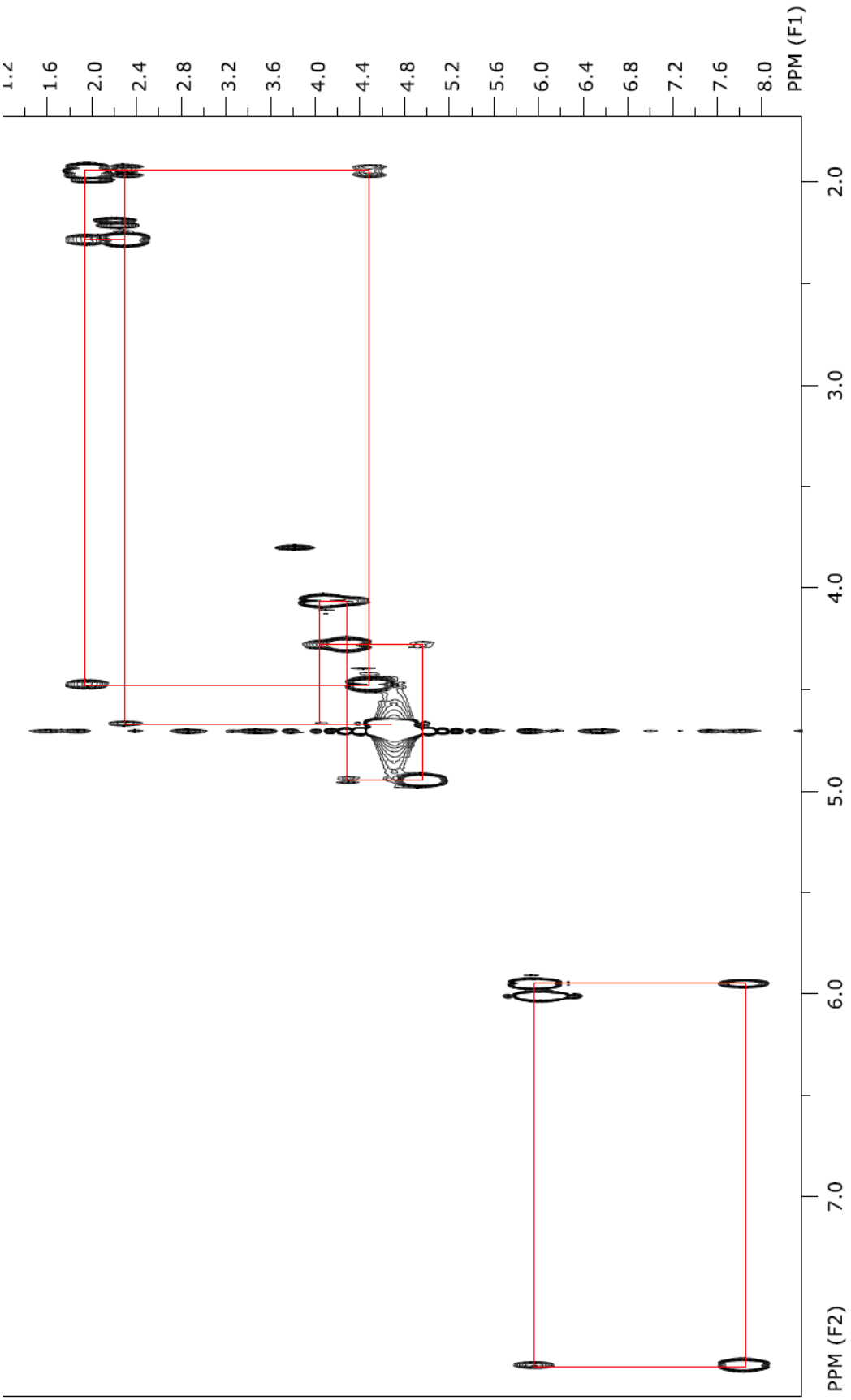

^{1}H-^{1}H COSY spectrum of 2'-OAP (12) at 700 MHz in D_2O.

The spectrum was determined at 40 °C. The chemical shifts were referenced to sodium 3-(trimethylsilyl)-2,2,3,3-d4-proponate.

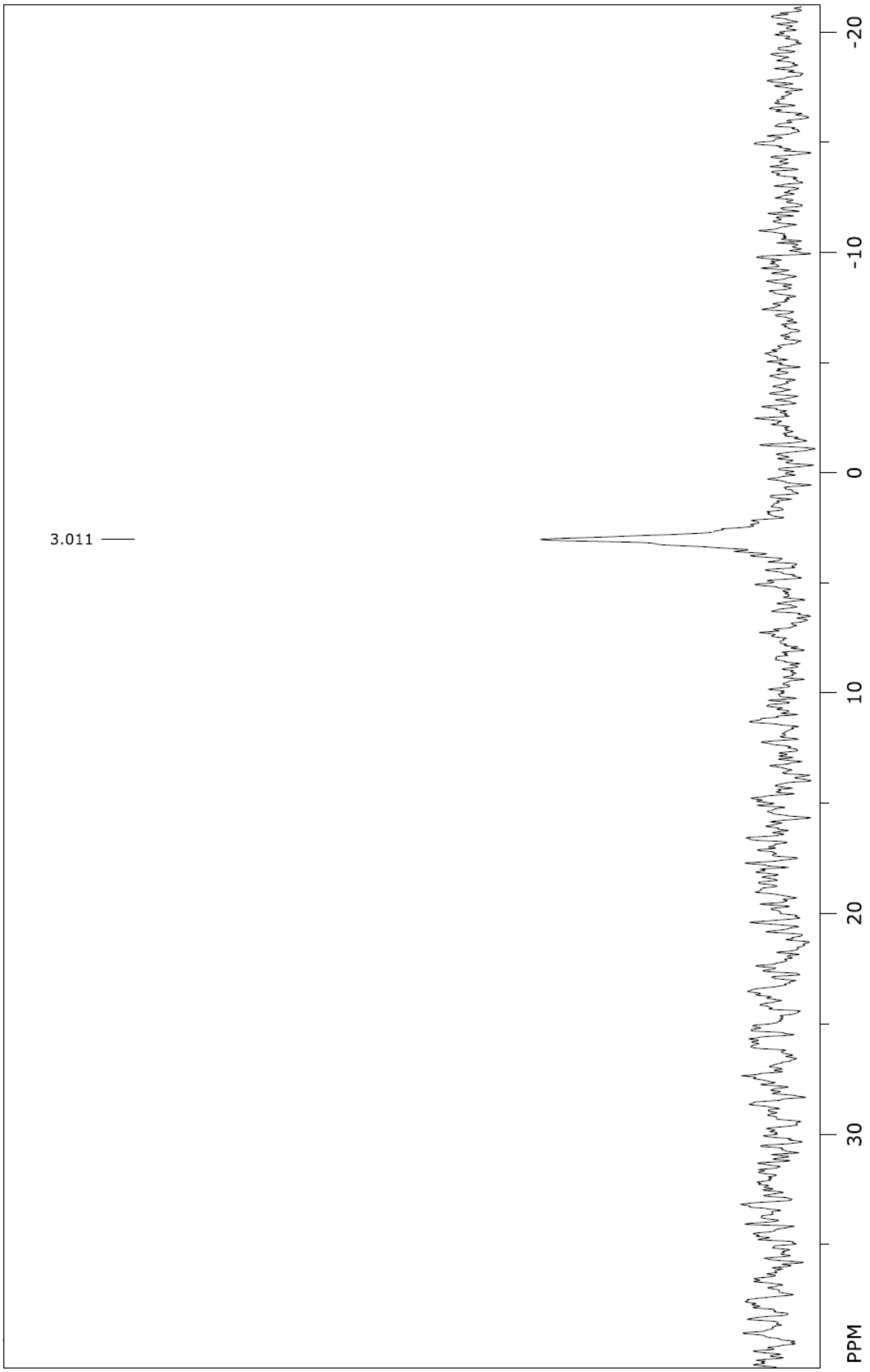

^{31}P NMR spectrum of 2'-OAP (12) at 201.6 MHz in D_2O.

The spectrum was determined at 40 °C. The chemical shifts were referenced to orthophosphoric acid.

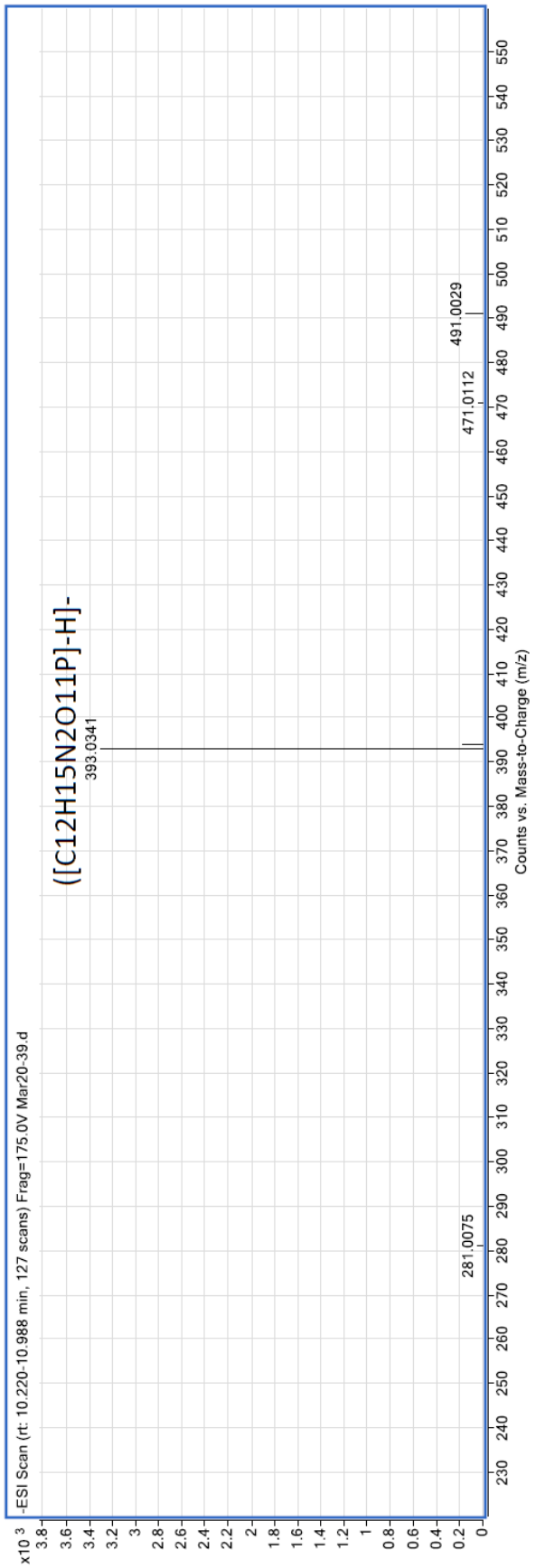

HRMS (ESI-TOF) of 2'-OAP (12).

m/z $[M-H]^-$ calculated for $C_{12}H_{14}N_2O_{11}P$ 393.034; found 393.034. Isolated from in vitro PolJ assay.

Preparation of heptosyl acid 2'-phosphate (2'-HAP, 13)

To isolate 2'-HAP, His-PolD (5 μM) was incubated with 300 mM of 2'-OAP, 500 μM $(NH_4)_2Fe(SO_4)_2 \cdot 6H_2O$, 1 mM ascorbate, and 1 mM α-KG in oxygen saturated Buffer A (50 mM Tris pH 7.6, 150 mM NaCl, 10% glycerol) at 25 °C . After 48 h incubation, the reaction was boil-quenched for 10 min at 95 °C, and the reaction was clarified by centrifugation at 10,000 x g for 10 min. The supernatant was loaded onto a QAE Sephadex A25 column (20 mL; bicarbonate form; GE Healthcare Life Sciences) in pre-equilibrated in dH_2O. Then, the column was washed with 10 CV of dH_2O, and elution was performed by a linear gradient 100 - 500 mM NH_4HCO_3 pH 7.6 over 10 CV. 2'-HAP was eluted after approximately seven CV. Fractions containing 2'-HAP were identified by HPAEC, combined and lyophilized three times. LC-HRMS (ESI-TOF) *m/z* $[M-H]^-$ calculated for $C_{12}H_{14}N_2O_{11}P$ 381.034; found 381.035.

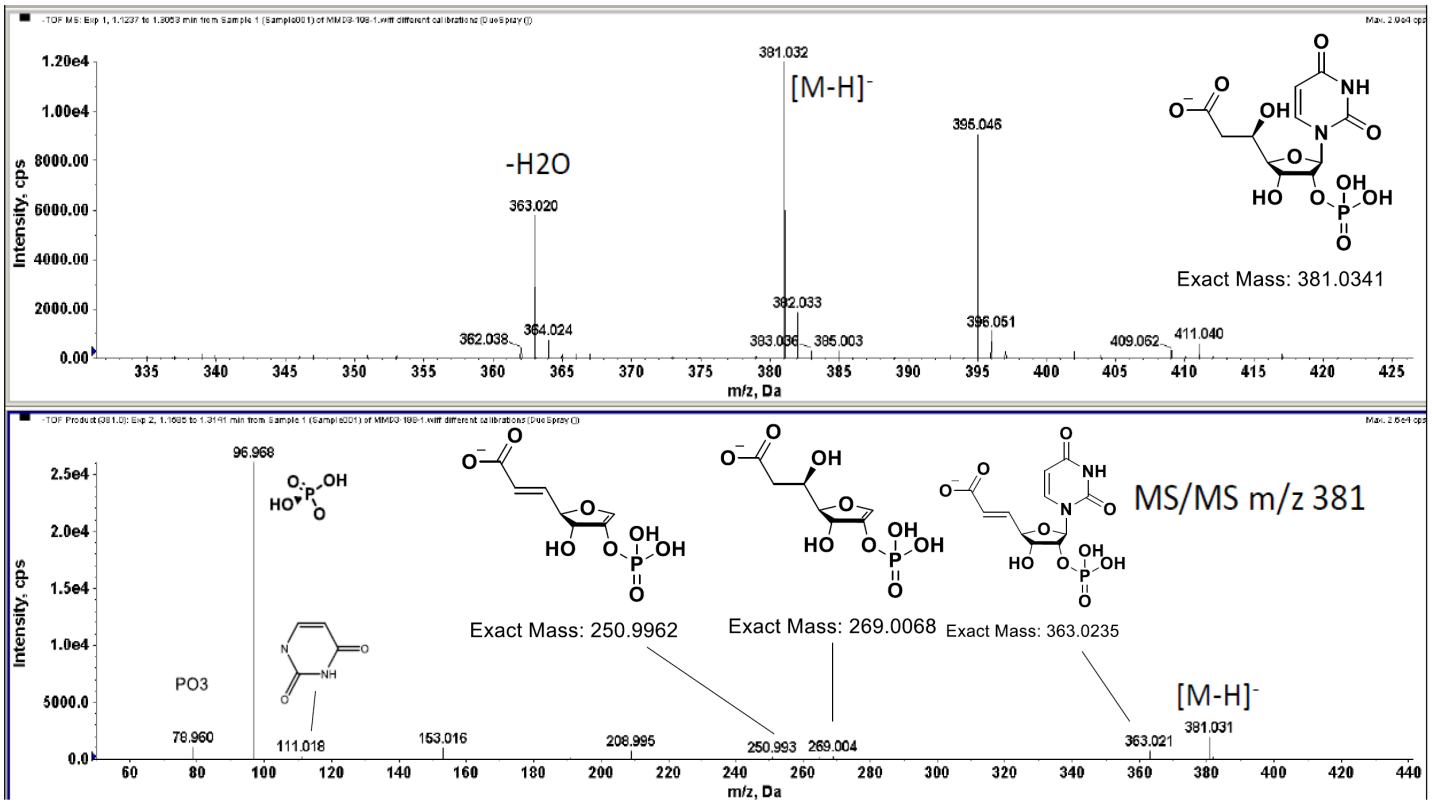

ESI-MS/MS of 2'-HAP (13).

m/z [M-H]$^-$ calculated for $C_{11}H_{15}N_2O_{11}P$ 381.034; found 381.032.

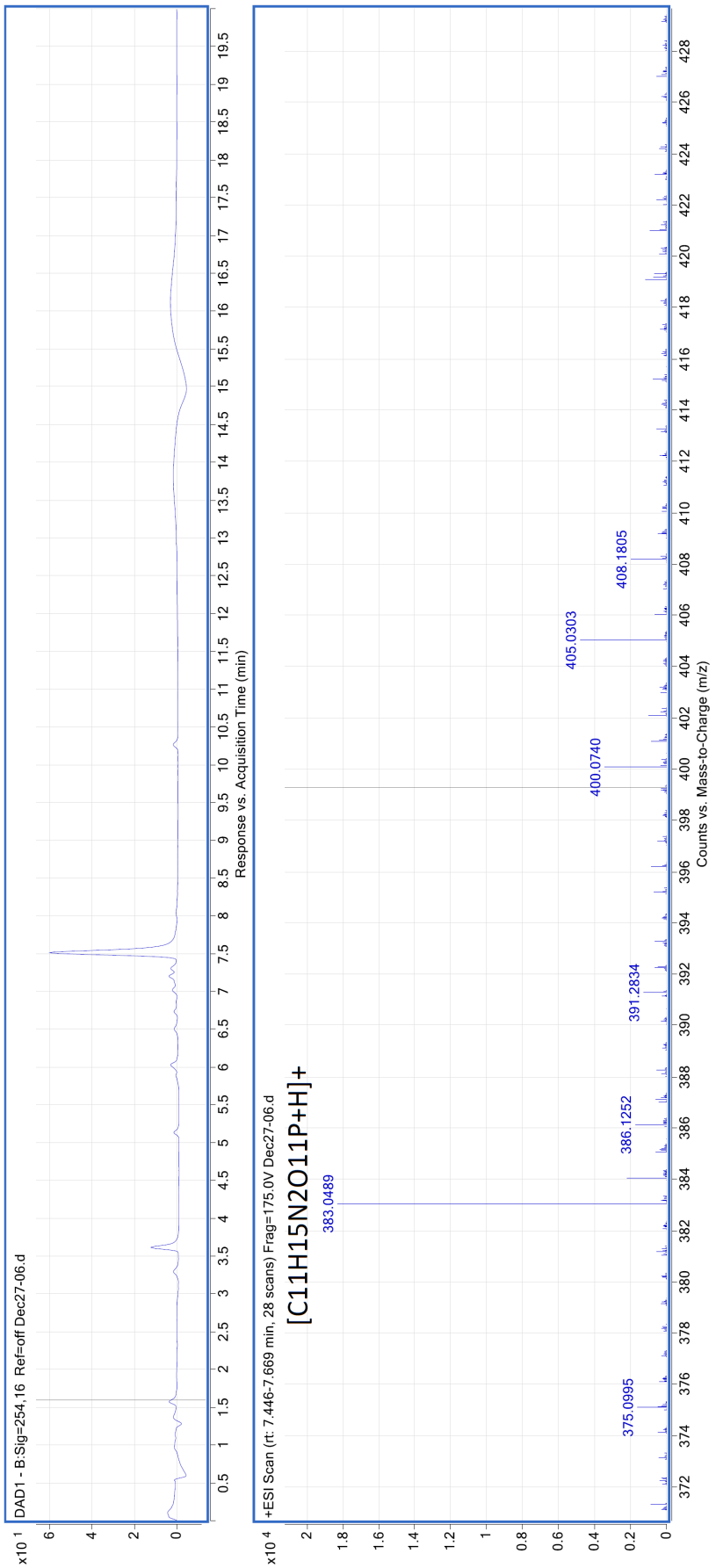

LC-HRMS of 2'-HAP (13).

m/z $[M+H]^+$ calculated for $C_{11}H_{15}N_2O_{11}P$ 383.049; found 383.049.

Preparation of 5'-keto-octosyl acid 2' phosphate (KOAP, 14) and 6'-hydroxyl-5'-keto-octosyl acid 2' phosphate (HKOAP, 15)

A large scale His-PolK reaction (60 mL) was performed as described in the Methods. After 24 h incubation, the reaction was boil-quenched for 5 min at 95 °C and then was filtered through a 0.2 μm membrane. The filtrate was diluted 10x in dH_2O, pH adjusted to 3.0 with formic acid, and loaded onto a DEAE Sephadex A25 column (50 mL; formate form; GE Healthcare Life Sciences). The column was washed with 10 CV of 50 mM ammonium formate pH 3.0, and KOAP and HKOAP were eluted with 200 mM ammonium formate pH 3.0. Fractions containing KOAP and HKOAP were identified by HPAEC, diluted to 50 mM ammonium formate with dH_2O and loaded onto a QAE Sephadex A25 column (70 mL; acetate form). The column was washed with 10 CV of 100 mM ammonium acetate pH 6.0, and then a stepwise elution was performed with 10 CV of 200 mM ammonium acetate pH 6.0 followed by 10 CV of 250 mM ammonium acetate pH 6.0. Fractions containing KOAP or HKOAP were identified by HPAEC, pooled separately and lyophilized twice prior to structural characterization. KOAP: ^{1}H NMR (700 MHz, D_2O): δ 1.91 (t; 12.2 Hz; 1H); 2.08 (dt; 13.5 Hz, 1.6 Hz; 1H); 4.11 (dd; 12.3 Hz; 2.0 Hz; 1H); 4.26 (bt; 1.4 Hz; 1H); 4.38 (dd; 3.7 Hz, 1.4 Hz; 1H); 5.23 (ddd; 9.2 Hz, 7.5 Hz, 3.7 Hz; 1H); 5.84 (d; 8.01 Hz; 1H); 6.01 (d; 7.4 Hz; 1H); 7.65 (d; 8.06 Hz; 1H). ^{13}C NMR (201.5 MHz, D_2O): δ 36.41, 73.80, 75.18, 76.16, 79.50, 91.04, 91.88, 102.72, 144.18, 146.07, 152.12, 166.32, 180.96. (ESI-TOF) *m/z* $[M+H]^+$ calculated for $C_{12}H_{13}N_2O_{11}P$ 393.033; found 393.034. HKOAP: LC-HRMS (ESI-TOF) *m/z* $[M+H+H_2O]^+$ calculated for $C_{12}H_{13}N_2O_{12}P$ 427.039; found 427.038.

Summary of NMR data for KOAP (14, hydrate form).

No.	^{1}H δ (ppm) (multiplicity; J_{H-H} (Hz))	^{13}C δ (ppm)	COSY
2	-	152.12	-
4	-	166.32	-
5	5.87 (d, 8.0)	102.72	H-6
6	7.68 (d, 8.0)	144.18	H-5
1'	5.94 (s)	91.04	H-2'
2'	5.05 (br)	76.16	H-3'
3'	4.36 (br)	75.18	H-2'
4'	4.26 (d, 10.5)	79.5	-
5'	-	91.88	-
6' a	2.06 (d, 13.2)	36.41	H-6'$_{b}$
6' b	1.86 (t, 13.5)		H-6'$_{a}$, H-7'
7'	4.06 (d, 12.4)	73.80	H-6'$_{b}$
8'	-	180.96	-

Chemical shifts were referenced to sodium 3-(trimethylsilyl)-2,2,3,3-d4-proponate.

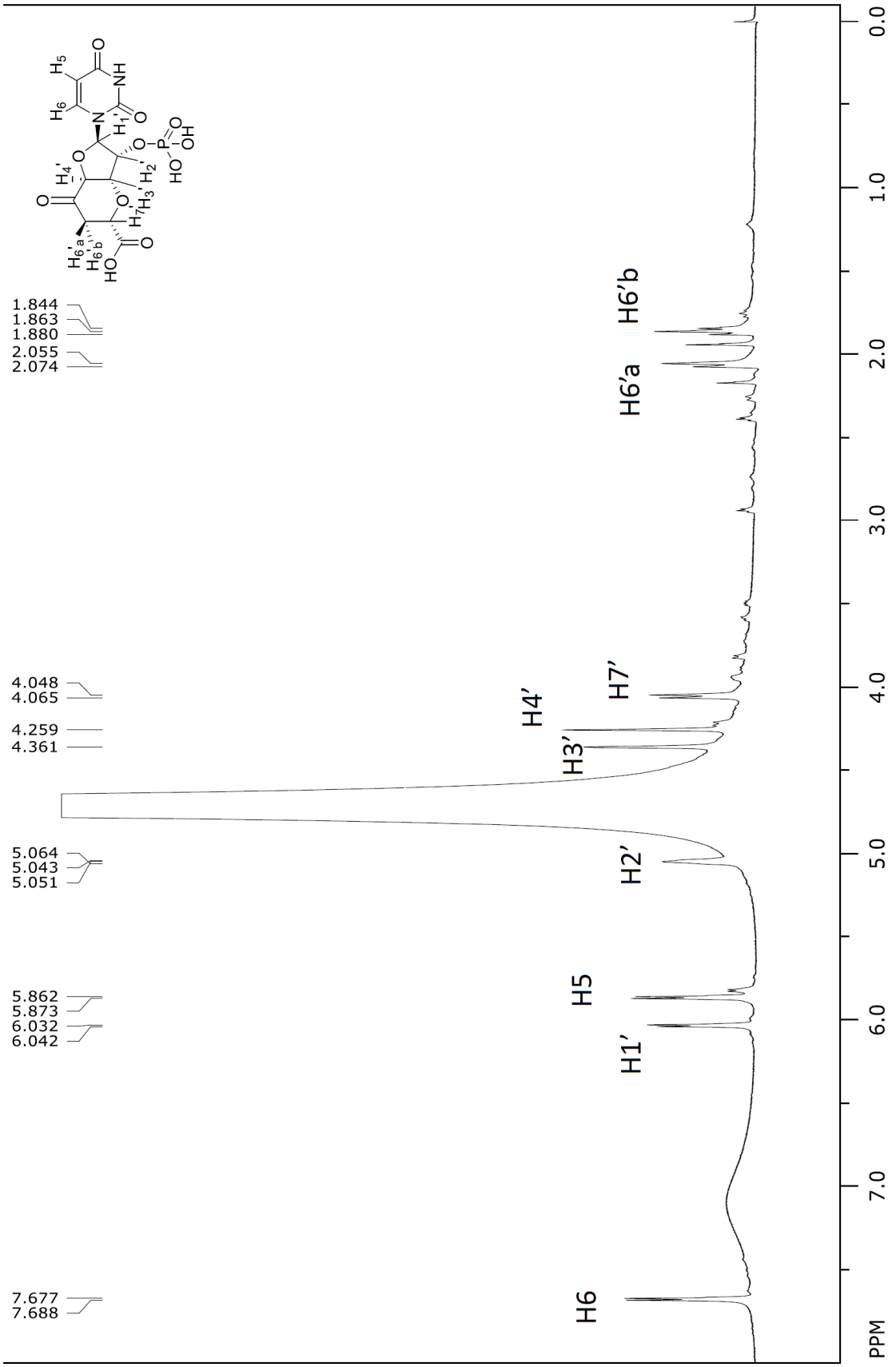

^{1}H NMR spectrum of KOAP (14) at 700 MHz in D_2O.

Isolated from in vitro PolK reaction with 2'-OAP. The chemical shifts were referenced to sodium 3-(trimethylsilyl)-2,2,3,3-d4-proponate.

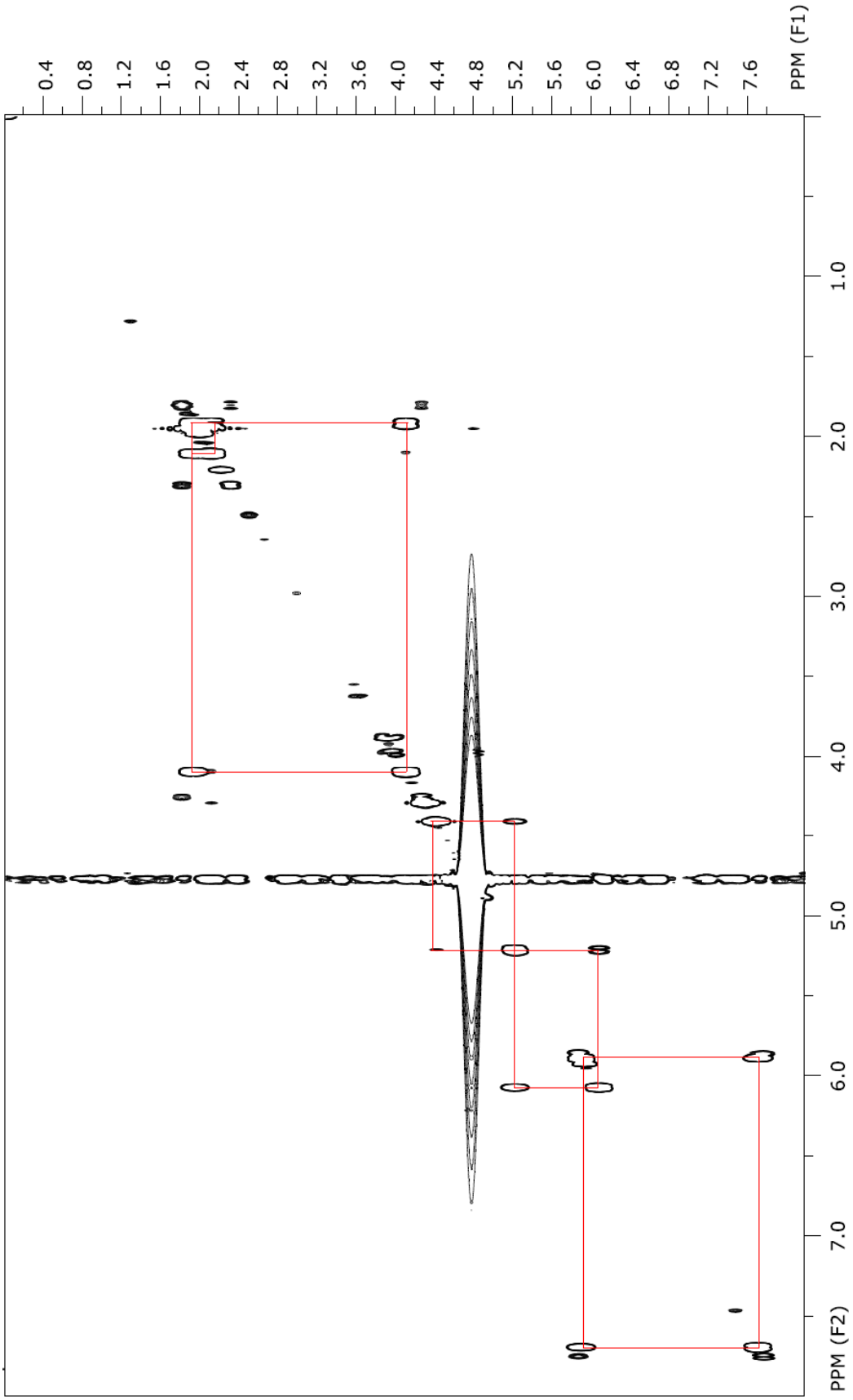

^{1}H-^{1}H COSY spectrum of KOAP (14) at 700 MHz in D_2O.

Isolated from *S. tendae* ΔnikK culture media. The chemical shifts were referenced to sodium 3-(trimethylsilyl)-2,2,3,3-d4-proponate.

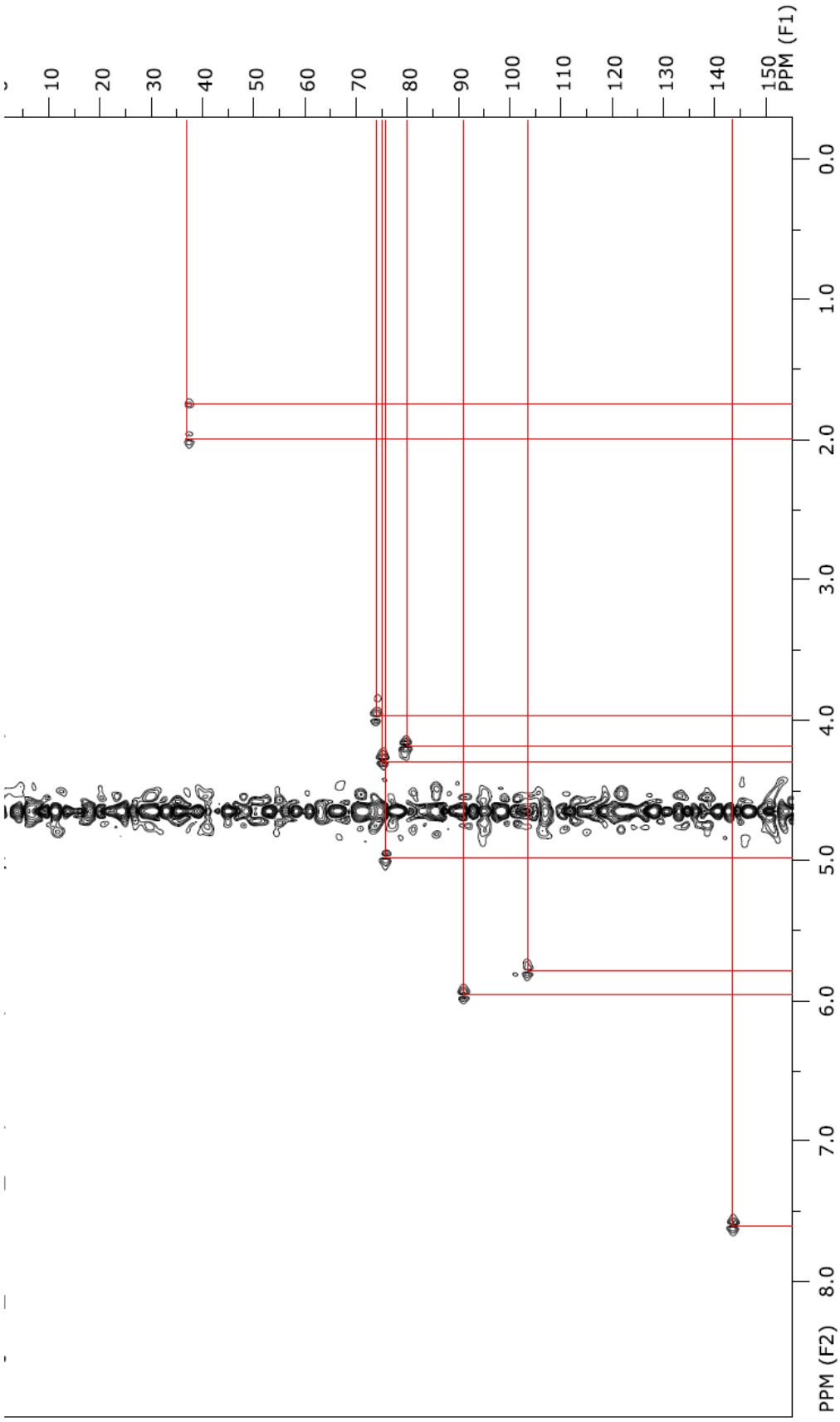

^{1}H-^{13}C HMQC spectrum of KOAP (14) at 700 MHz in D_2O.

Isolated from *S. tendae* ΔnikK culture media. The chemical shifts were referenced to sodium 3-(trimethylsilyl)-2,2,3,3-d4-proponate.

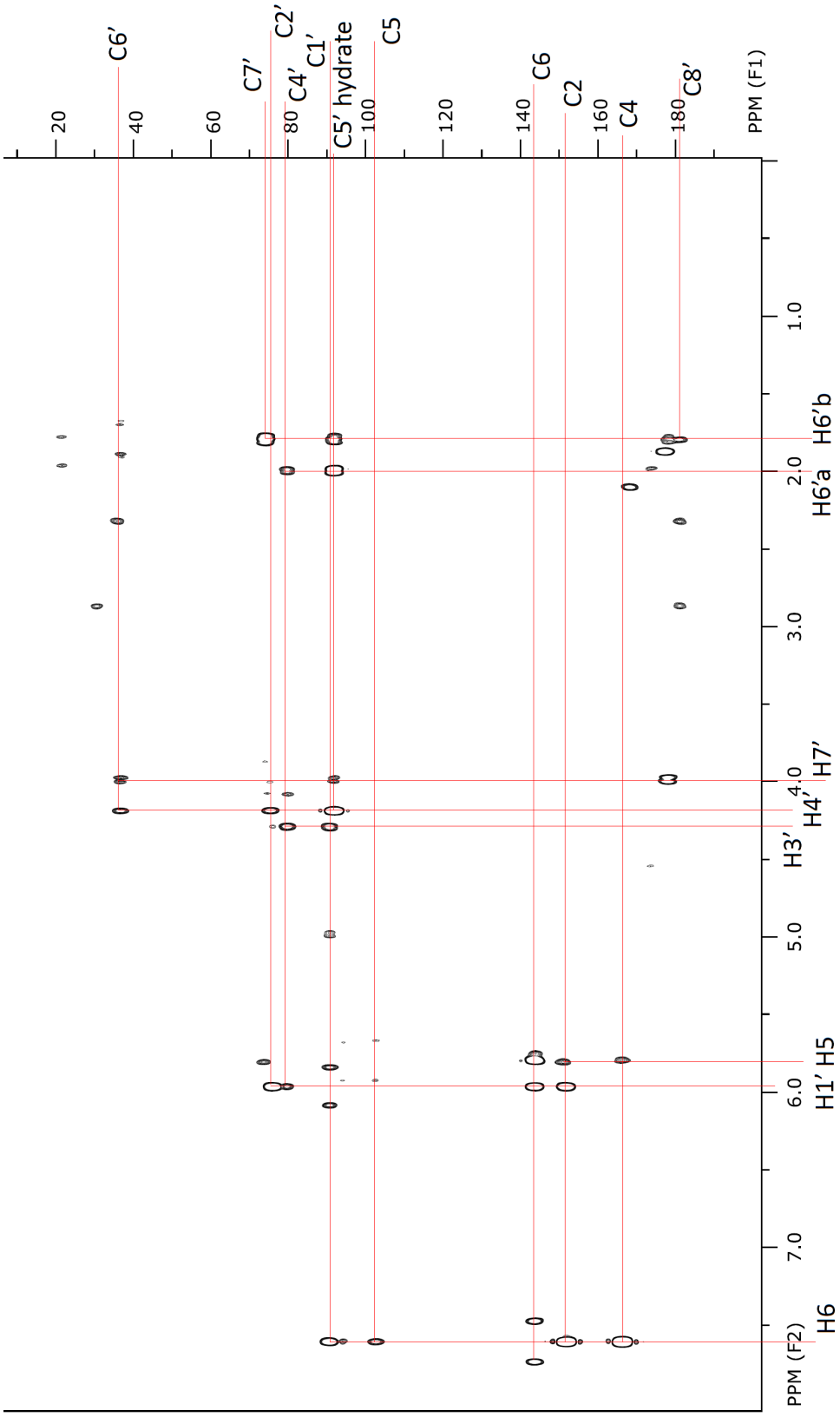

^{1}H-^{13}C HMBC spectrum of KOAP (14) at 700 MHz in D_2O.

Isolated from *S. tendae* ΔnikK culture media. The chemical shifts were referenced to sodium 3-(trimethylsilyl)-2,2,3,3-d4-proponate.

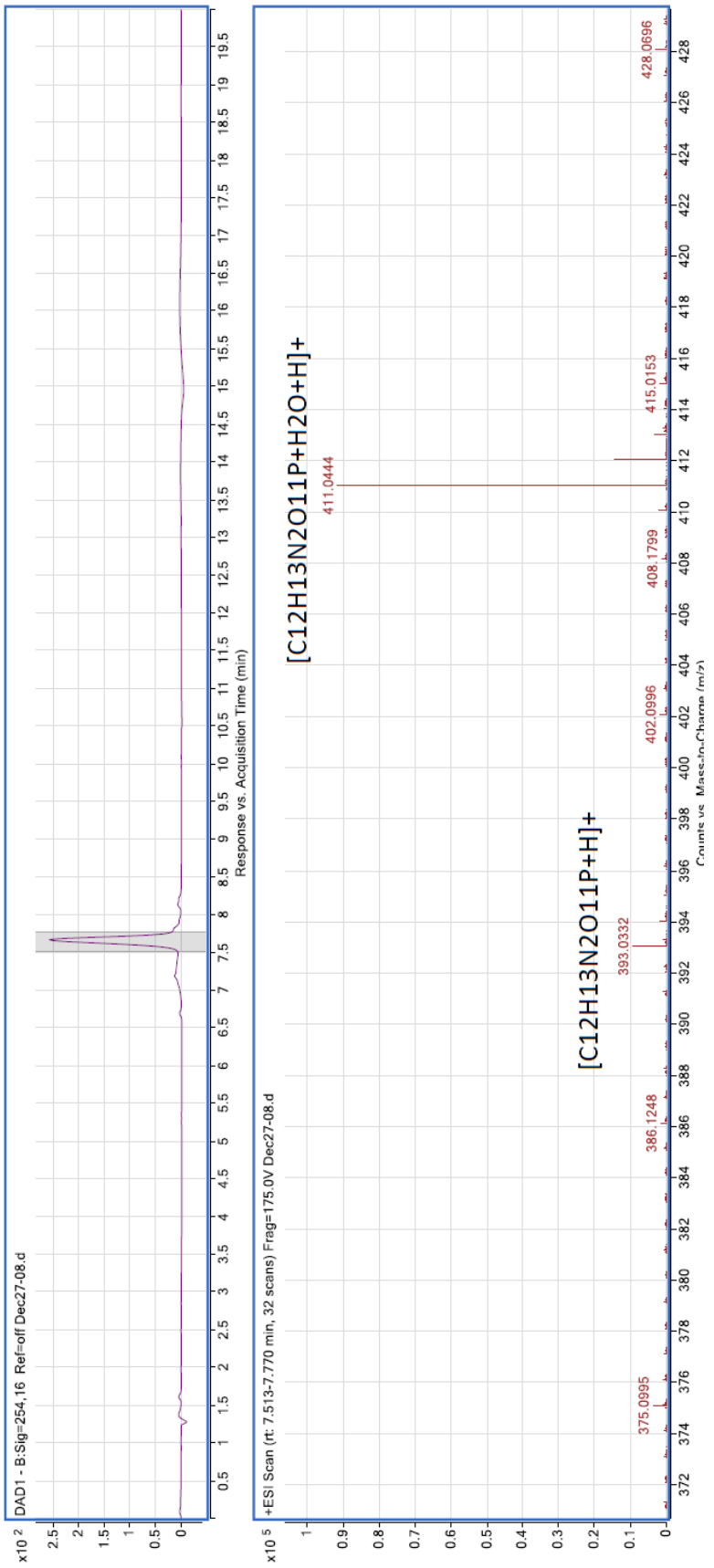

LC-HRMS of KOAP (14) from PolK Assay.

Isolated from in vitro PolK enzyme assay. *m/z* $[M+H]^+$ calculated for $C_{12}H_{13}N_2O_{11}P$ 393.033; found 393.0332.

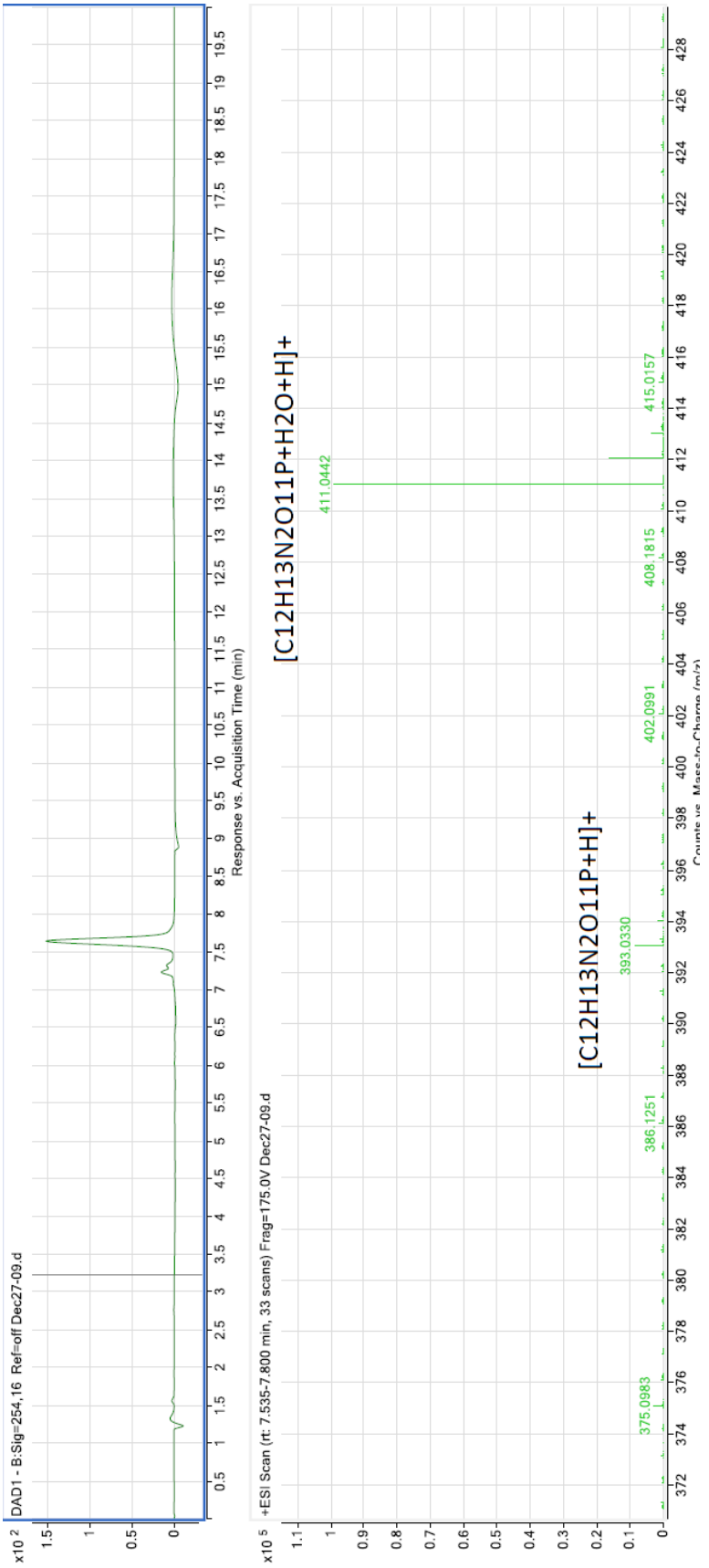

LC-HRMS of KOAP (14) isolated from culture media.

KOAP was isolated from *S. tendae ΔnikK* culture media. *m/z* $[M+H]^+$ calculated for $C_{12}H_{13}N_2O_{11}P$ 393.033; found 393.033.

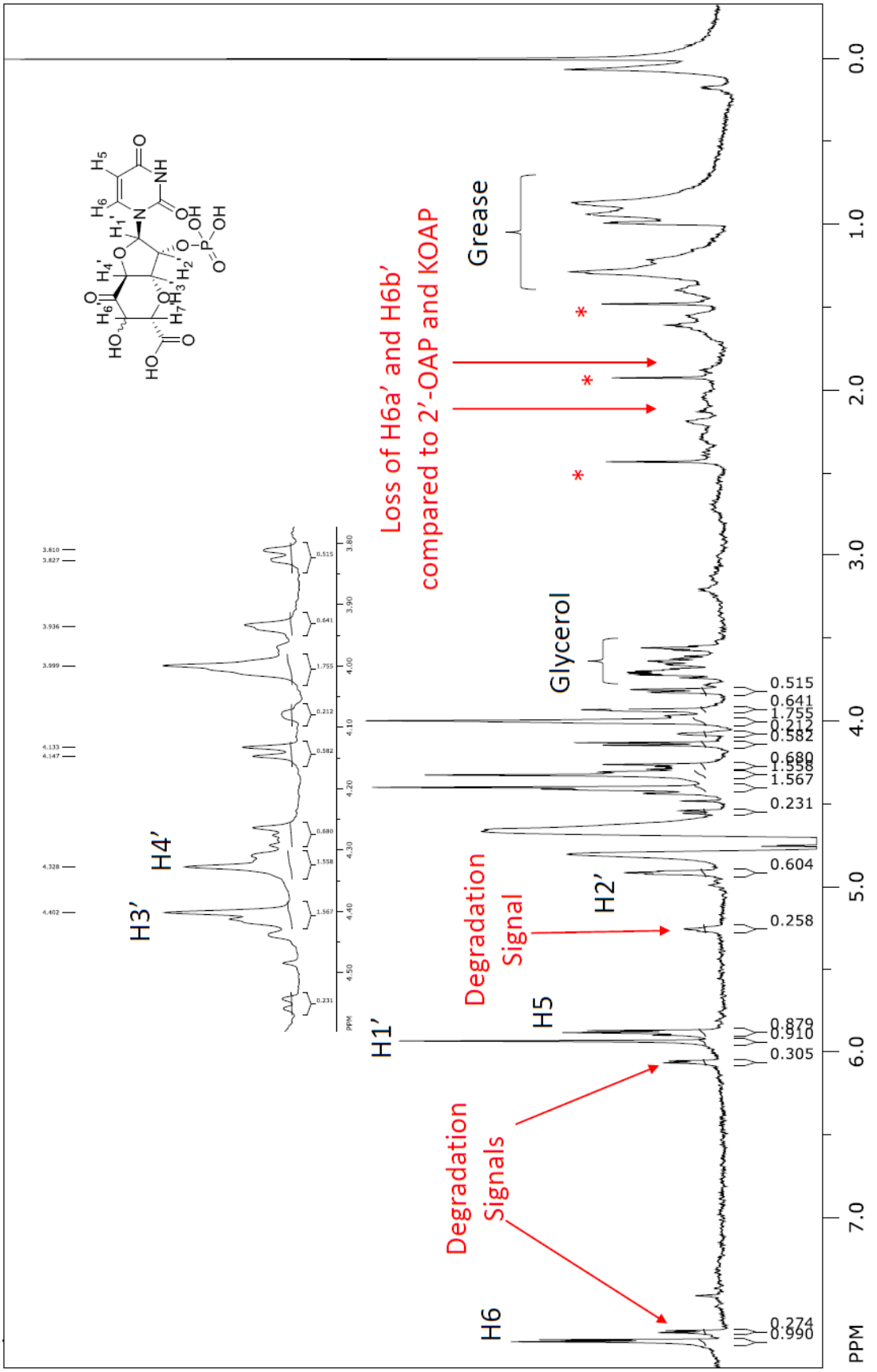

[1]H NMR of HKOAP (15) at 700 MHz in D2O.

Red asterisks (*) indicate unknown impurities. Analysis of compound was hindered by degradation. Proton assignments are tentative. The chemical shifts were referenced to sodium 3-(trimethylsilyl)-2,2,3,3-d4-proponate.

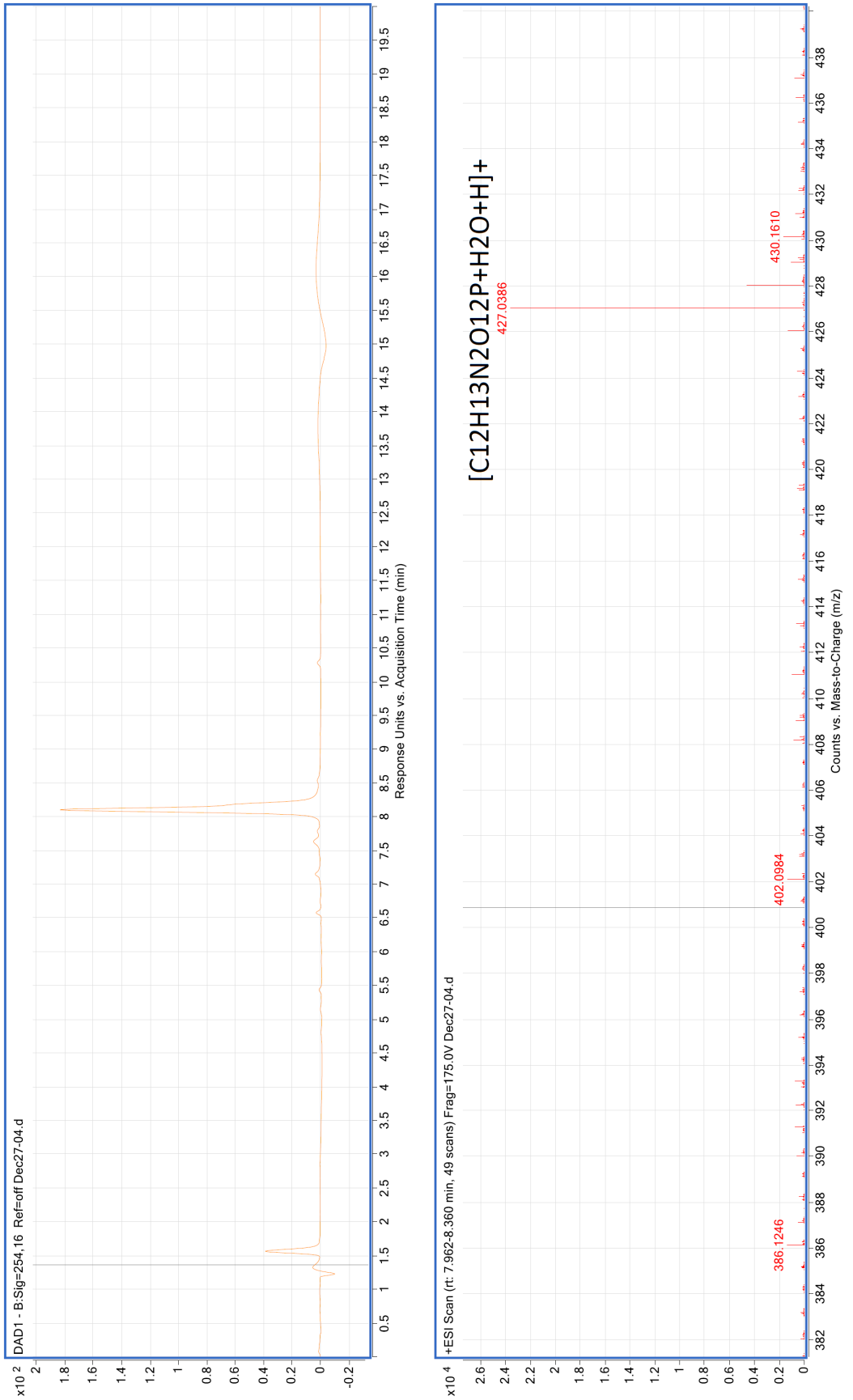

LC HRMS of HKOAP (15).

m/z $[M+H2O+H]^+$ calculated for $C_{12}H_{13}N_2O_{12}P$ 427.039; found 427.039.

Preparation of 5'-amino-6'-hydroxyl-octosyl acid-2'-phosphate (AHOAP, 16)

A large scale MBP-NikK reaction (10 mL) containing 15 μM enzyme, 6 mM L-Phe, 0.5 mM HKOAP, and 40 mM Tris pH 9.0 was prepared and incubated at 25 °C for 12 h. Then, an additional 8 mL of 90 mM enzyme was added, and the reaction was monitored for an additional 12 hours. Upon completion as determined by HPAEC analysis, the reaction was boil-quenched at 95 °C for 5 min, and clarified by centrifugation. The supernatant was diluted 10x in dH_2O and loaded onto a QAE Sephadex A25 column (40 mL new resin; bicarbonate form). The column was washed with 5 CV of 100 mM ammonium bicarbonate pH 7.6, and the product was eluted stepwise with 200 mM ammonium bicarbonate pH 7.6 (10 CV) followed by 250 mM ammonium bicarbonate pH 7.6 (10 CV). Fractions containing AHOAP were identified by HPAEC, combined and lyophilized three times prior to structural characterization. LC-HRMS (ESI-TOF) *m/z* $[M-H]^-$ calculated for $C_{12}H_{16}N_3O_{11}P$ 408.045; found 408.049.

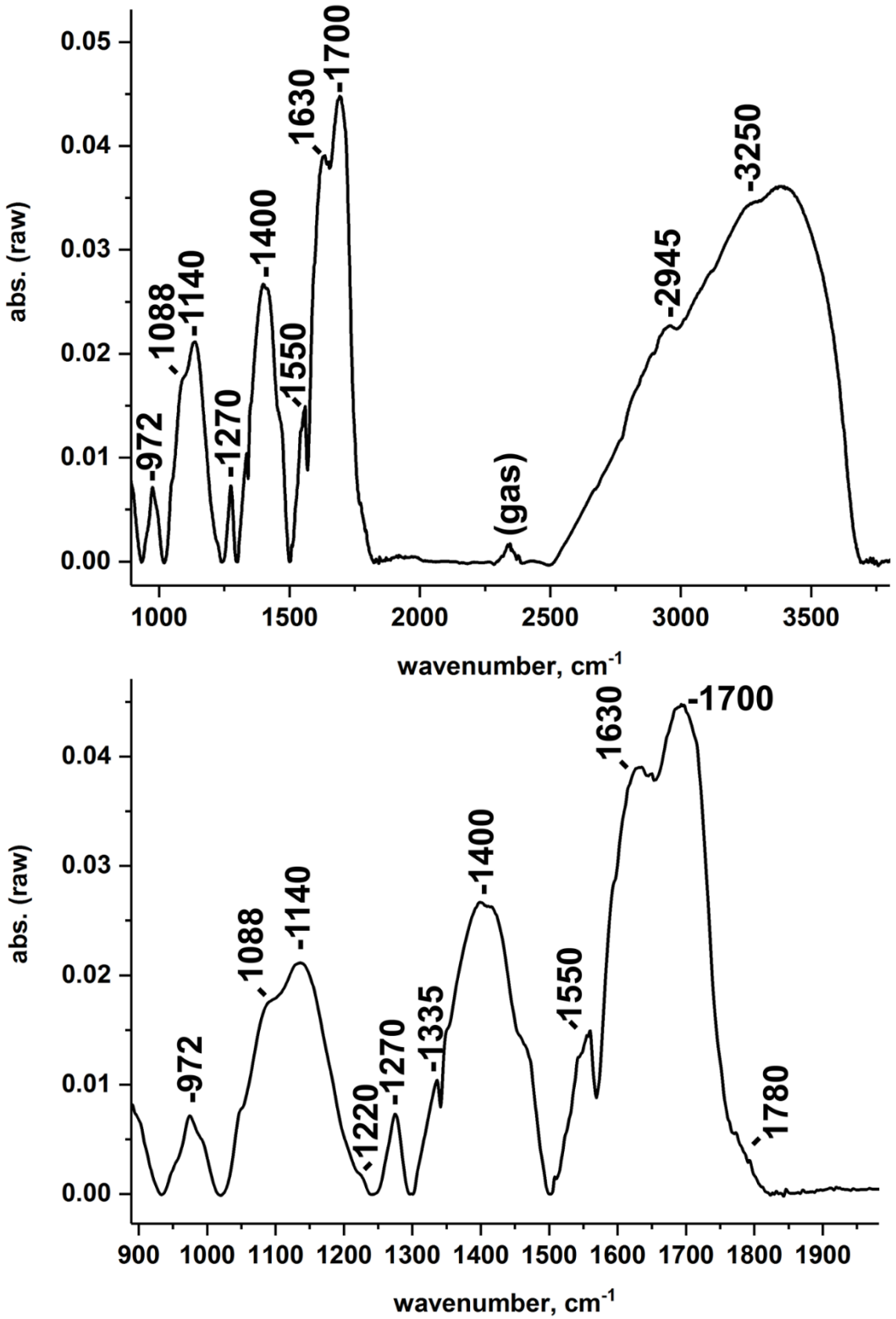

FT-IR of AHOAP (16).

Assignments for FT-IR of AHOAP (16).

Wavenumber (cm^{-1})	Assignments
2945	C-H stretching
1780 (sh)	conjugated anhydride?
1700	C=O
1630	NH_2 bending, C=C stretching
1550	C=C stretching, conjugated
1400	C-C stretching, C-H bending, O-H bending
1335	O-H bending, C-N stretching
1270	C-O stretching, C-N stretching
1220 (w)	O-P-O antisymmetric stretching
1140	C-C/C-N stretching
1088	O-H/O-P-O symmetric stretching
972	C-C stretching, C=C bending

w, weak; sh, shoulder

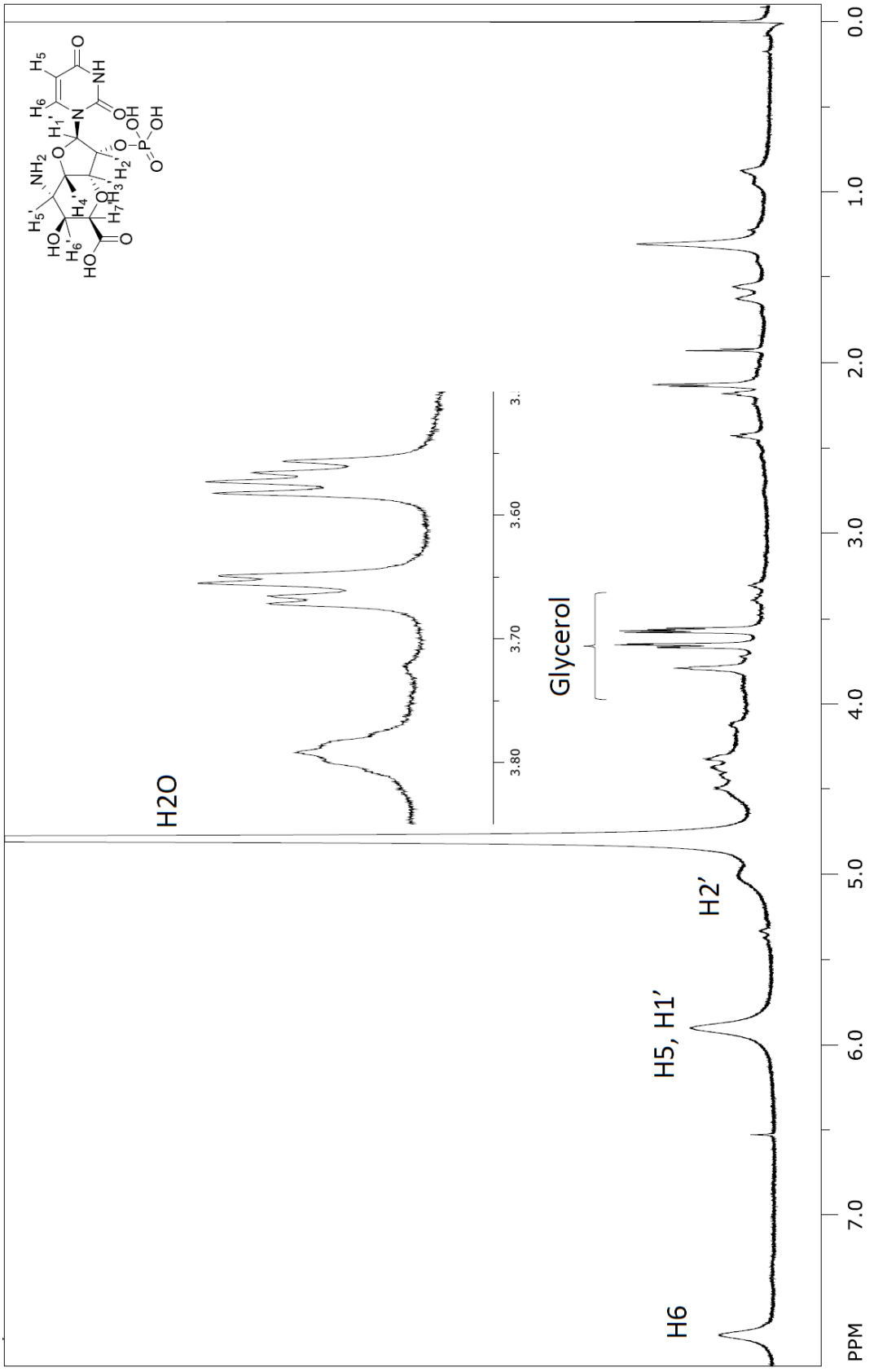

^{1}H NMR of AHOAP (16) at 700 MHz in D_2O.

AHOAP has a T1 relaxation time of between 0.15 s (nucleobase signals) to 1.0 s (sugar signals). Contaminating glycerol has a T1 relaxation time of < 0.15 s. Good tuning and shimming of the instrument is demonstrated by the crisp glycerol signals. The chemical shifts were referenced to sodium 3-(trimethylsilyl)-2,2,3,3-d4-proponate.

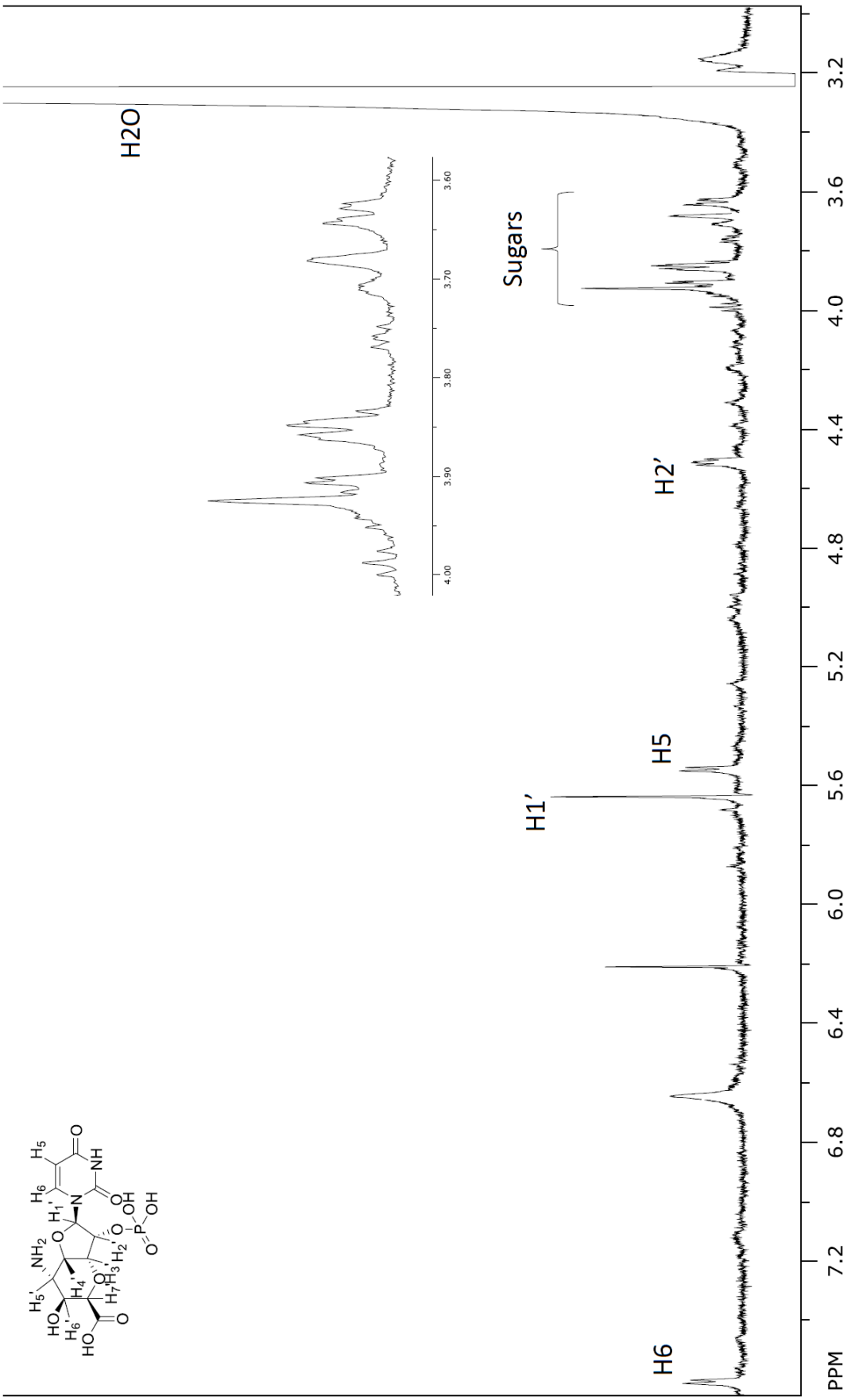

[1]H NMR of AHOAP (16, dilute) at 700 MHz in d6-DMSO.

The chemical shifts were referenced to sodium 3-(trimethylsilyl)-2,2,3,3-d4-proponate.

Preparation of 5'-amino-6'-hyrodroxyl-octosyl acid (AHOA)

AHOAP (0.93 mM) in ~10% DMSO (0.45 mL), 0.05 mL of 10x CutSmart Buffer (NEB), and CIP (40 units) were combined and the mixture was incubated at 37 °C for 2 h. The reaction was boil-quenched at 95 °C for 2 min and clarified by centrifugation. AHOA was isolated by HPLC with an Xbridge Amide 3.5 mm – 4.6 x 250 mm column (Waters) using 10 mM ammonium acetate pH 10.0 and acetonitrile as eluents. Fractions containing AHOA were lyophilized three times prior to structural characterization. ^{1}H NMR (700 MHz, D_2O): δ 3.76 (t; 3.5 Hz; 1H), 3.95 (dd; 10.5 Hz, 4.9 Hz; 1H), 4.13 (t; 2.1 Hz; 1H), 4.33 (dd; 10.7 Hz, 3.7 Hz; 1H), 4.42 (d; 2.1 Hz; 1H), 4.47 (d; 5.6 Hz; 1H), 5.83 (s; 1H), 5.87 (d; 8.4 Hz; 1H), 7.68 (d; 8.4 Hz; 1H). ^{13}C NMR (201.5 MHz, D_2O): δ 53.7, 72.4, 73.4, 73.9, 76.3, 79.4, 94.8, 103.8, 143.6, 157.0, 177.3, 183.2. LC-HRMS (ESI-TOF) *m/z* $[M+H]^+$ calculated for $C_{12}H_{15}N_3O_8$ 330.093; found 330.092.

Summary of NMR data for AHOA.

No.	^{1}H δ (ppm) (multiplicity; J_{H-H} (Hz))	^{13}C δ (ppm)	COSY
2	-	157.0	-
4	-	177.3	-
5	7.68 (d; 8.4)	103.8	H-6
6	5.87 (d; 8.4)	143.6	H-5
1'	5.83 (s)	94.8	-
2'	4.42 (d; 2.1)	79.4	-
3'	4.13 (t; 2.1)	73.4	H-4'
4'	3.76 (t; 3.5)	53.7	H-3', H-5'
5'	4.33 (dd; 10.7, 3.5)	76.3	H-4', H-5'
6'	3.95 (dd; 10.5; 4.9)	72.4	H-5', H-7'
7'	4.47 (d; 5.6)	73.9	H-6'
8'	-	183.2	-

Chemical shifts were referenced to sodium 3-(trimethylsilyl)-2,2,3,3-d4-proponate.

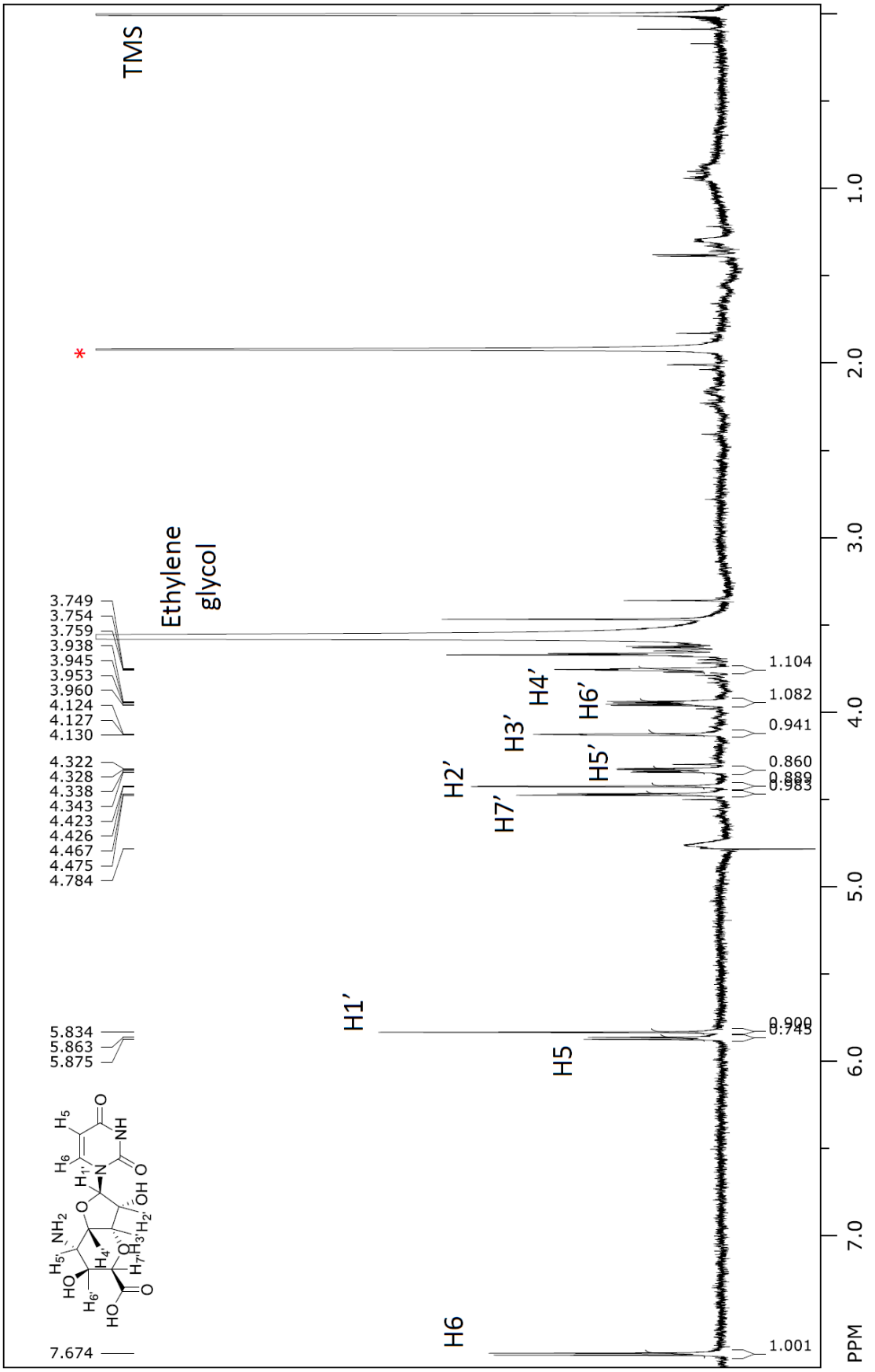

^{1}H NMR of AHOA at 700 MHz in D_2O.

Red asterisk (*) indicates unknown impurity. The chemical shifts were referenced to sodium 3-(trimethylsilyl)-2,2,3,3-d4-proponate.

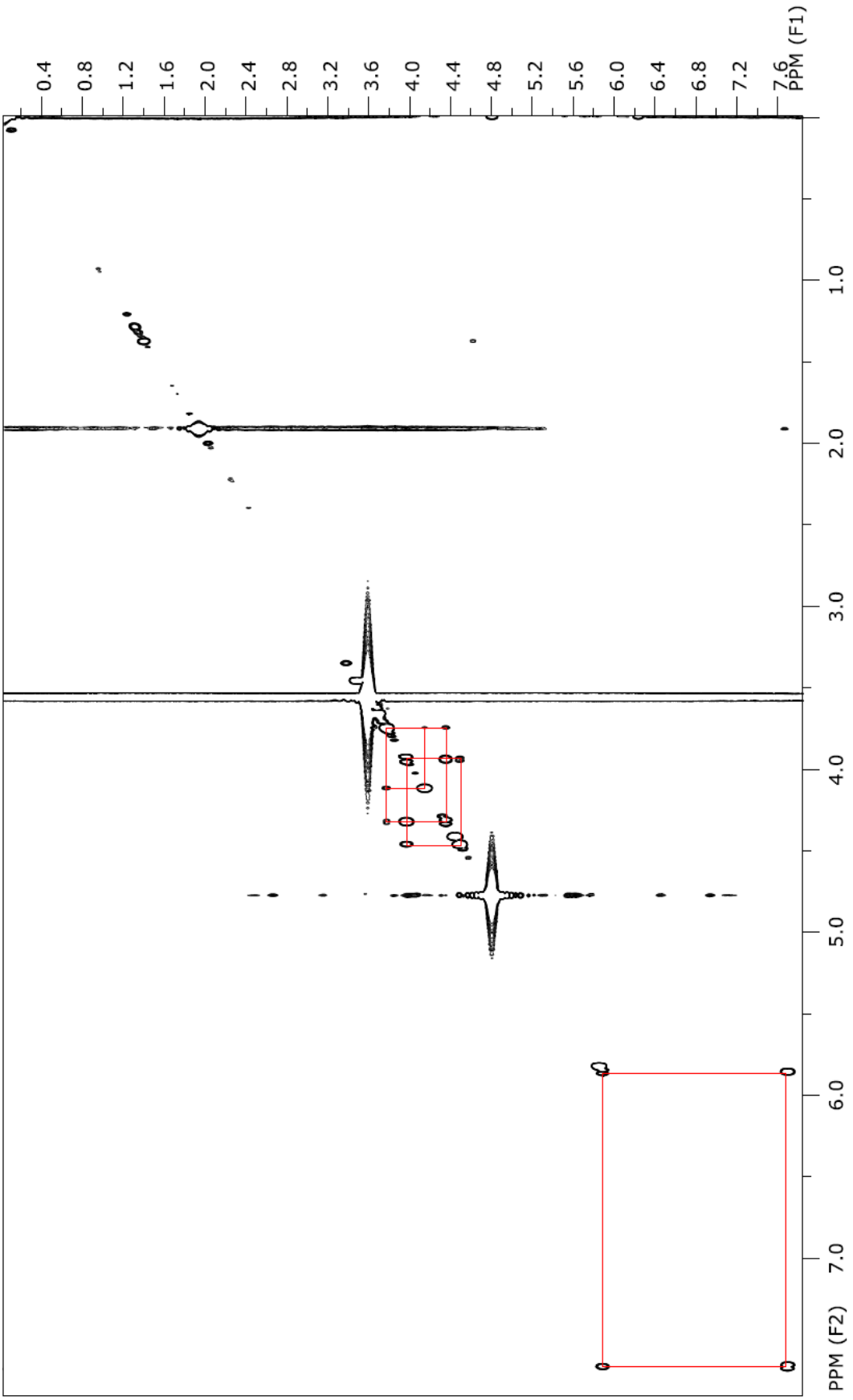

^{1}H-^{1}H COSY NMR of AHOA at 700 MHz in D_2O.

The chemical shifts were referenced to sodium 3-(trimethylsilyl)-2,2,3,3-d4-proponate.

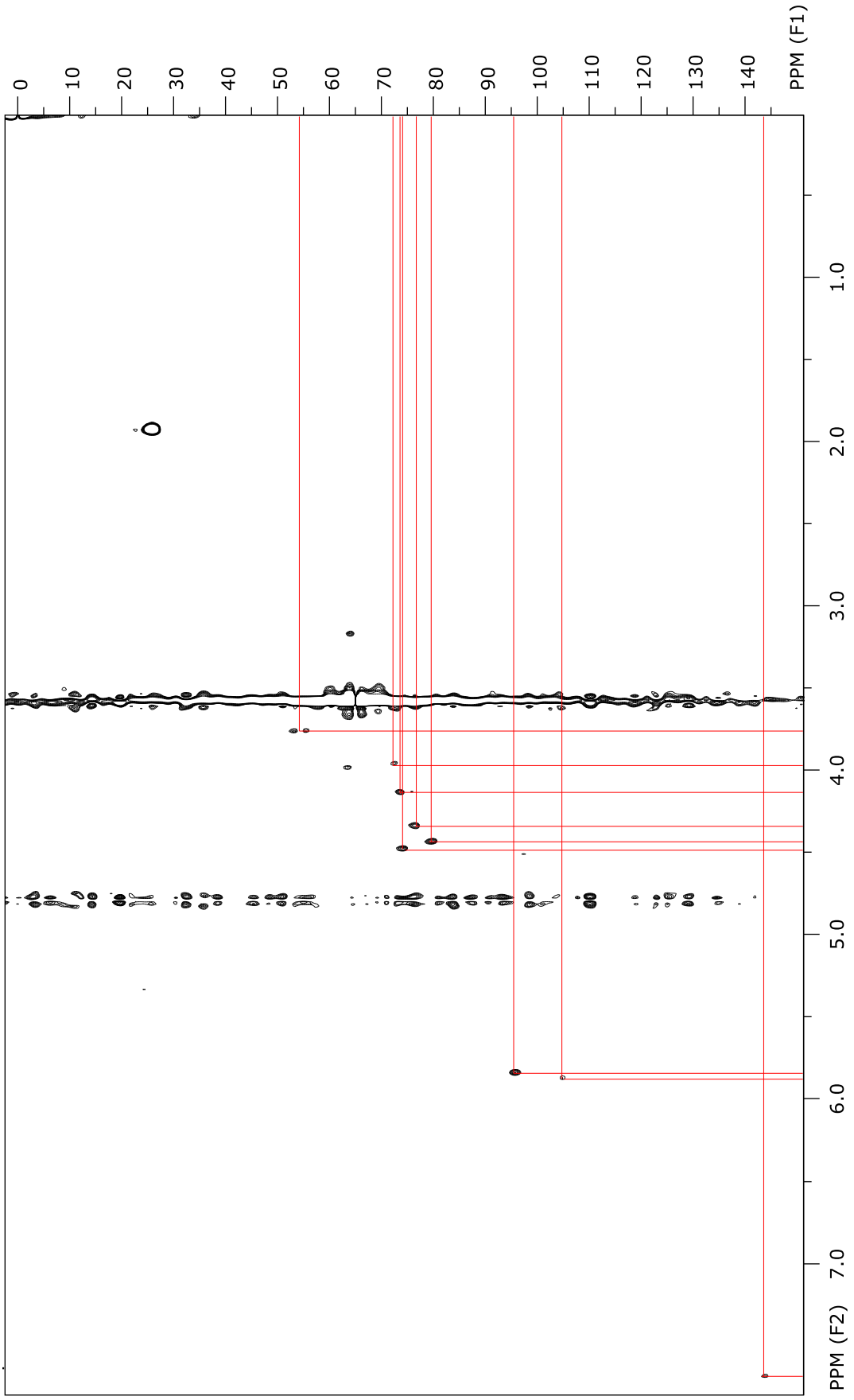

^{1}H-^{13}C HMQC of AHOA at 700 MHz in D_2O.

The chemical shifts were referenced to sodium 3-(trimethylsilyl)-2,2,3,3-d4-proponate.

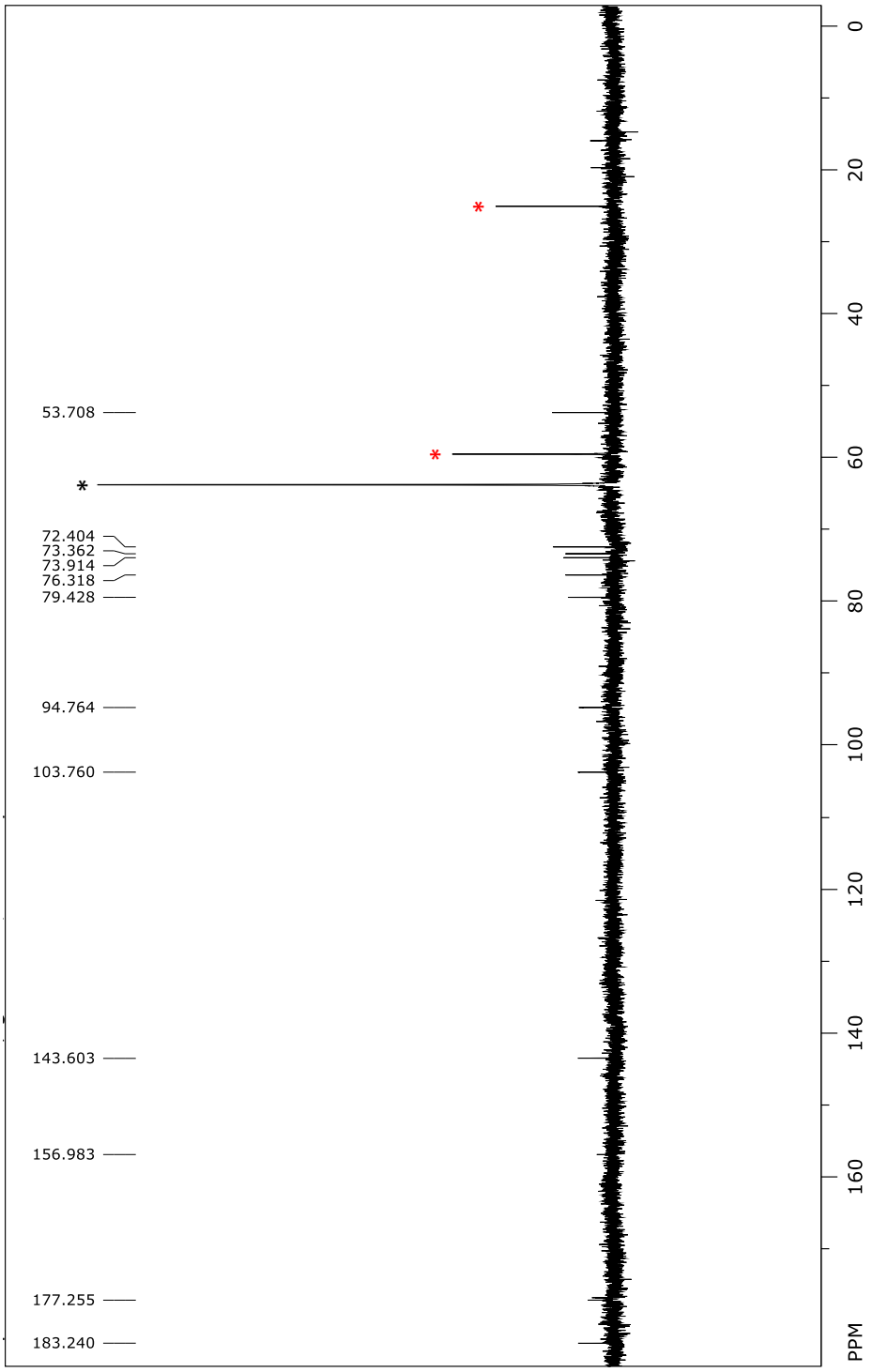

^{13}C NMR of AHOA at 175 MHz in D_2O.

The black asterisk indicates a signal of ethylene glycol. The red asterisks are signals from an unknown impurity, as determined by cross correlation in the HMQC spectrum. The chemical shifts were referenced to sodium 3-(trimethylsilyl)-2,2,3,3-d4-proponate.

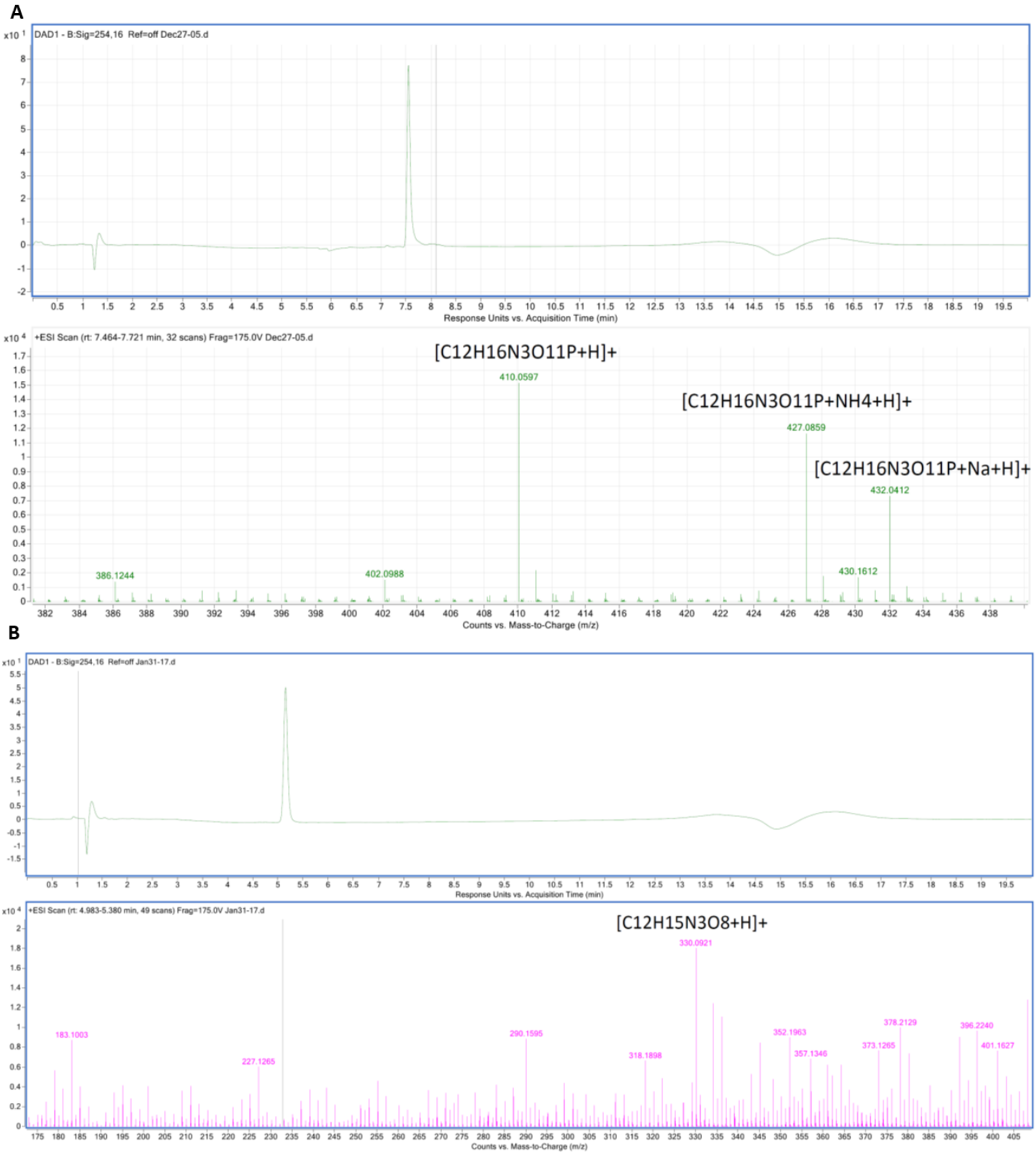

LC HRMS of AHOAP (16) and AHOA.

A. Purified AHOAP: *m/z* $[M+H]^+$ calculated for $C_{12}H_{16}N_3O_{11}P$ 410.060; found 410.060. **B.** Purified AHOA: *m/z* $[M+H]^+$ calculated for $C_{12}H_{15}N_3O_8$ 330.0932; found 330.0921.

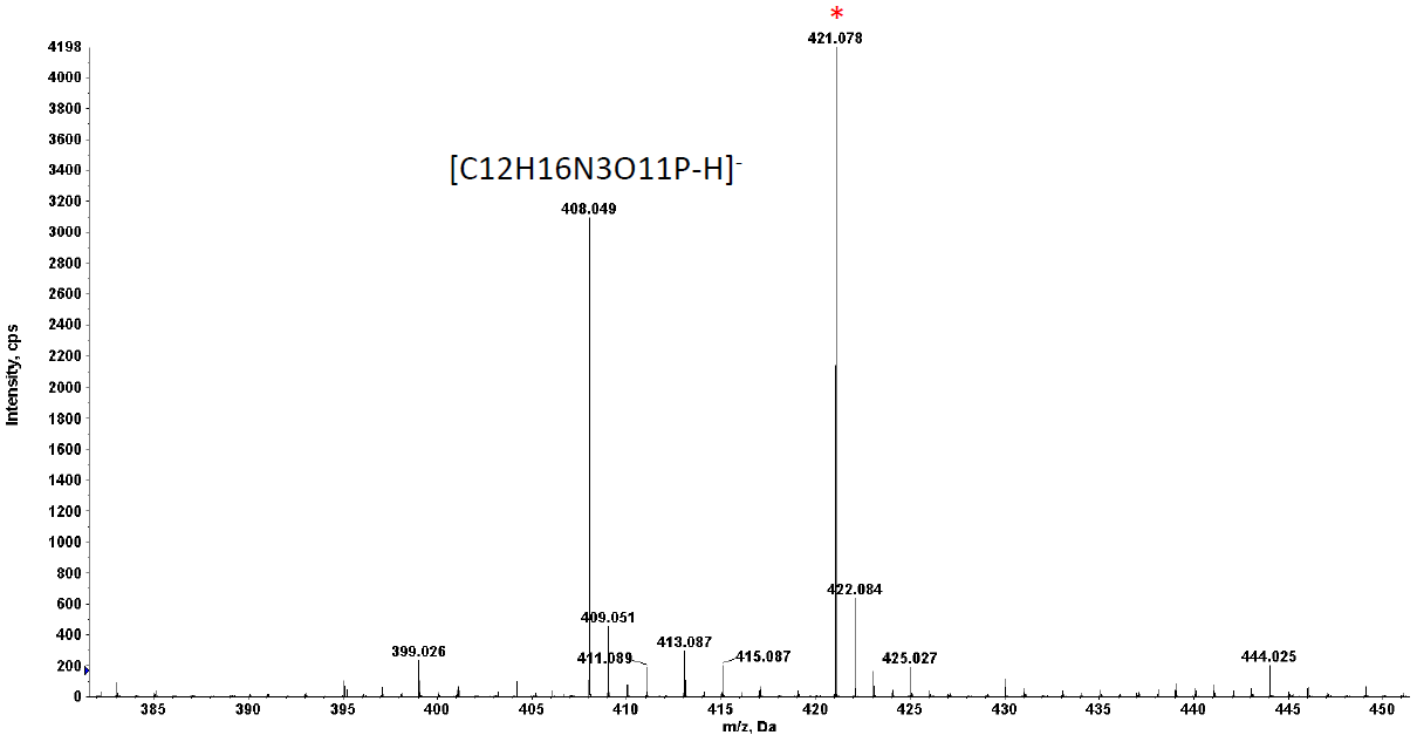

ESI-TOF-MS of AHOAP (16).

Purified AHOAP was analyzed by direct infusion without chromatographic separation. *m/z* $[M-H]^-$ calculated for $C_{12}H_{16}N_3O_{11}P$ 408.045; found 408.049. Red asterisk (*) indicates an unknown contaminant.

Preparation of 2'-aminohexuronic acid phosphate (AHAP, 9)

A large scale His-PolD reaction (15 mL) was performed as in Methods for 2 h. Upon completion as determined by HPAEC analysis, the reaction was boil-quenched at 95 °C for 5 min and clarified by centrifugation. The supernatant was diluted 10x in H_2O and was loaded onto a QAE Sephadex A25 column (20 mL; bicarbonate form). The column was washed with 10 CV of H_2O, followed by 10 CV of 100 mM ammonium bicarbonate pH 7.6. AHAP was eluted under a gradient from 100-300 mM ammonium bicarbonate pH 7.6 over 10 CV. Fractions containing AHAP were identified by HPAEC, combined and lyophilized three times prior to structural characterization. ^{1}H NMR (700 MHz, D_2O): δ 3.75 (s; 1H); 4.18 (d; 2.8 Hz; 1H); 4.39 (dd; 2.7 Hz, 6.0 Hz; 1H); 4.73 (t; 6.0 Hz; 1H); 5.88 (d; 4.0 Hz; 1H); 5.91 (d; 7.0 Hz; 1H); 7.64 (d; 8.1 Hz; 1H). 58.19, 62.25, 71.80, 84.01, 94.10, 105.43, 146.75, 154.56, 165.17, 169.17. LC-HRMS (ESI-TOF) *m/z* $[M+H]^+$ calculated for $C_{10}H_{14}N_3O_{10}P$ 368.049; found 368.049.

Summary of NMR data for AHAP (9).

No.	1H δ (ppm) (multiplicity; JH-H (Hz))	13C δ (ppm)	COSY
2	-	154.6	-
4	-	165.2	-
5	5.91 (d; 7.0)	105.4	H-6
6	7.64 (d; 8.1)	146.8	H-5
1'	5.88 (d; 4.0)	94.1	H-2'
2'	4.73 (t; 6.0)	71.8	H-1', H-3'
3'	4.39 (dd; 6.0, 2.7)	84.0	H-2'
4'	4.18 (d; 2.8)	58.2	ND
5'	3.75 (s)	62.3	ND
6'	-	169.2	-

Chemical shifts were referenced to sodium 3-(trimethylsilyl)-2,2,3,3-d4-proponate.

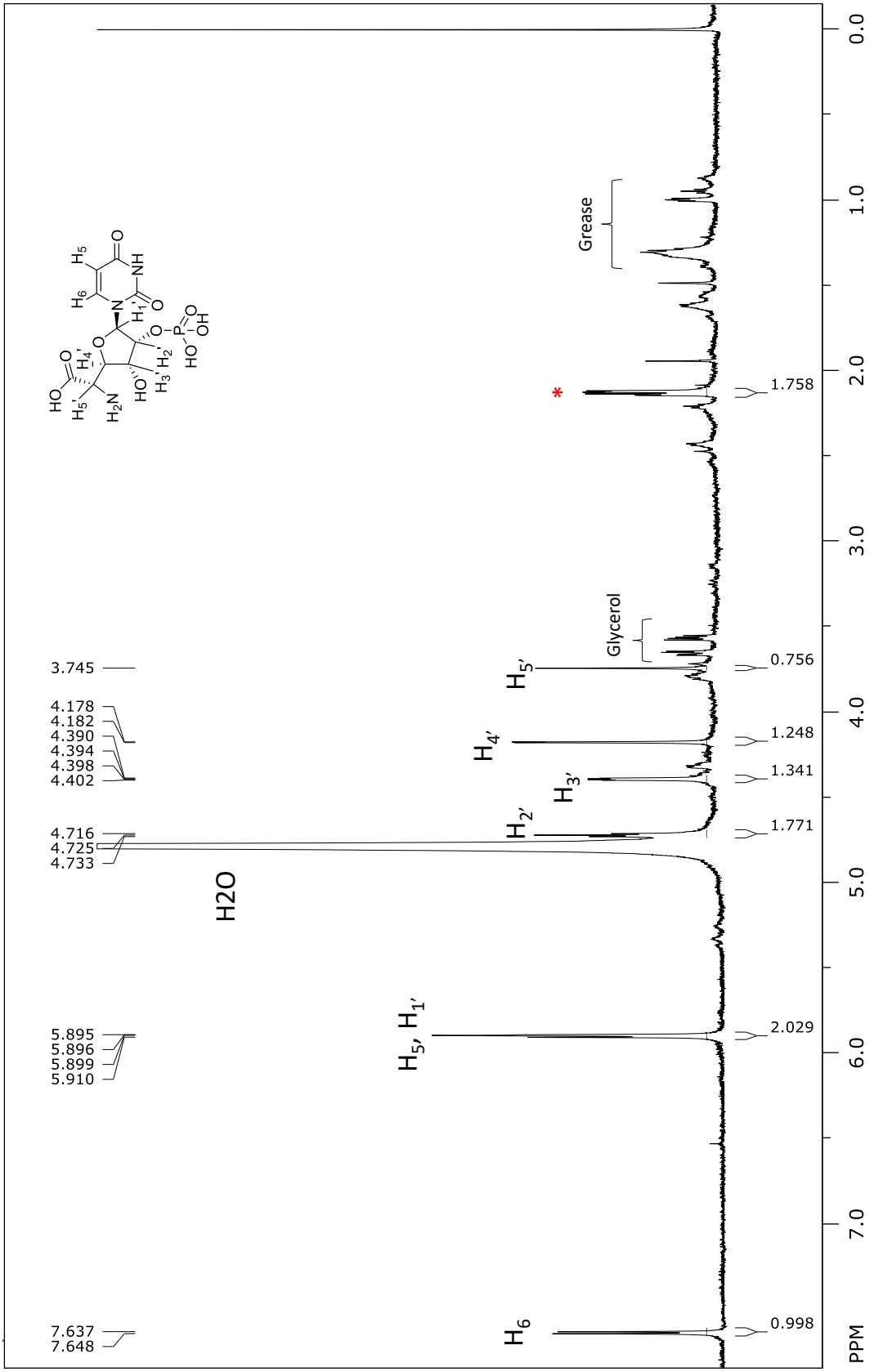

^{1}H NMR spectrum of AHAP (9) at 700 MHz in D_2O.

Red asterisk (*) indicates signals from an unknown contaminant. The chemical shifts were referenced to sodium 3-(trimethylsilyl)-2,2,3,3-d4-proponate.

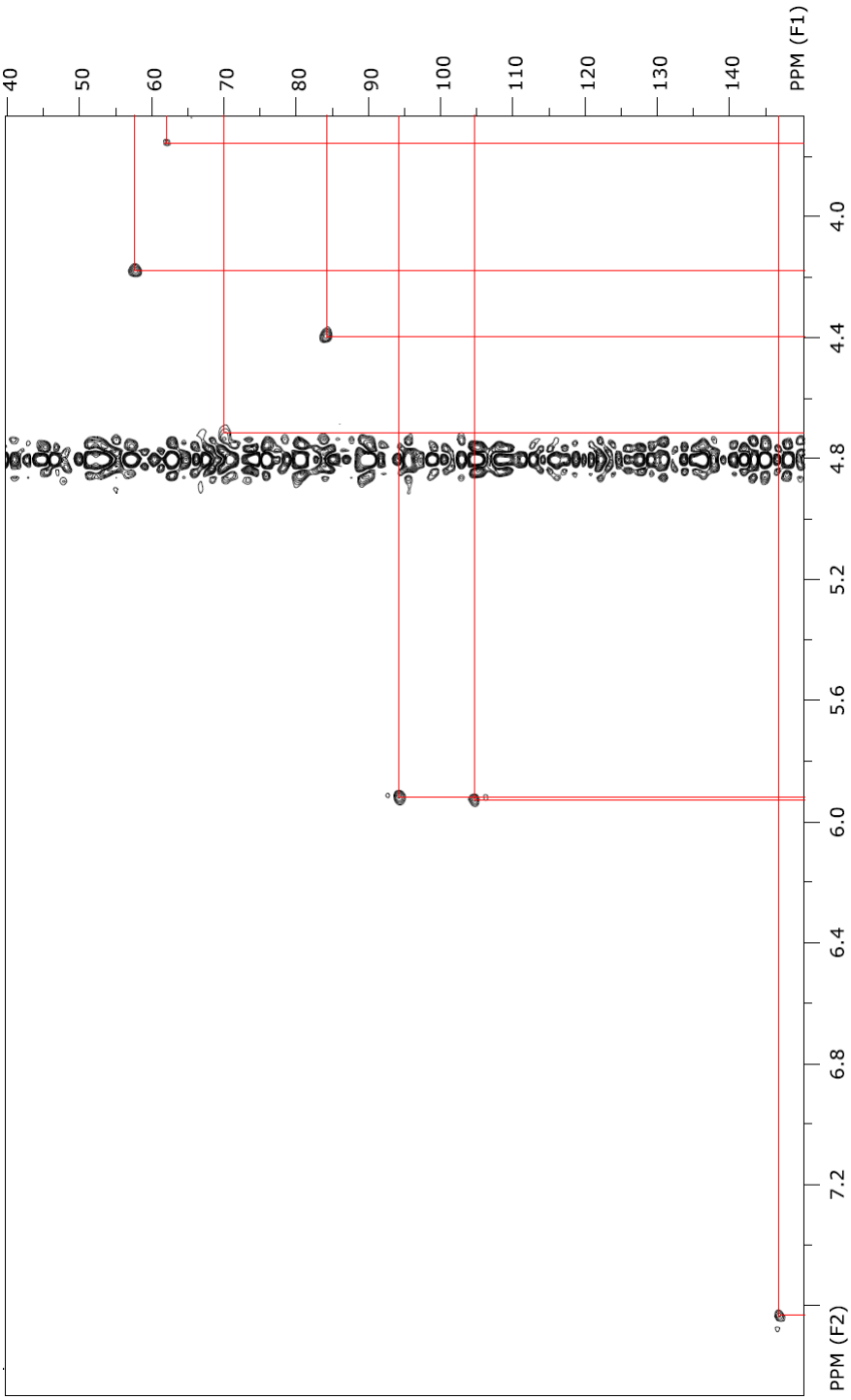

^{1}H-^{13}C HMQC of AHAP (9) at 700 MHz in D_2O.

The chemical shifts were referenced to sodium 3-(trimethylsilyl)-2,2,3,3-d4-proponate.

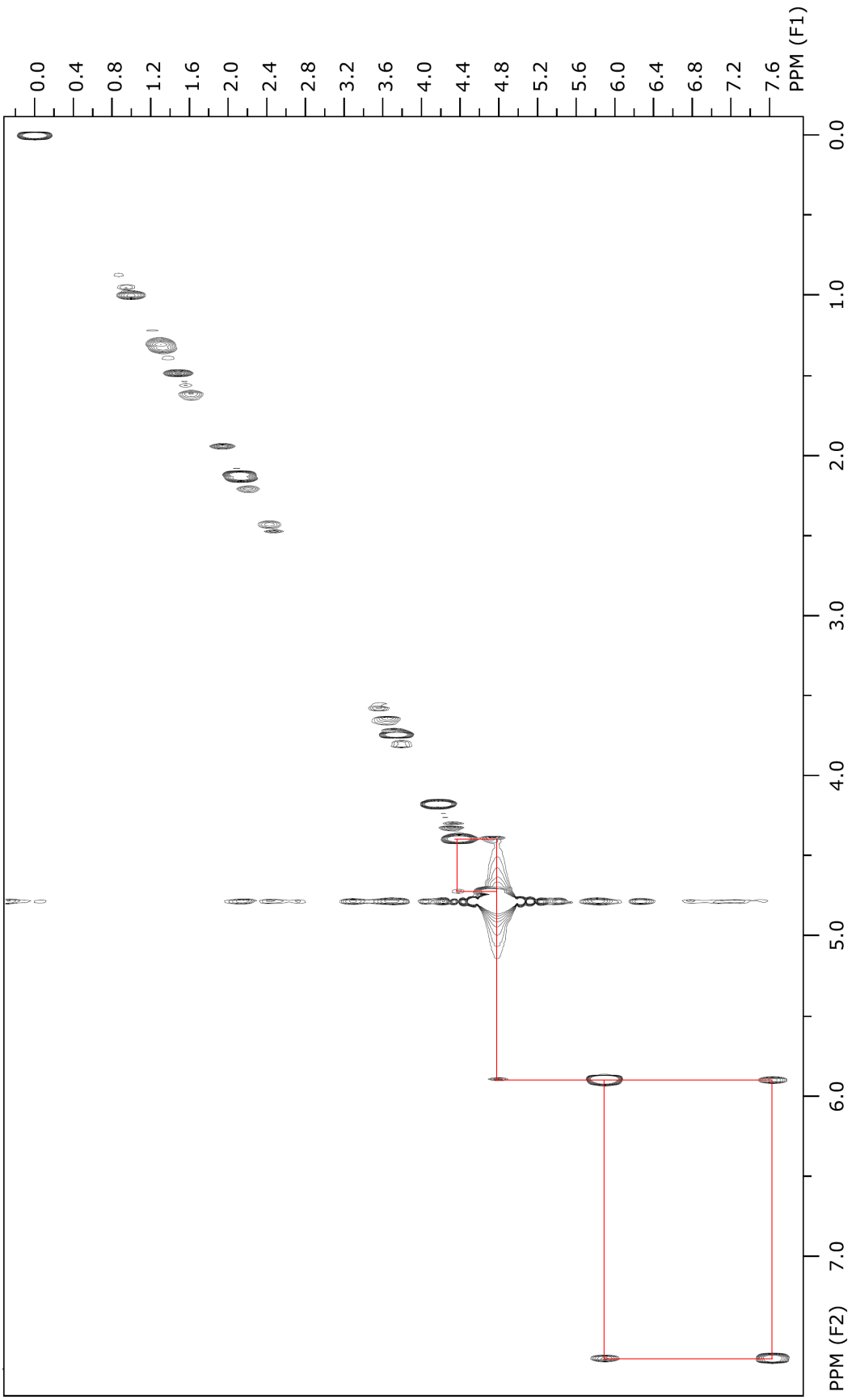

^{1}H-^{1}H COSY NMR of AHAP (9) at 700 MHz in D_2O.
The chemical shifts were referenced to sodium 3-(trimethylsilyl)-2,2,3,3-d4-proponate.

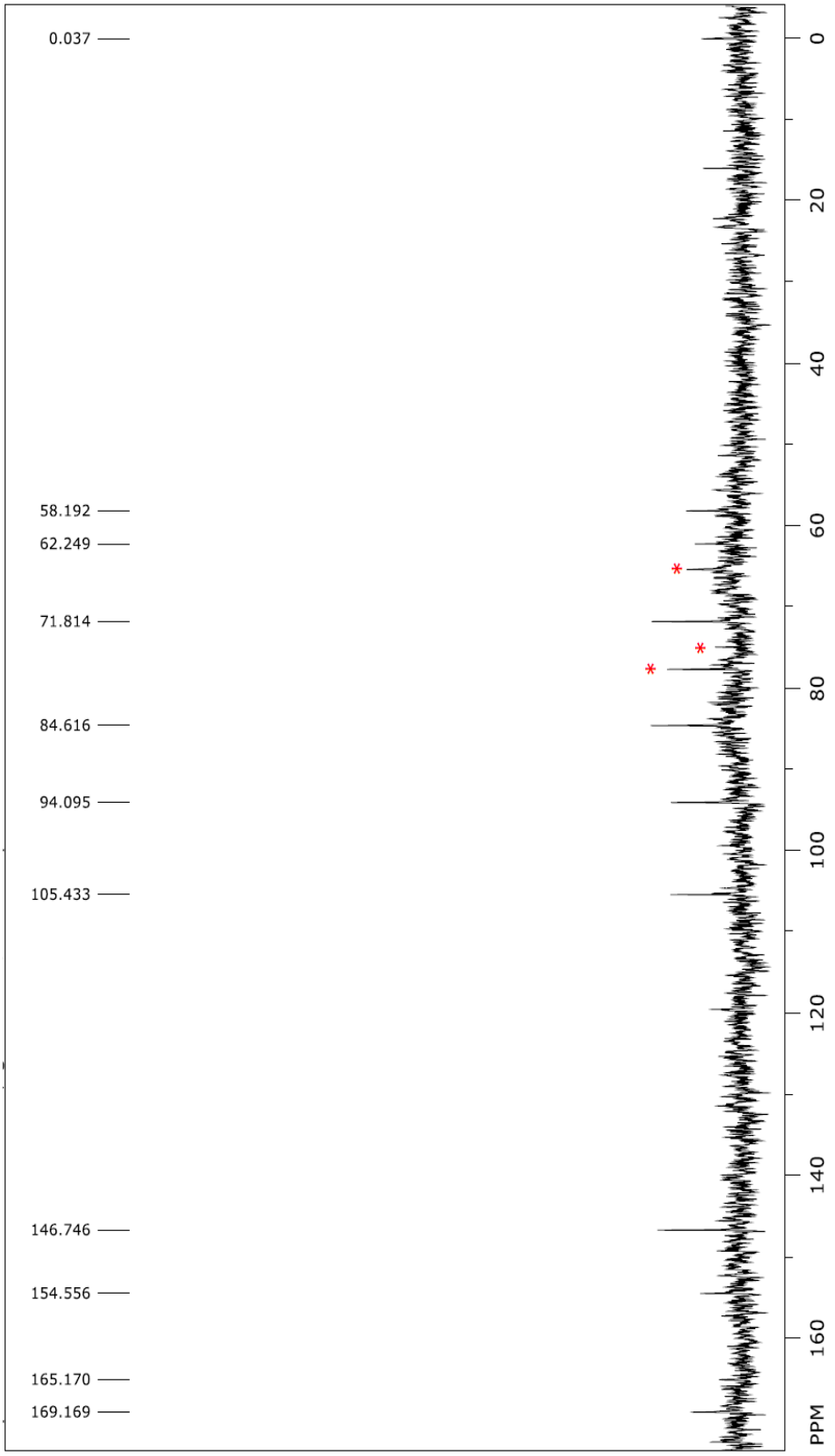

^{13}C NMR of AHAP (9) at 201.6 MHz in D_2O.

Red asterisks (*) indicate glycerol contamination or unknown contaminant. The chemical shifts were referenced to sodium 3-(trimethylsilyl)-2,2,3,3-d4-proponate.

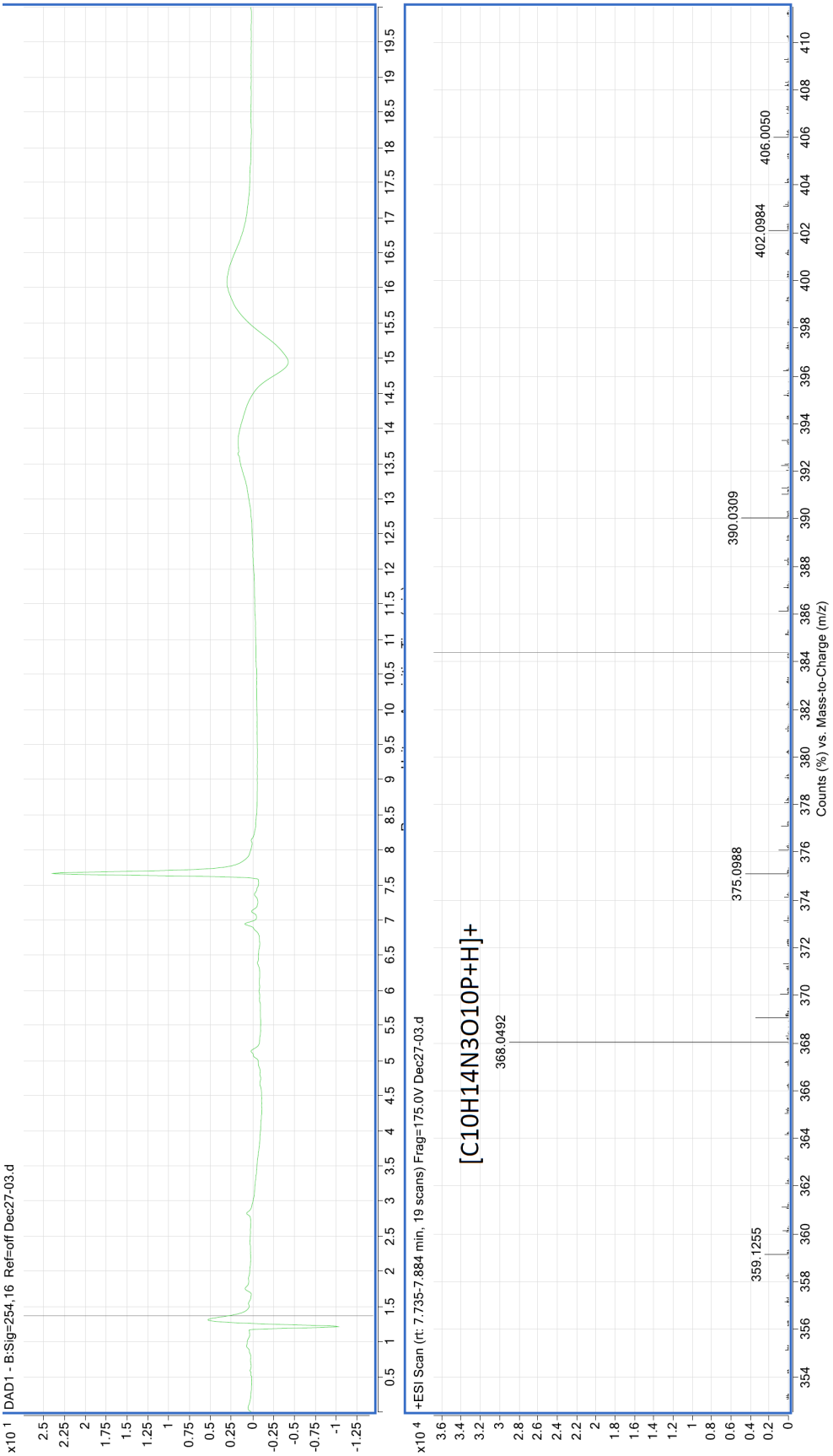

LC ESI-TOF-MS of AHAP (9).

m/z $[M+H]^+$ calculated for $C_{10}H_{14}N_3O_{10}P$ 368.0490; found 368.0492.

Preparation of Nikkomycin Z (1)

Streptomyces tendae Tü901 was grown in 50 mL of media (43 g/L mannitol, 12 g/L soluble starch, 20 g/L soy peptone, 3.75 mg/L iron sulfate hexahydrate, 10 g/L yeast extract pH adjusted to 6) in a 250 mL baffled flask at 28 °C and 180 rpm for three days. An aliquot (1 mL) of the saturated culture is then used to inoculate 500 mL of the same media in 2.8 L baffled flasks for nine days at 28 °C and 180 rpm. The pH was adjusted with 1 N sulfuric acid daily to 6.0. The culture was periodically checked by microscope to check for contaminating bacteria. After nine days, the cells were removed by centrifugation at 5,000 x *g* for 15 min at 4 °C. The fermentation broth then was decanted, frozen, and stored at -20 °C until further purification. For the purification, fermentation broth (200 mL) was thawed and centrifuged to remove cell debris. The supernatant was lyophilized, resuspended in 50 mL of deionized water (dH_2O), pH adjusted to 4 with 1 M AcOH, and then immediately loaded onto a DOWEX 50X8-200 (Sigma-Aldrich; sodium form; 50 mL) column. The column was washed with dH_2O until absorbance at 260 nm was at baseline. Then, nikkomycin Z was eluted by a linear gradient (250 x 250 mL) from 0 to 50 mM NH_4OH. Fractions were collected every 10 mL and were immediately pH adjusted individually to 7.0 with 1 M AcOH. The fractions were assessed by UV absorbance at 260 nm and all fractions with $A_{260nm} > 0.5$ (typically ~ 100 mL, from 20 – 40 mM NH_4OH) were combined and concentrated by rotary evaporation to ~10 mL. The concentrate then was loaded onto an Amberchrom CG300M (Sigma-Aldrich; 100 mL) reverse phase column, and eluted with dH_2O. The elution was fractionated every 10 mL, and monitored by UV absorbance at 260 nm. Nikkomycin Z was eluted after ~ 100 mL of elution. The NMR spectra (Fig. S60), UV-vis spectra, and HR LC/MS of the isolated compound agree with the published literature. ^{1}H NMR (500 MHz, D_2O): δ 0.44 (d, 7 Hz, 1H); 2.55-2.62 (m; 1H); 4.15 (s; 1H); 4.19 (s; 1H); 4.27 (s; 1H); 4.36 (s; 1H); 4.43 (s; 1H); 4.98 (s; 1H); 5.73 (s; 1H); 5.74 (s; 1H); 7.27 (q; 8.35 Hz; 2H); 7.56 (d; 8.0 Hz; 1H); 7.94 (s; 1H). LC-HRMS (ESI-TOF) *m/z* $[M+H]^+$ calculated for $C_{20}H_{25}N_5O_{10}$ 496.167; found 496.170.

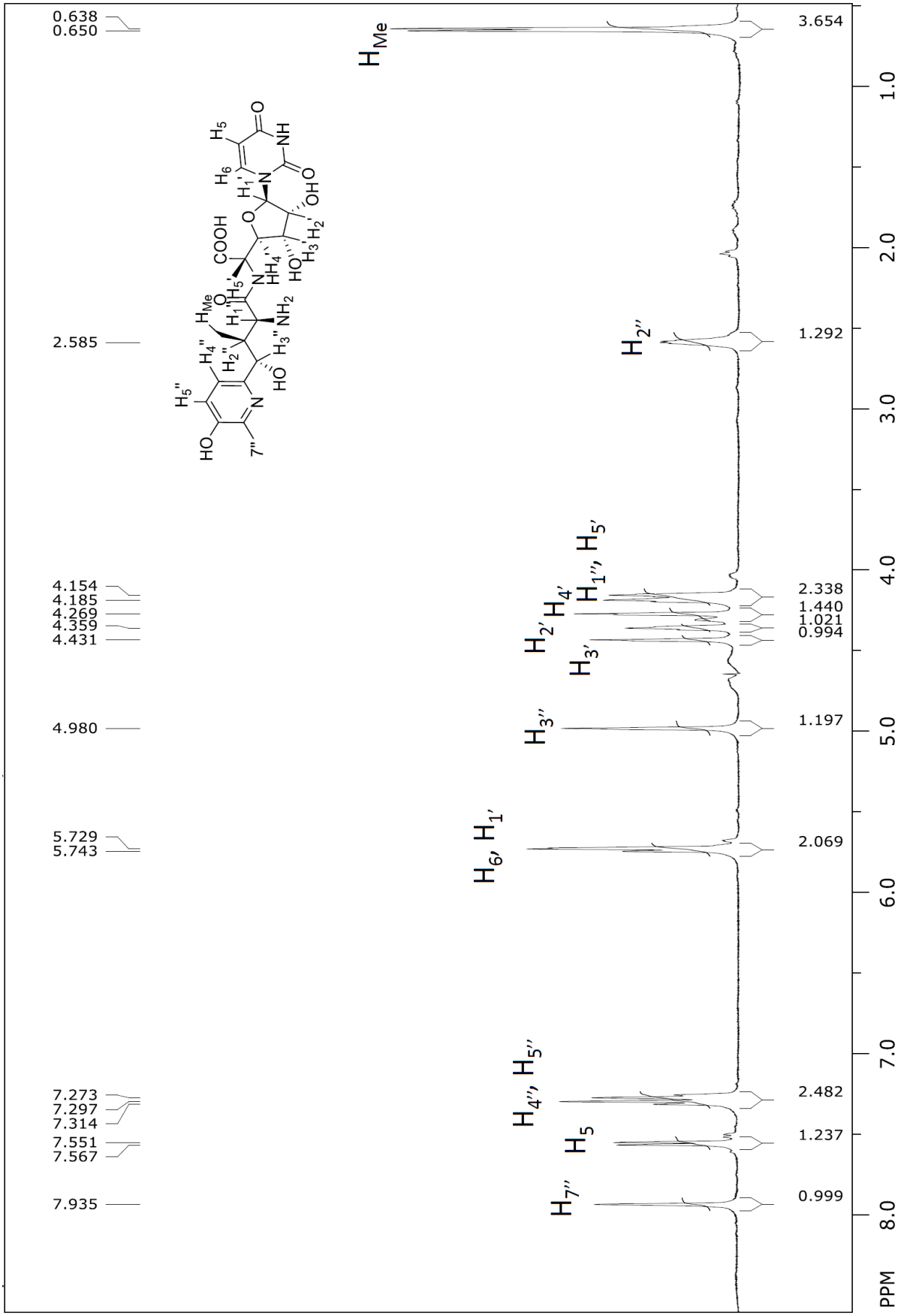

^{1}H NMR of Nikkomycin Z (1) at 500 MHz in D_2O.

Preparation of AHA (3) and 4-hydroxypyridinyl homothreonine (HPHT, 10)

Nikkomycin Z (20 mg, 20 mM) was dissolved in 10 mM NaOH (0.01 mL), and incubated at 80 °C for 6 h. The reaction was adjusted to pH 4.0 with 1 M AcOH, and loaded onto a DOWEX 50WX8-200 column (20 mL; sodium form). The column was washed with 1 CV dH_2O. AHA and HPHT were eluted by a linear gradient 0-50 mM NH_4OH. Fractions containing AHA and HPHT were identified by UV-vis spectra, pH adjusted to 7.0 with 1 M AcOH and combined separately for lyophilization. ^{1}H NMR spectra (Fig. S61 and S62), UV-vis spectra, and HR LC/MS agreed with the published literature. AHA: ^{1}H NMR (500 MHz, D_2O): δ 3.71 (d; 2.5 Hz; 1H); 4.11 (dd; 4.85 Hz, 4.0 Hz; 1H); 4.18 (t; 5.5 Hz; 1H); 4.35 (t; 5.5 Hz; 1H); 5.73 (d; 5.5 Hz; 1H); 5.77 (d; 8.0 Hz; 1H); 7.58 (d; 8.0 Hz; 1H). HRMS (ESI-TOF) *m/z* $[M+H]^+$ calculated for $C_{10}H_{13}N_3O_7$ 288.083, found 228.083. HPHT: ^{1}H NMR (500 MHz, D_2O): δ 0.78 (d; J = 7.5 Hz; 3H); 2.47 (qd; 7.05 Hz, 2.35 Hz; 1H); 3.71 (d; 2.5 Hz; 1H); 4.59 (d; 7.0 Hz; 1H); 7.24 (d; 2.5 Hz; 1H); 7.26 (d; 2.5 Hz; 1H); 7.95 (s; 1H). LC-HRMS (ESI-TOF) *m/z* $[M+H]^+$ calculated for $C_{10}H_{14}N_2O_4$ 227.103; found 227.103.

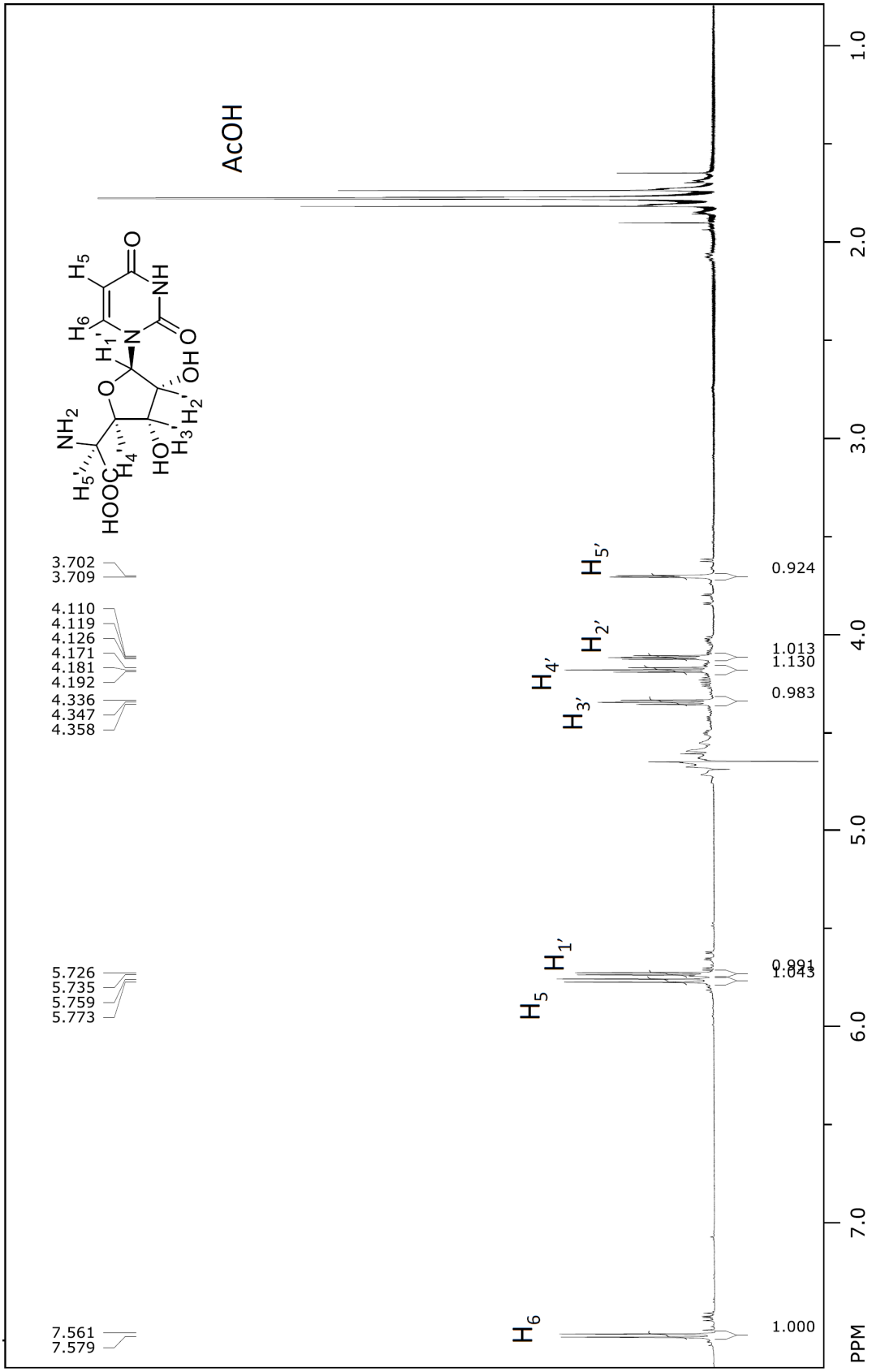

^{1}H NMR of AHA (3) at 500 MHz in D_2O.

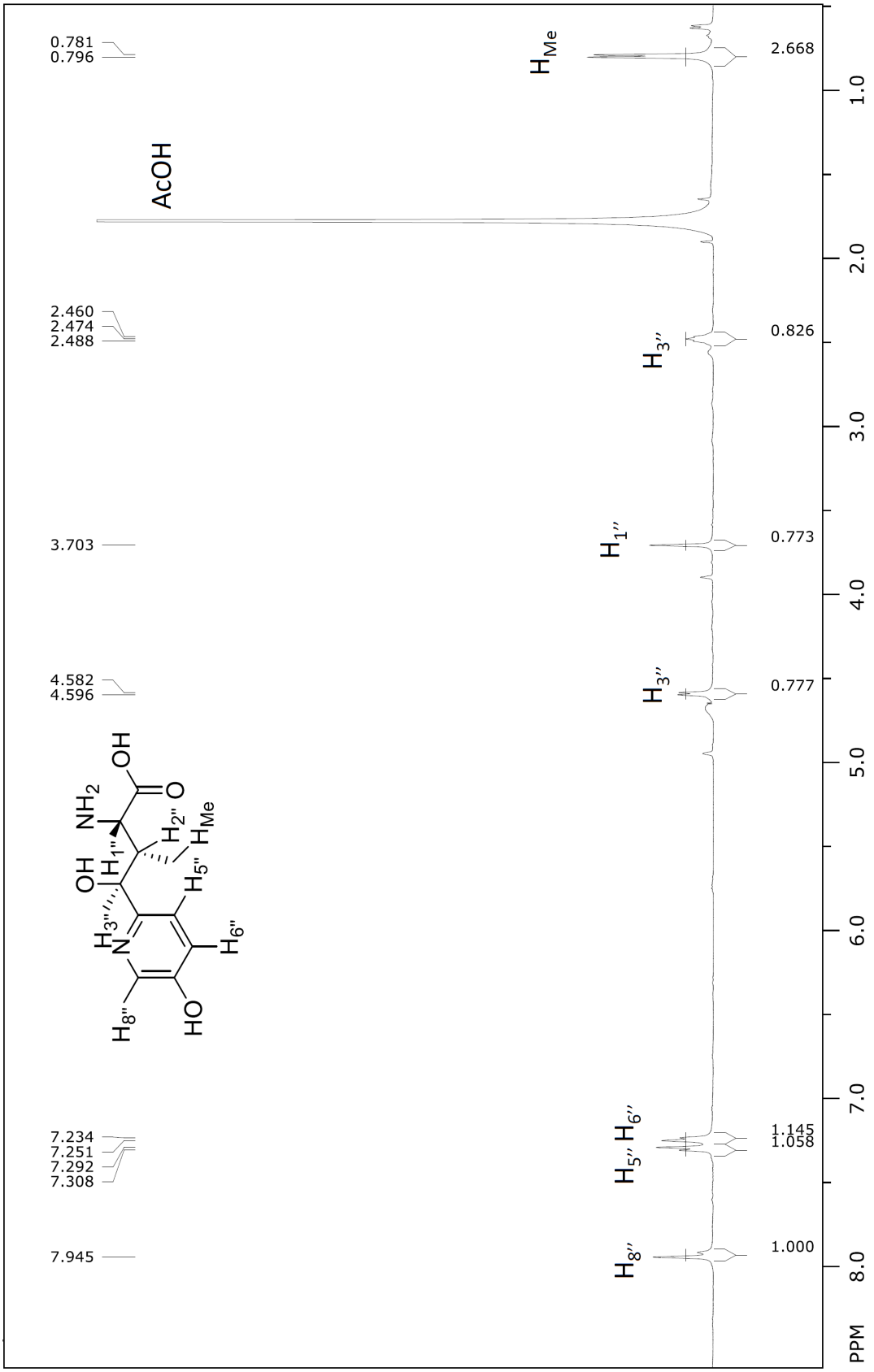

^{1}H NMR of HPHT (10) at 500 MHz in D_2O.

Isolation of 2'-OAP (12) and KOAP (14) from *S. tendae* Δ*nikK* Culture Media

S. tendae Δ*nikK* culture media (35 mL) was diluted to 300 mL with dH_2O and loaded onto a DEAE Sephadex A25 column (50 mL; formate form; GE Healthcare Life Sciences). The column was washed with 5 CV of dH_2O. Elution was performed with 20 mM ammonium formate pH 3.0. Fractions containing 2'-OAP were identified by HPAEC, combined, and pH adjusted to 6 with 1 M sodium hydroxide. Then, the solution was diluted to 600 mL with dH_2O and loaded onto a QAE Sephadex A25 column (100 mL; acetate form; GE Healthcare Life Sciences). The column was washed with 10 CV of 100 mM ammonium acetate pH 6.0, and 2'-OAP was eluted with a gradient from 200-225 mM ammonium acetate pH 6.0 over 10 CV. The column was then washed with 500 mM ammonium acetate pH 6.0 for 5 CV. Fractions containing 2'-OAP were identified by HPAEC, combined, and lyophilized twice.

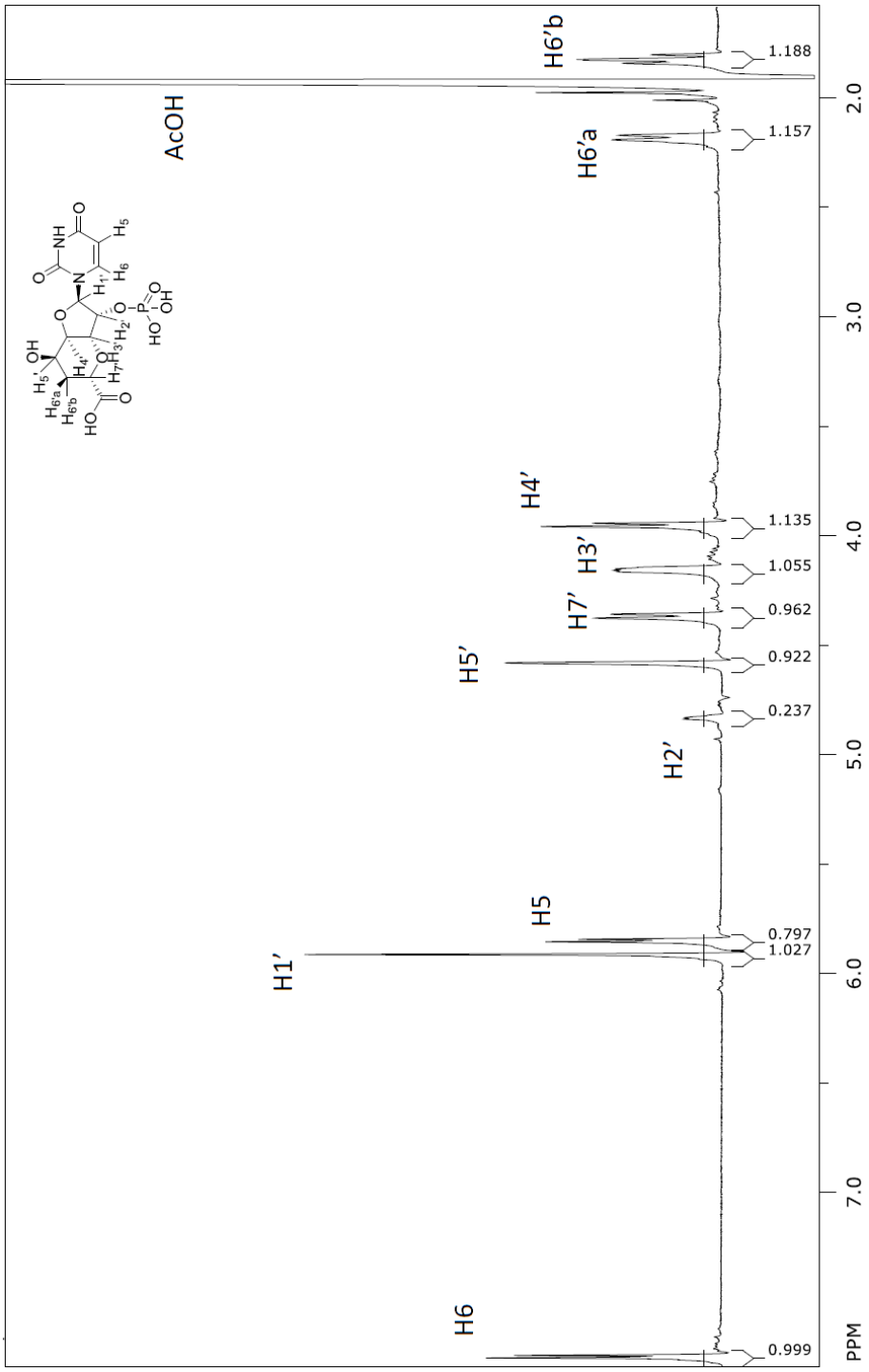

^{1}H NMR spectrum of 2'-OAP (12) from culture media at 700 MHz in D_2O.

The spectrum was determined at 25 °C. Chemical shifts were referenced to sodium 3-(trimethylsilyl)-2,2,3,3-d4-proponate. 2'-OAP was isolated from *S. tendae* Δ*nikK* culture media.

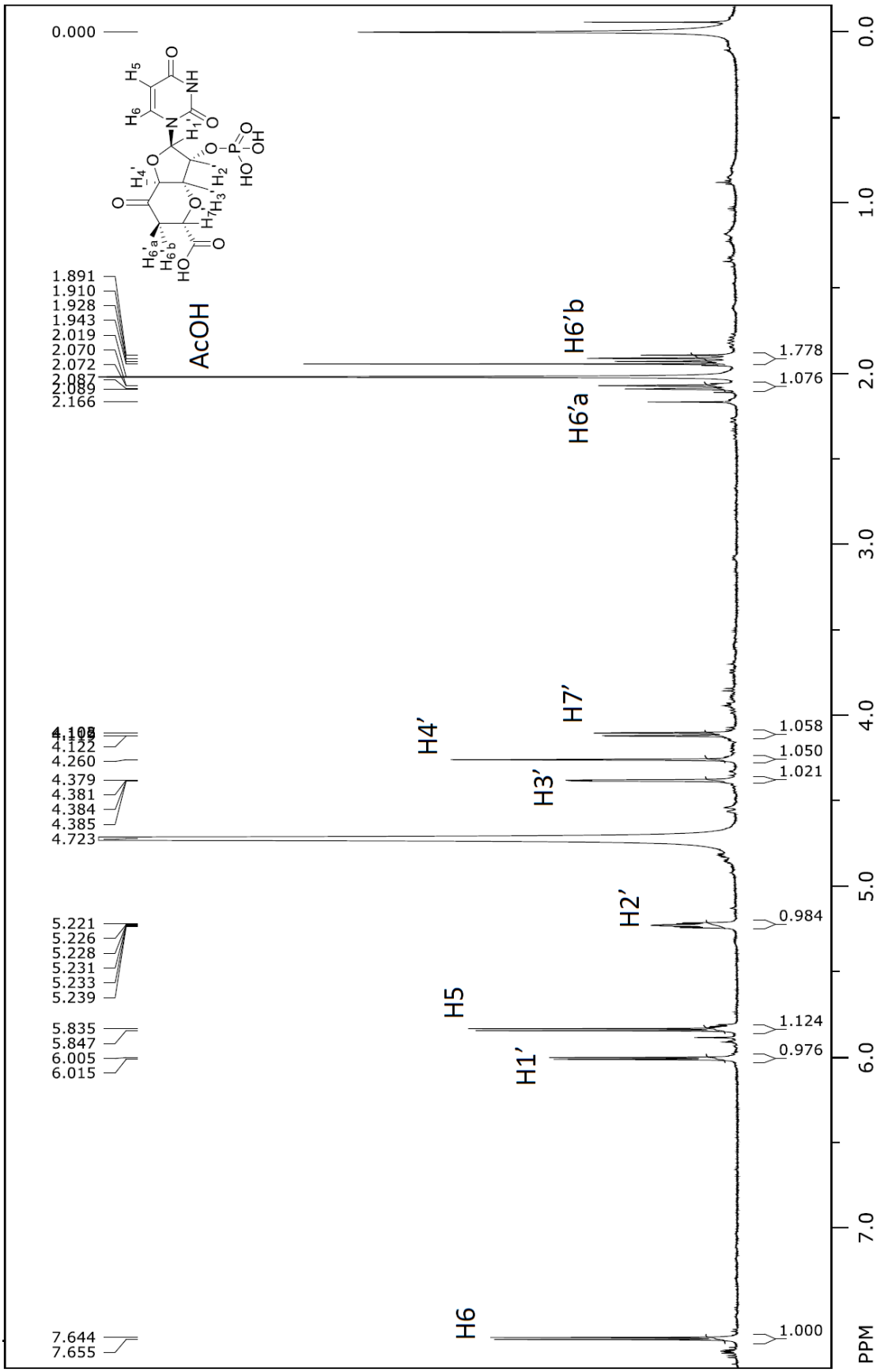

^{1}H NMR spectrum of KOAP (14) isolated from culture media (700 MHz in D_2O).

Isolated from *S. tendae* ΔnikK culture media. The chemical shifts were referenced to sodium 3-(trimethylsilyl)-2,2,3,3-d4-proponate.

Isolation of 5'-OAP (6) from *S. tendae ΔnikL* Culture Media

S. tendae Δ*nikL* culture media (25 mL) was diluted to 300 mL in dH_2O and loaded onto a QAE Sephadex A25 column (40 mL; bicarbonate form). The column was washed with 10 CV of 0.1 M ammonium bicarbonate pH 7.6. Then, the 5'-OAP was elute in a gradient from 200-500 mM ammonium bicarbonate pH 7.6. Fractions containing 5'-OAP were identified by HPAEC, combined, and lyophilized twice. The resulting powder was resuspended in 3 mL of dH_2O and passed through an Amberchrom CG300 column (Sigma-Aldrich; 100 mL). 5'-OAP was eluted with dH_2O and lyophilized twice prior to NMR characterization.

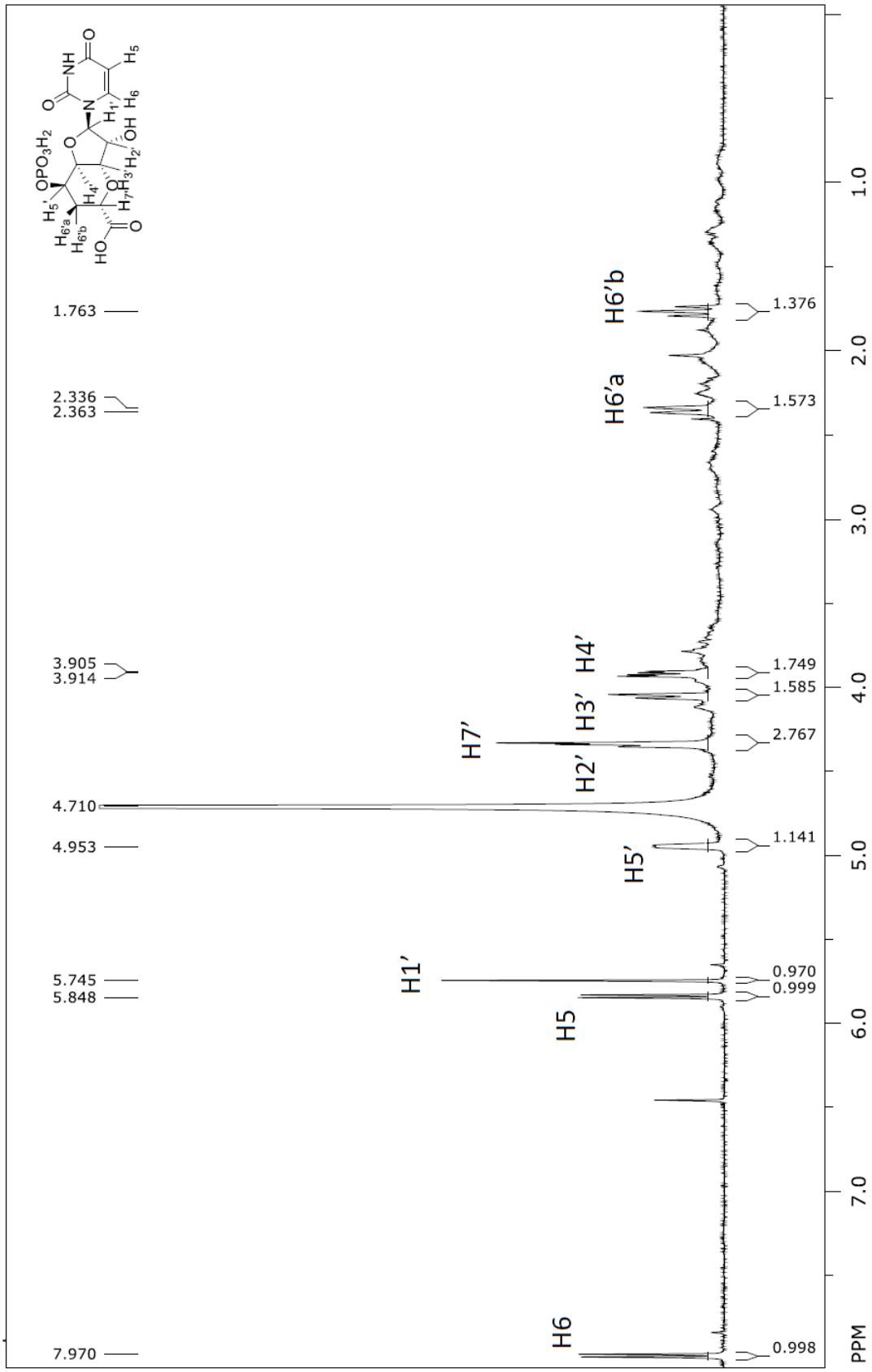

^{1}H NMR of 5'-OAP (6) at 700 MHz in D_2O.

5'-OAP was isolated from *S. tendae* Δ*nikL* culture media. The spectrum was identical to the previously reported spectrum of 5'-OAP isolated from *in vitro* enzyme assays.